Università degli Studi di Padova

DIPARTIMENTO DI BIOLOGIA

SCUOLA DI DOTTORATO DI RICERCA IN BIOSCIENZE E BIOTECNOLOGIE

INDIRIZZO IN NEUROBIOLOGIA
CICLO XXVI

Quantitative estimate of biochemical and electrical intercellular coupling in the developing cochlea of wild type and DFNB1 mouse models

Direttore della Scuola: Ch.mo Prof. Giuseppe Zanotti

Coordinatore di Indirizzo: Ch.mo Prof. Daniela Pietrobon

Supervisore: Ch.mo Prof. Fabio Mammano

Dottorando: Federico Ceriani

Contents

List of Figures

List of Tables

Summary

Hearing loss is the most common form of sensory impairment, with approximately one infant/1000 born with profound congenital deafness. Nonsyndromic hearing loss and deafness (DFNB1) is an inherited condition with a mild to severe deafness phenotype caused by mutations in GJB2 (which encodes the protein connexin26) and GJB6 (which encodes connexin30). Gap junction channels formed primarily by these two connexin protein subunits couple non-sensory cells (supporting and epithelial cells) of the mammalian cochlea, forming vast functional syncytia. Previous work has shown that electrical and metabolic coupling mediated by gap junction channels is fundamental for the development and maintenance of hearing. However, precise estimates of the degree of coupling and its alterations under DFNB1 conditions are lacking, notwithstanding the vast body of studies conducted in recombinant expression systems.

In this thesis work, we combined large scale optical recordings, single cell electrophysiology and computer simulations to elucidate the mechanisms that underlie intercellular communication in cochlear supporting cells from juvenile mice (first postnatal week). First, we developed a novel technique based on voltage imaging to map the extent and the degree of electrical coupling in non-sensory cell networks of the developing mouse cochlea. We also quantified precisely the reduction of electrical coupling in cochlear organotypic cultures from transgenic mice with hearing defects due to absence or mutation of connexin30 compared to wild type animals. By comparing our experimental results with numerical simulations, we estimated that cochlear supporting cells in the mouse are already well coupled in the first postnatal week by as many as $\sim$ 1500 channels per cell pair. In age-matched cultures from connexin30(T5M/T5M) and connexin30($-/-$) mice, junctional conductance was reduced respectively by 14% and 91%, and these data account for the increased hearing thresholds exhibited by these animals in the adult stage.

Besides electrical coupling, inner ear gap junction channels and hemichannels have been shown to participate in ATP- and IP_3- dependent intercellular Ca^{2+} signaling, and alterations of these signaling mechanisms in the postnatal cochlea have been linked to impairment of hearing acquisition. We thus performed Ca^{2+} imaging experiments aimed at elucidating the mechanisms underlying the generation and intercellular propagation of ATP-mediated Ca^{2+} signals in cochlear non-sensory cells. We determined that ATP- and IP_3- dependent Ca^{2+} oscillations in cochlear non-sensory cells can occur at constant intracellular IP_3 concentration. We then combined the information

gathered from the two types of experimental approaches in a mathematical model that (i) correctly reproduces the range and propagation speed of intercellular Ca^{2+} waves and (ii) indicates that inception and culmination of self-sustained Ca^{2+} oscillations are marked by supercritical Hopf bifurcations at ATP concentrations of $\sim$ 100 nM and $\sim$1 µM, respectively.

Finally, we investigated the relationship between spontaneous Ca^{2+} transients in cochlear non-sensory cells and spontaneous Ca^{2+} action potentials in sensory inner hair cells. Our preliminary results suggest that Ca^{2+} signaling in non-sensory cells may have a modulating effect on spontaneous electrical activity, which is intrinsically generated in inner hair cells.

Riassunto dell'attivitá svolta

La perdita dell'udito è la forma più comune di disabilità sensoriale: circa un bambino su 1000, infatti, è affetto alla nascita da sordità congenita profonda. La sordità non sindromica (DFNB1) è una malattia ereditaria con un fenotipo di sordità che va da lieve a grave, causata da mutazioni nei geni GJB2 (che codifica la proteina connessina26) e GJB6 (che codifica la connessina30). Canali giunzionali formati prevalentemente da queste due proteine accoppiano le cellule non sensoriali (cellule di sostegno e cellule epiteliali) della coclea dei mammiferi, le quali formano vasti sincizi funzionali. Studi precedenti hanno dimostrato che l'accoppiamento elettrico e metabolico mediato da canali giunzionali è fondamentale per lo sviluppo e il mantenimento dell'udito. Tuttavia, nonostante il gran numero di studi condotti in sistemi di espressione, mancano stime precise del grado di accoppiamento e delle sue alterazioni in condizioni DFNB1.

In questo lavoro di tesi, sono state combinate registrazioni ottiche su larga scala , registrazioni elettrofisiologiche su singola cellula e simulazioni al computer per chiarire i meccanismi che sono alla base della comunicazione intercellulare nelle cellule cocleari non sensoriali in topi giovani (prima settimana post-natale) . In primo luogo, abbiamo sviluppato una nuova tecnica basata sull'imaging del potenziale di membrana cellulare per mappare l'estensione e il grado di accoppiamento elettrico nelle reti cellulari non sensoriali della coclea in via di sviluppo . Abbiamo anche quantificato con precisione la riduzione dell'accoppiamento elettrico in colture organotipiche cocleari da topi transgenici con difetti uditivi causati dall'assenza o da mutazioni della connessina30 rispetto ad animali wild type. Confrontando i nostri risultati sperimentali con simulazioni numeriche , abbiamo stimato che le cellule non sensoriali della coclea nel topo sono già ben accoppiate nella prima settimana post-natale da ben $\sim$ 1500 canali per ogni coppia di cellule. Nelle colture di pari età provenienti da topi connexin30(T5M/T5M) e connexin30($-/-$), la conduttanza giunzionale è ridotta rispettivamente del 14% e del 91% , e questi dati sono in accordo con l'aumento delle soglie uditive mostrato da questi animali nella fase adulta .

Oltre a fornire l'accoppiamento elettrico , é stato dimostrato che i canali giunzionali dell'orecchio interno partecipano alla segnalazione Ca^{2+} intracellulare dipendente dall'ATP e dall'IP_3, e l'alterazione di questi meccanismi di segnalazione nella coclea postnatale é stata collegata alla compromissione dell'acquisizione dell'udito. Abbiamo quindi eseguito esperimenti di imaging dello ione Ca^{2+} volti a chiarire i meccanismi alla base della ge-

nerazione e propagazione intercellulare dei segnali Ca^{2+} mediati da ATP nelle cellule non sensoriali della coclea. Abbiamo determinato che le oscillazioni Ca^{2+} dipendenti dall'ATP e dall'IP_3 nelle cellule non sensoriali cocleari possono verificarsi in presenza di una concentrazione intracellulare di IP_3 costante. Abbiamo poi combinato le informazioni raccolte attraverso i due diversi approcci sperimentali in un modello matematico che (i) riproduce correttamente la velocità e il range di propagazione delle onde Ca^{2+} intercellulari e (ii) indica che l'inizio e il culmine delle oscillazioni Ca^{2+} sono contrassegnati da biforcazioni di Hopf supercritiche a concentrazioni di ATP di ~ 100 nM e ~ 1 µM, rispettivamente .

Infine , abbiamo studiato la relazione tra transienti Ca^{2+} spontanei delle cellule non sensoriali e i potenziali d'azione spontanei delle cellule ciliate interne. I nostri risultati preliminari suggeriscono che i transienti Ca^{2+} delle cellule non sensoriali potrebbero avere un effetto modulante sull'attività elettrica spontanea , che è intrinsecamente generata nelle cellule ciliate interne.

Original publications

Part of the data reported in the present thesis has been published in the following papers:

1. Ceriani, F., and Mammano, F. (2013). A rapid and sensitive assay of intercellular coupling by voltage imaging of gap junction networks. *Cell Communication and Signaling*, 11(1), 78. doi:10.1186/1478-811X-11-78

2. Ceriani, F., and Mammano, F. (2012). Calcium signaling in the cochlea - Molecular mechanisms and physiopathological implications. *Cell Communication and Signaling*, 10(1), 20. doi:10.1186/1478-811X-10-20

1 Introduction

Our auditory system provides us with an incredibly rich source of information about the world around us. From a physical point of view, what we refer to as "sounds" are pressure waves generated by vibrating air molecules. The job of the auditory system is to transform these sound waves into distinct patterns of neural activity, which are then integrated with information from other sensory systems to guide behavior, including intraspecies communication.

The first stage of this transformation occurs at the external and middle ears, which collect sound waves and amplify their pressure, so that the sound energy in the air can be successfully transmitted to the fluid-filled cochlea of the inner ear. The external ear, which consists of the pinna, concha, and auditory meatus, gathers sound energy and focuses it on the eardrum, or tympanic membrane. The external ear collects sound and channels via the ear canal to the tympanic membrane, or eardrum (Figure 1.1).

As oscillations in air pressure hit on the eardrum, its vibrations are transmitted to the middle ear's ossicles, named malleus, incus, and stapes. The major function of the middle ear is to match relatively low-impedance airborne sounds to the higher-impedance fluid of the inner ear (the term "impedance" in this context describes a medium's resistance to movement). The middle ear ensures transmission of the sound energy across the air–fluid boundary by boosting the pressure measured at the tympanic membrane almost 200-fold by the time it reaches the inner ear (Figure 1.1).

In the inner ear, a series of biomechanical processes occur that break up the signal into simpler, sinusoidal components, with the result that the frequency, amplitude, and phase of the original signal are all faithfully transduced by the sensory hair cells and encoded by the electrical activity of the auditory nerve fibers. One product of this process of acoustical decomposition is the systematic representation of sound frequency along the length of the cochlea, referred to as tonotopy, which is an important organizational feature preserved throughout the central auditory pathways.

1.1 Inner ear

The *inner ear* is situated within the petrous portion of the temporal bone and is composed of the *vestibular system* (semicircular canals, utricle, and saccule), which senses linear and angular acceleration and inclination of the head with respect to gravity, and the *cochlea*, which mediates sound perception . In the inner ear, the membranous labyrinth is contained within the bony labyrinth. The bony labyrinth consists of the vestibular system (composed by the vestibule and the semicircular canals) and the spirally coiled cochlea. Within each structure is the corresponding portion of the membranous labyrinth:

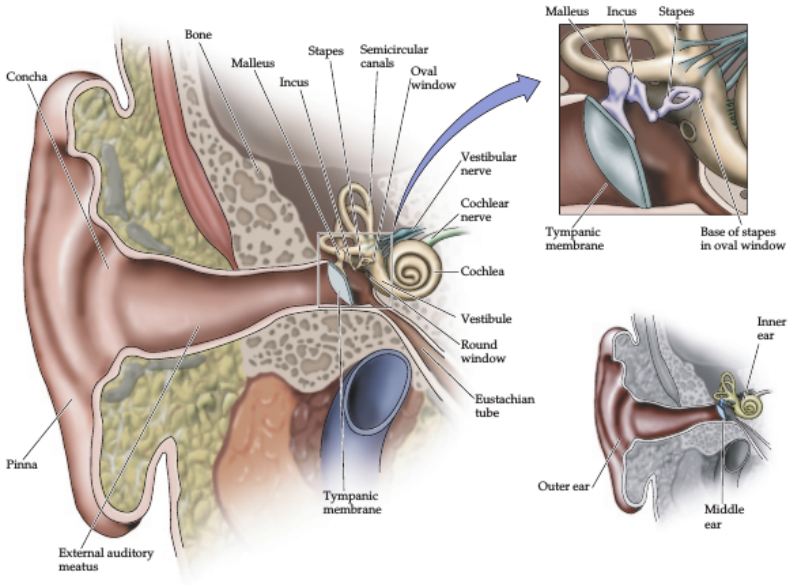

Figure 1.1: Anatomy of the human ear. The external ear, which consists of the pinna, concha, and auditory meatus, collects sound and channels via the ear canal to the tympanic membrane, or eardrum. As oscillations in air pressure hit on the eardrum, its vibrations are transmitted to the middle ear's ossicles, named malleus, incus, and stapes. Finally, the stapes transmits vibrations to the oval window, a membrane-covered opening to the inner ear. (Figure from Ref. [Purves et al., 2001])

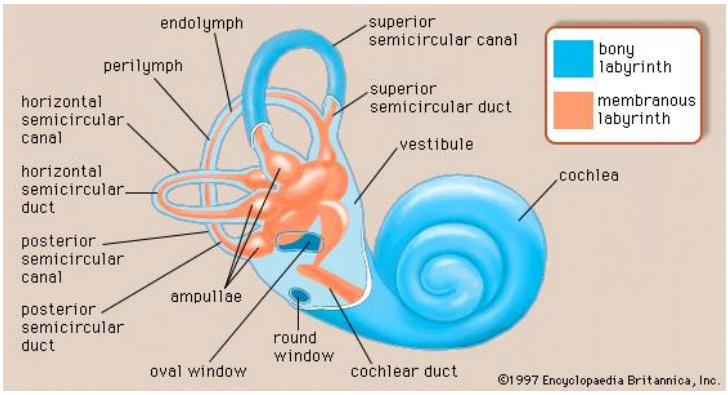

Figure 1.2: The two labyrinths of the inner ear. The bony labyrinth, a cavity in the temporal bone, is divided into three sections: the vestibule, the semicircular canals, and the cochlea. Within the bony labyrinth there is a membranous labyrinth, which is also divided into three parts: the semicircular ducts; two saclike structures, the saccule and utricle, located in the vestibule; and the cochlear duct, which is the only part of the inner ear involved in hearing. (Figure from `http://www.britannica.com/EBchecked/topic/288499/inner-ear`)

the vestibule contains the utricle and the saccule, each semicircular canal contains a semicircular duct (Figure 1.2).

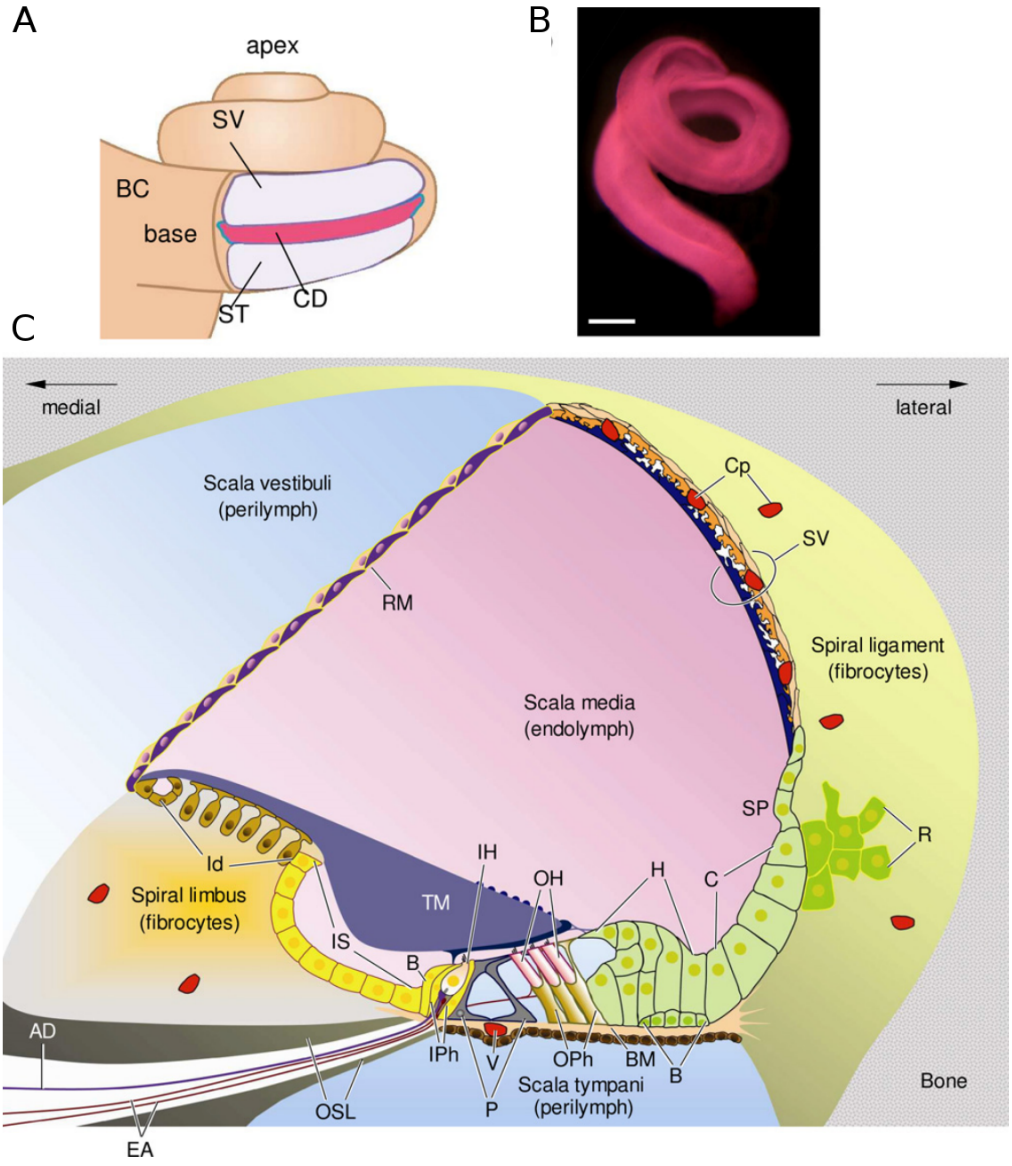

Figure 1.3: Anatomy of the cochlea and cochlear duct.
(A) Schematic drawing of the cochlea: BC, bony capsule shown fenestrated near the base to expose scala vestibuli (SV) and scala tympany (ST), both filled with perilymph; CD, cochlear duct, filled with endolymph. (B) CD from a P5 mouse after removal of the bony capsule; scale bar, 1 mm. (C) Schematic diagram of a cross section of the cochlear canals. Scala media (or cochlear duct) lies between the larger vestibular and tympanic scalae. The base of scala media is formed by the osseous spiral lamina (OSL) and the basilar membrane (BM). The organ of Corti rests on the basilar membrane. The organ of Corti contains inner and outer hair cells (IH, OH), separated by pillar cells (P) that form the tunnel of Corti. In the mature mouse cochlea afferent synapses typically have a single ellipsoid ribbon per active zone in both inner and outer hair

cells. Inner hair cells form afferent synapses only with afferent dendrites (AD) of type I spiral ganglion neurons. Lateral olivocochlear neurons synapse onto boutons of type I spiral ganglion neurons in close proximity to inner hair cells. Medial olivocochlear neurons contact outer hair cells directly. Each outer hair cell is supported by an outer phalangeal cell (OPh), or supporting cell of Deiters, which holds the base of the hair cell in a cup-shaped depression. From each Deiters' cell, a phalangeal projection extends upward to a stiff membrane, the reticular lamina, that forms the upper layer of the organ of Corti. The apices of the outer hair cells are firmly held by the reticular lamina but the cell bodies are suspended in fluid that fills the space of Nuel and the tunnel of Corti. Although this fluid is sometimes referred to as cortilymph, its composition is thought to be similar, if not identical, to that of the perilymph. Inner hair cells are supported and enclosed by inner phalangeal cells (IPh) which rest on the thin outer portion, called the tympanic lip, of the spiral limbus. The latter rests on the margin of the osseous spiral lamina and hosts interdental cells (Id) and fibrocytes (not shown). Inner border (B) and cuboidal epithelial cells line the spiral limbus on the inner sulcus (IS) side. Stereocilia on the apical tips of inner hair cells are arranged in parallel rows. In contrast, stereocilia on outer hair cells form a "W"-shaped pattern. The longest stereocilia of outer hair cells contact the overlying acellular structure, the tectorial membrane (TM). The tectorial membrane covers the reticular lamina and reaches the cells of Hensen (H). Two other types of epithelial cells, cells of Claudius (C) and Böttcher (B), cover the outer sulcus. The spiral prominence (SP) and the stria vascularis (SV) are situated at the upper margin of the outer sulcus. Some cells of the outer sulcus send projections, called root cells (R), into the substance of the fibrous spiral ligament. The spiral ligament lies between the stria vascularis and the bony wall of the cochlea and hosts numerous fibrocytes (not shown). Like the adjacent stria vascularis, the spiral ligament is well supplied with blood capillaries (Cp). The vas spiralis (V) is a blood vessel running in the tympanic layer of the basilar membrane just beneath the tunnel of Corti. The transparent vestibular membrane of Reissner (RM), which consists of only two layers of flattened cells, stretches from the stria vascularis to the medial margin of the spiral limbus.(Figure from Ref. [Mammano, 2013])

1.1.1 Developmental anatomy of the mammalian cochlea

The cochlea is a snail–shaped inner ear structure divided in three chambers, namely the scala vestibuli, the scala tympani, and the scala media (also known as cochlear duct) [Krstic, 1997, Raphael and Altschuler, 2003] (Figure 1.3A and B). The scala tympani is connected by the cochlear aqueduct to the subarachnoidal space of the cranial cavity, which is filled with cerebrospinal fluid. The scalae vestibuli and tympani are connected through an opening at the apical end of the cochlea, called the helicotrema and are both filled with perilymph, a fluid whose composition is similar to that of cerebrospinal fluid. The mature cochlear duct is filled with endolymph, an unusual extracellular fluid containing 150 mM K^+, 2 mM Na^+ and as little as 20 µM extracellular free Ca^{2+} concentration ($[Ca^{2+}]_o$) [Bosher and Warren, 1978].

The isolation of endolymph from perilymph depends on cells that form the cochlear duct epithelium. These epithelial cells are connected by a network of tight and adherens junctions near their apical surfaces (i.e. in facing the scala media). The duct epithelium includes the organ of Corti (Figure 1.3C) [Lim, 1986], which is the sensory organ responsible for sound transduction. The organ of Corti rests on the basilar membrane and has the form of an epithelial ridge encompassing highly specialized sensory inner

and outer hair cells. Hair cells possess an apical stereociliary bundle that is the site of sound transduction. In the adult human cochlea there are about 3500 inner hair cells, organized in a single row. There are approximately three times as many outer hair cells, organized in three parallel rows. Preceding the acquisition of hearing, the sensory epithelium comprises the greater epithelial ridge (GER), which gives rise to the inner hair cells and medial non–sensory cells, and the adjacent lesser epithelial ridge (LER), which is thought to generate the outer hair cells and lateral non–sensory cells [Eggston and Wolff, 1947, Lim and Rueda, 1992]. Cells providing mechanical support to hair cells are designated as supporting cells. In the mature organ of Corti, supporting cells include inner phalangeal cells, inner and outer pillar cells, outer phalangeal cells (also known as Deiters' cells), and Hensen's, Böttcher's and Claudius' cells. The rows of inner and outer hair cells are separated by the triangle of Corti, formed by the apposition of inner and outer pillar cells. The inner phalangeal cells completely surround the inner hair cells. The outer phalangeal cells form cups holding the synaptic poles of the outer hair cells and send fine processes, or phalanges, to the reticular lamina. This is a thin, stiff cytoplasmic plate that extends from the innermost row of outer hair cells to the Hensen's cells sealing the apical (endolymphatic) poles of outer hair cells within a mosaic of apposing phalangeal process of outer pillar cells and outer phalangeal cells. The tectorial membrane covers the organ of Corti throughout the cochlea, from base to apex. It is medially attached at the spiral limbus to interdental cells. The inferior aspect of the tectorial membrane is in contact with the stereocilia of outer hair cells and with Hensen's cells at the lateral edge of the organ of Corti. Hensen's stripe is an area in the inferior aspect of the TM, with which inner hair cell stereocilia are thought to interact. Medial to the organ of Corti, the cochlear duct epithelium comprises interdental cells of the spiral limbus. Lateral to the organ of Corti, the duct epithelium consists of spiral prominence cells and marginal cells of the stria vascularis. The remainder of the duct wall is formed by the Reissner's membrane [Krstic, 1997, Raphael and Altschuler, 2003].

1.1.2 Physiology and development of the cochlea

The stria vascularis transports K^+ into the endolymph and generates the endocochlear potential [Hibino and Kurachi, 2006, Zdebik et al., 2009, Patuzzi, 2011a, Patuzzi, 2011b]. This is an electrical potential difference between endolymph and perilymph. The endocochlear potential appears around postnatal day 5 (P5, where P0 indicates the day of birth) in rodents and increases progressively to reach levels in excess of +100 mV by P17 [Schmidt and Fernandez, 1963, Uziel et al., 1981, Rybak et al., 1992]. The high potassium concentration in mature endolymph (150 mM) is a necessary but not sufficient condition for the endocochlear potential. A study perfomed by Yamasaky et al. [Yamasaki et al., 2000] was specifically designed to clarify the chronological developmental process of monovalent ions (Na^+, K^+, Cl^-) in the endolymph of the mouse in relation to the development of the endocochlear potential. In that study, the concentrations of all three monovalent ions in endolymph reached adult levels at P7, when the endocochlear potential was still under +20 mV, whereas the endocochlear potential increased abruptly after P7 and reached approximately +80 mV at P14 [Yamasaki et al., 2000].

Both the endocochlear potential and the high endolymphatic potassium are key factors for the mechanotransduction process performed by cochlear hair cells [Wangemann, 2006, Fettiplace et al., 2006, Schwander et al., 2010, Richardson et al., 2011]. Mechanotransduction is initiated by mechanical stimuli applied to the stereociliary bundle due to the sound–evoked shearing motion between the reticular lamina and the tectorial membrane. Movement of the hair cell stereocilia in the direction of the taller row opens transduction ion channels in the stereocilia [Beurg et al., 2009]. The large potential difference between the endolymph and the cytoplasm of inner and outer hair cells drives potassium ions into hair cells through these mechanically gated channels. In adult hair cells, K^+ influx generates a receptor potential, which is a graded change of membrane potential, V_m. Hair cell depolarization triggers glutamate release at specialized afferent synapses, known as ribbon synapses, located on their basal pole [Glowatzki et al., 2008, Meyer and Moser, 2010, Matthews and Fuchs, 2010]. Ribbon synapses connect hair cells to (afferent dendrites of) spiral ganglion neurons, which transmit impulses into central nervous system activating central pathways that lead to hearing [Rusznak and Szucs, 2009, Meyer and Moser, 2010, Nayagam et al., 2011]. Type I spiral ganglion neurons are large bipolar neurons that comprise the major population (90–95%) of spiral ganglion cells and are postsynaptic to inner hair cells, the auditory sensory cells of the mammalian cochlea. The features of the inner hair cell ribbon synapses combine with the firing properties of spiral ganglion neurons to generate the auditory temporal code with high precision [Rutherford et al., 2012].

It is well established that receptor potentials in outer hair cells drive a local mechanical amplification process [Ashmore, 2008, Dallos, 2008], carried out by the motor protein prestin [Zheng et al., 2000, Schaechinger et al., 2011]. This mechanical amplification is required for the high sensitivity and sharp frequency selectivity of mammalian hearing ([Dallos, 2008, Ashmore, 2011, Johnson et al., 2011a]). In contrast, the synaptic function performed by outer hair cells is poorly understood. They are presynaptic to type II spiral ganglion neurons that have small unmyelinated axons and constitutes only 5% of the cochlear nerve. While the type I fibers turn upwards toward the inner hair cells, the type II fibers cross the tunnel of Corti along its floor in a radial trajectory and then turn toward the basal end of the cochlea (these fibers were called outer spiral fibers before it was known that they were connected to type II neurons). The peripheral endings of type II spiral ganglion neurons branch extensively and innervate a dozen outer hair cells, generally in the same row. Recent data suggest that type II fibers could communicate centrally by maximal activation of their entire pool of presynaptic outer hair cells [Weisz et al., 2012]. Type II afferents also contact Deiters' and Hensen's cells in the apical cochlear turn, but these cells lack presynaptic ultrastructure and are considered postsynaptic to type II afferents [Burgess et al., 1997, Fechner et al., 2001]. Thus it is possible that type II fibers establish local circuit interactions between outer hair cells and supporting cells; however the function of this putative interaction remains elusive. Reciprocal synapses between outer hair cells and their type-II terminals have been detected in human, chimpanzee, cat, guinea pig, and mouse throughout the cochlear spiral and in all three rows of outer hair cells [Nayagam et al., 2011]. Thiers et al. [Thiers et al., 2008] think that this local circuitry

may mediate feedback control of, and bidirectional communication among, outer hair cells. In addition, modulatory top-down control is effected by neurons of the superior olive forming efferent synapses on hair cells and postsynaptic boutons [Robertson, 2009,Guinan Jr., 2006].

While the human full–term neonate can hear at birth, auditory function in most rodents begins between P10 and P14, reaching adult–level thresholds between by the 3rd postnatal week [Mikaelian et al., 1965, Ehret, 1977, Uziel et al., 1981]. Of notice, inner hair cells of neonatal mice and gerbils generate spontaneous Ca^{2+} action potentials [Marcotti, 2012] throughout pre-hearing stage of development [Johnson et al., 2012, Johnson et al., 2011b]. Beurg et al. [Beurg et al., 2008] reported that also immature outer hair cells fire regenerative action potentials, which are presumably Ca^{2+}–dependent as they are not eliminated by tetrodotoxin but are abolished by nifedipine, a blocker of L-type Ca^{2+} channels. The complete disappearance of spontaneous action potentials and replacement by graded receptor potentials is mainly due to the expression of K^+ ion channels characteristic of mature cells [Kros et al., 1998].

While spontaneous action potentials are occurring in immature hair cells, the auditory afferent fibers undergo extensive reorganization (reviewed in refs. [Defourny et al., 2011,Appler and Goodrich, 2011,Bulankina and Moser, 2012]; summarized schematically in Figure 1 of ref. [Greenwood et al., 2007])The more numerous type I spiral ganglion neurons that initially innervate both inner hair cells and outer hair cells undergo pruning. This pruning results in the retraction of neurites that innervate outer hair cells and the refinement of innervation to the inner hair cells. The end result is a one–to–one axosomatic innervation characteristic of mature inner hair cells. Conversely, the less abundant type II spiral ganglion neurons that also initially innervate both inner and outer hair cells lose their connections with inner hair cells. Maturation of mechanotransduction parallels these events. Details of mechanotransduction have been investigated in acute explants and in organotypic cultures of cochlear tissue [Waguespack et al., 2007,Lelli et al., 2009]. These explant cultures (Figure 1.4) preserve the architecture and functional relationships among the cells observed in vivo and are readily obtained from mice before the onset of hearing [Van de Water and Ruben, 1971, Sobkowicz et al., 1975, Sobkowicz et al., 1993]. Electrophysiological recordings indicate that hair cells in rat organotypic cultures show normal immature development of mechanotransduction properties [Waguespack et al., 2007].

1.2 Connexins and gap junctions

Hearing relies not only on the functional maturation of hair cells, but also on differentiation and proper organization of non–sensory cell networks that transfer signaling, ion, and nutrient molecules through gap junction channels [Cohen-Salmon et al., 2005, Kelly and Chen, 2009]. The network of epithelial gap junctions forms around embryonic day 16 and interconnects all supporting cells in the organ of Corti as well as adjacent epithelial cells. The epithelial gap junction network apparently subdivides further in two separate, medial and lateral, buffering compartments. These two distinct compartments

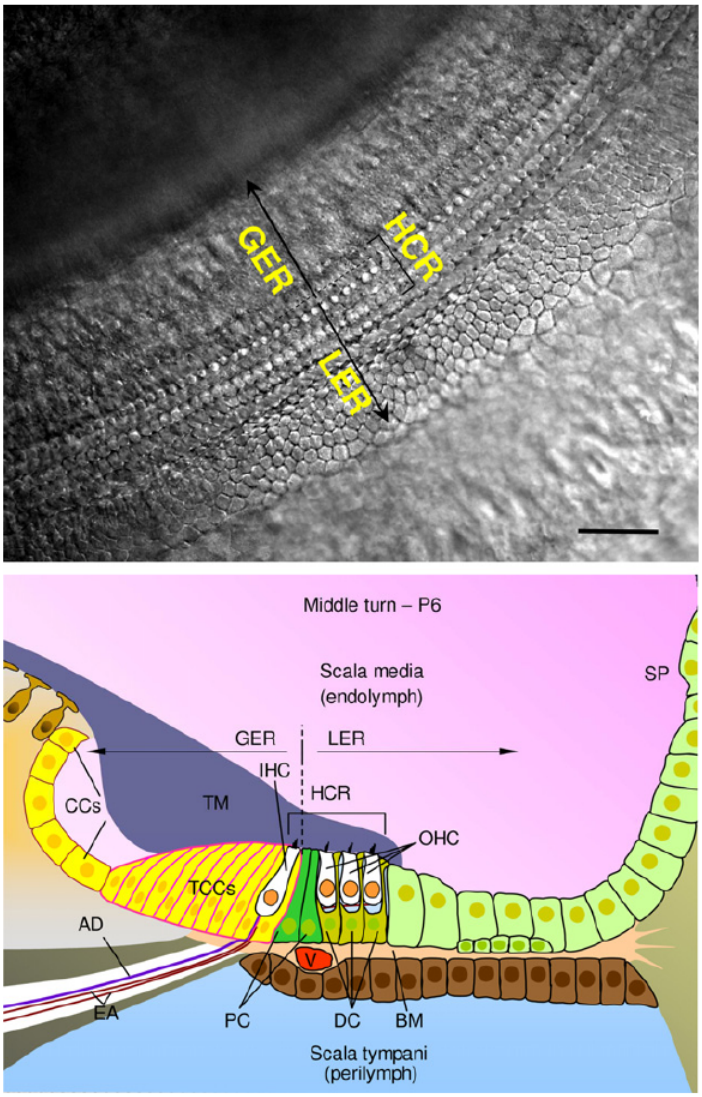

Figure 1.4: The sensory epithelium of the developing cochlea. Top: Differential interference contrast (DIC) micrograph of the sensory epithelium in the basal turn of an organotypic cochlear culture, viewed from the scala media. LER, lesser epithelial ridge; GER, greater epithelial ridge; HCR, hair cell region; scale bar, 50 µm. Bottom: Schematic diagram of the epithelium viewed in transverse section, i.e. in a plane that contains the axis of the modiolus. Abbreviations as in Figure 1.3 (Figure from Ref. [Mammano, 2013])

are believed to be individually dedicated to the homeostasis of inner and outer hair cells, respectively [Spicer and Schulte, 1998, Jagger and Forge, 2006]. A second network, named the connective tissue gap junction network, starts to develop around birth. This latter network comprises interdental cells and fibrocytes in the spiral limbus, fibrocytes of the spiral ligament, basal and intermediate cells of the stria vascularis [Cohen-Salmon et al., 2005].

1.2.1 The potassium recycle hypothesis

A long–standing tenet is that gap junction networks of mature cochlea intervene in the recycling of potassium ions to the endolymph (reviewed in refs. [Kikuchi et al., 2000, Wangemann, 2002, Zhao et al., 2006, Mistrik and Ashmore, 2009]). In such K^+ recycle hypothesis, cochlear non–sensory cells are presumed to buffer the K^+ that enters apical channels on the stereocilia of hair cells during auditory transduction, diffuses to the soma, and is released there through basolateral K^+ channels. Because epithelial and connective gap junction networks are discontinuous at the lateral wall of the cochlea, the recycle scheme requires K^+ leaving the epithelial or diffusing through perilymph to be taken up by the fibrocytes in the spiral limbus [Cohen-Salmon et al., 2005]. To complete the circuit, intercellular transport of K^+ might occur along the cochlear wall via gap junctions that link fibrocytes with basal and intermediate cells of the stria vascularis [Kelly et al., 2011]. After reaching the stria vascularis, potassium ions are then released by intermediate cells into the lumen of the stria vascularis and are finally transported into strial marginal cells for secretion back into endolymph, thereby completing the K^+ cycle (Figure 1.5) [Kikuchi et al., 2000, Wangemann, 2002, Zhao et al., 2006, Mistrik and Ashmore, 2009]. The K^+ recycle hypothesis, although lacking experimental proof, is indirectly supported by the widespread distribution of gap junction channels [Lautermann et al., 1999, Lautermann et al., 1998, Kikuchi et al., 1995], K/Cl cotransporters [Boettger et al., 2002], and aquaporins [Huang et al., 2002]. The K^+ recycle hypothesis is also consistent with the observation that several classes of supporting cells in the cochlear sensory epithelium express glial fibrillary acidic protein (GFAP) [Rio et al., 2002]. GFAP is a classic marker for astrocytes that, in the central nervous system, spatially buffer K^+ through the glial syncytium [Kofuji and Newman, 2004]. However the K^+ recycle hypothesis also meets some difficulties, as detailed hereafter.

1.2.2 Cochlear connexins and deafness

Gap junction channels in the mammalian cochlea are formed primarily by connexin26 and connexin30 protein subunits [Lautermann et al., 1999, Lautermann et al., 1998] encoded by nonsyndromic hearing loss and deafness (DNFB1) genes GJB2 and GJB6, respectively (reviewed in refs. [Nickel and Forge, 2008, Martinez et al., 2009]); see also `http://www.ncbi.nlm.nih.gov/books/NBK1272/`). The fact that DFNB1 is the most common form of inherited deafness in Caucasian populations highlights the importance of connexins for hearing (reviewed in refs. [Hilgert et al., 2009, del Castillo and del Castillo, 2011]). Connexin26 and connexin30 share 77% amino acid identity and may assemble

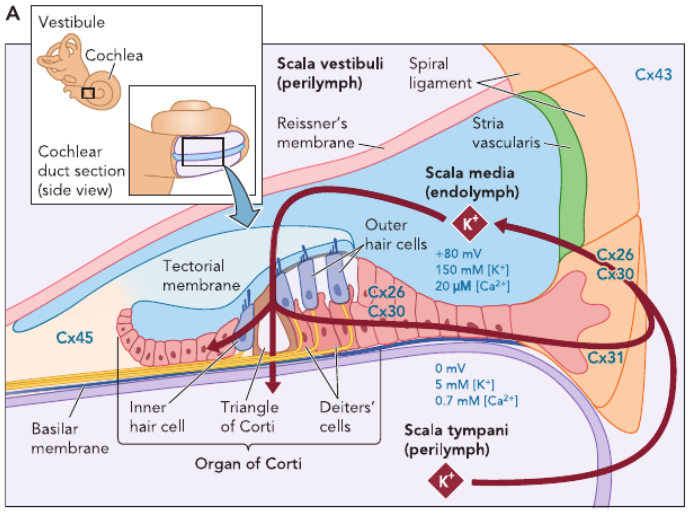

Figure 1.5: Potassium spatial buffering in the cochlea. K^+ released from the hair cells has been proposed to flow through scala tympani perilymph before entering the spiral ligament and being secreted back into endolymph. Conversely, according to the potassium recycle hypothesis, K^+ released from cochlear hair cells is taken up by adjacent supporting cells and flows from cell to cell through the gap junction network towards the spiral ligament, thereby never entering the perilymph. Figure from [Mammano et al., 2007]

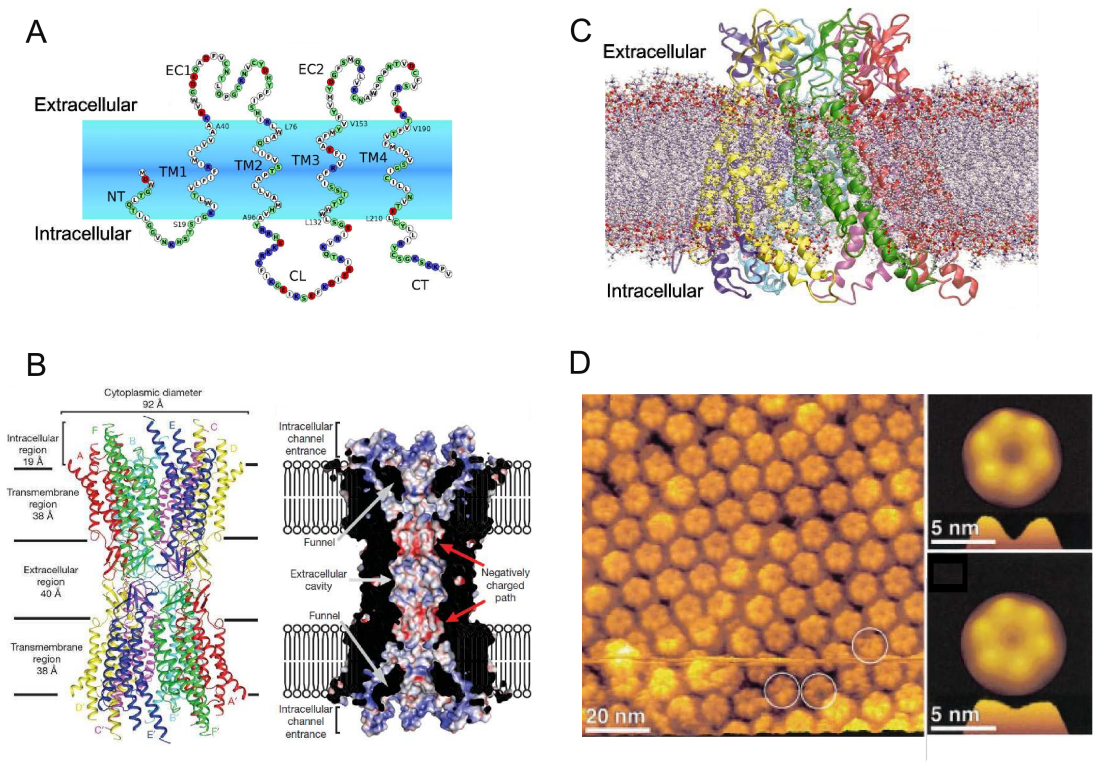

Figure 1.6: Connexin26 channels and hemichannels. (A) Topology representation and sequence alignment of the human connexin26. NT, N-terminus; CT, C-terminus; TM1-TM4, transmembrane helices 1 to 4; CL, cytoplasmic loop connecting TM2, TM3; EC1, EC2, extracellular loops connecting TM1 to TM2 and TM3 to TM4, respectively. Residue color code: blue, positive; red, negative; white, hydrophobic; green, hydrophilic. (from [Zonta et al., 2012]) (B) Left: side view of the structure of the human connexin26 gap junction channel in ribbon representation. The corresponding protomers in the two hemichannels, which are related by a two-fold axis, are shown in the same colour. Right: Vertical cross-section through the gap junction channel, showing the surface potential inside the channel. The channel features a wide cytoplasmic opening, which is restricted by the funnel structure, a negatively charged path and an extracellular cavity at the middle. The electrostatic potentials range from 240 (red) to 40 (blue) kT e^{-1} (from [Maeda et al., 2009]). (C) Connexin26 connexon model in a lipid bilayer (from [Zonta et al., 2012]).(D) Left: atomic force microscopy tomograph showing the connexon arrangement in the extracellular surface. Right: average atomic force microscopy tomograph of connexon hemichannels in Ca^{2+} free (top) and 0.5 mM Ca^{2+} extracellular solution (bottom) (from [Muller et al., 2002])

to form heteromeric and heterotypic gap junction channels [Forge et al., 2003, Ahmad et al., 2003, Yum et al., 2007]. To date, the human connexin26 gap junction channel is the only structure that has been resolved by X-ray diffraction (at 3.5 åresolution, Figure 1.6) [Maeda et al., 2009]. The structure of connexin30 channels has been inferred by a combination of homology modeling and molecular dynamics [Zonta et al., 2012]. Mouse models confirm that connexin26 and connexin30 are essential for auditory function and for survival and development of the organ of Corti [Cohen-Salmon et al., 2002, Kudo, 2003, Teubner, 2003, Chang et al., 2008, Sun et al., 2009, Schutz et al., 2011, Schutz et al., 2010]. These animal models also reveal critical gaps in our current understanding of the role played by connexins in the inner ear and the etiology of deafness due to absent or mutated connexins. Deafness and absence of an endocochlear potential in mice lacking connexin30 correlate with: (1) disruption of the endothelial barrier of the capillaries supplying the stria vascularis before endocochlear potential onset; (2) down–regulation of betaine–homocysteine S–methyltransferase; and (3) local increase in homocysteine, a known factor of endothelial dysfunction [Cohen-Salmon et al., 2007] with no obvious link to gap junction channel function. Similarly, the hypothesis that connexin dysfunction impacts primarily on K^+ recycling is challenged by the identification of connexin26 human recessive deafness mutants, e.g. V84L [Kelley et al., 1998], that are capable of forming functional channels [Bruzzone et al., 2003]. Studies performed in model cells indicate that connexin26 V84L mutant channels are as permeable to K^+ as wild type channels. However, the transfer of the second messenger IP_3 (and possibly of other key metabolites) through the mutant channels is impaired [Beltramello et al., 2005, Decrock et al., 2011]. Thus, the permeability of connexin gap junction channels to metabolites [Hernandez et al., 2007, Harris, 2007], and not simply to small inorganic ions, is likely to play an important role in development, physiology and etiology of connexin–related hearing impairment. For an in–depth analysis of other difficulties confronting the K^+ recycle hypothesis, see refs. [Patuzzi, 2011a, Patuzzi, 2011b] . Chloride ions also play an important role in cochlear function. For example, a mouse model of Bartter syndrome (an autosomal recessive disorder characterized by congenital deafness and severe renal salt and fluid loss) showed that barttin in the marginal cells of stria vascularis is essential for the generation of the endocochlear potential [Rickheit et al., 2008]. Barttin is an important subunit of certain chloride channels (ClC–Ka, ClC–Kb). Impairment of this Cl^- path causes a reduction of endocochlear potential, but not the high K^+ concentration of endolymph, leading to deafness [Rickheit et al., 2008].

1.3 Calcium signaling in the cochlea

Calcium ions (Ca^{2+}) play numerous and fundamental roles in the inner ear. In section 1.3.1 and 1.3.2 of this chapter, we focus on the aspects of sound transduction that are influenced by Ca^{2+}, including mechanotransduction function and neurotransmitter release at the hair cell synapse. In the last part, we concentrate on Ca^{2+} signaling in the network of non-sensory cells in the developing cochlea.

1.3.1 Calcium signaling at the hair cell endolymphatic pole

In the cochlea, the relative motion between the sensory cells and their overlaying structure, the tectorial membrane, causes the deflection of the hair bundle and the opening of mechanotransduction channels, one of the few ion channels not yet conclusively identified [Peng et al., 2011]. Stereocilia in the hair bundle are arranged in rows of graded height [Lin et al., 2005] and a fine extracellular filament, termed the tip link, connects the top of each stereocilium to the side of its taller neighbor, parallel to the bundle's axis of mechanical sensitivity [Kachar et al., 2000]. Tip-links are mechanically in series with a yet unidentified elastic element, termed gating spring [Kachar et al., 2000, Gillespie et al., 2005], which pulls on transduction channels and whose stiffness may be Ca^{2+}-dependent [Cheung and Corey, 2006]. It is thought that the hair cell receptor potential is caused by deflection of the hair bundle towards the tallest stereocilia, which increases the tension in the tip link causing the opening of mechanotransduction channels located at its bottom end [Beurg et al., 2009]. Indeed, application of the Ca^{2+} chelator BAPTA to the hair bundle disrupts the tip links and abolishes mechanotransduction currents [Assad et al., 1991, Zhao et al., 1996, Furness et al., 2008]. Cadherin 23 and protocadherin 15, respectively comprising 27 and 11 cadherin repeats, with Ca^{2+} binding sites in the interrepeat regions, interact at their N termini forming the upper (cadherin 23) and lower (protocadherin 15) part of tip links [Kazmierczak et al., 2007]. Furthermore, Molecular Dynamics simulations of the first two repeats of cadherin 23 suggest that binding at interrepeat sites is essential to determine cadherin 23 stiffness and folding strength [Sotomayor et al., 2010]. A Ca^{2+} binding motif has also been identified at the N terminus of cadherin 23 [Elledge et al., 2010], which could play an important role in the formation of the tip link and might also account for the disruptive effects of BAPTA [Assad et al., 1991, Zhao et al., 1996]. Recent results in transgenic mice provide genetic evidence consistent with protocadherin 15 and cadherin 23 being part of the tip-link complex and necessary for normal mechanotransduction [Alagramam et al., 2011]. Further support to the tip-link model of transduction is derived from the evidence that mutations in genes encoding for cadherin 23 and protocadherin 15 have been associated with Usher syndrome type 1 and nonsyndromic hearing loss DFNB12 and DFNB23 [Bolz et al., 2001, Bork et al., 2001, Ahmed et al., 2003].

Not only is Ca^{2+} essential to preserve the structure of the tip-links, but it also contributes to the mechanotransduction current. Based on early experiments performed under mM levels of extracellular Ca^{2+} concentration ($[Ca^{2+}]_o$), it had been concluded that ∼10% of the total mechanotransduction current was carried by Ca^{2+} [Ricci et al., 1998]. However, as previously mentioned, $[Ca^{2+}]_o$ in endolymph is as low as a few tens of µM [Bosher and Warren, 1978, Corey and Hudspeth, 1983] and recent work indicates that the fraction of mechanotransduction current attributable to Ca^{2+} decrease in proportion to $[Ca^{2+}]_o$; at endolympatic levels of $[Ca^{2+}]_o$, it accounts for only the ∼0.2% of the total mechanotransduction current [Beurg et al., 2010b]. In a standard experimental protocol, adaptation is measured by the decrease in mechanotransduction current, which occurs during a sustained deflection of the hair bundle [Howard and Hudspeth, 1987]. Under these experimental conditions, adaptation shifts the relationship between the channel

open probability (P_0) and the bundle displacement (X) in the direction of the applied stimulus, canceling the effects due to sustained stimuli while maintaining the sensitivity to transient stimuli [Fettiplace and Ricci, 2003]. In this complex phenomenon, at least two phases, both Ca^{2+}-dependent, can be distinguished: (i) fast adaptation, which occurs when Ca^{2+} enters transduction channels, then closes them within a few milliseconds or less; (ii) slow adaptation, which occurs with a time constant that spans a wide range of 10-50 ms depending on the type of hair cells studied (reviewed in [Peng et al., 2011]).

Fast adaptation is thought to be caused by the direct binding of Ca^{2+} to an intracellular site of the mechanotransduction channel or a closely associated subunit which closes the channel itself [Cheung and Corey, 2006, Howard and Hudspeth, 1988, Crawford et al., 1991, Ricci et al., 2005, Wu et al., 1999]. Slow adaptation, which has been studied extensively in vestibular hair cells, has been linked to activity of molecular motors [Howard and Hudspeth, 1987], composed of unconventional myosin molecules [Holt et al., 2002, Kros et al., 2002, Grati and Kachar, 2011], which interact in a Ca^{2+}-dependent manner with actin filaments at the core of stereocilia [Gillespie and Muller, 2009]. The known stereocilia myosins that could affect adaptation in both inner hair cells and outer hair cells are myosin-Ic, VIIa, and IIIa [Hasson et al., 1995, Schneider et al., 2006, Dumont et al., 2002]. Another unconventional myosin, XVa, which is required for normal growth of hair cell stereocilia, has been implicated in fast adaptation based on a study of P1-P4 shaker 2 mice (that have no functional myosin-XVa) [Stepanyan and Frolenkov, 2009]. This study indicates that: (i) Ca^{2+} sensitivity of the mechanotransduction channels and the fast adaptation require a structural environment that is dependent on this unconventional myosin; (ii) this environment is disrupted in inner hair cells of this mutant strain, but not in outer hair cells. However, available data indicate that myosin-XVa is present at the tips of wild-type stereocilia in both inner hair cells and outer hair cells [Belyantseva et al., 2003, Rzadzinska et al., 2004]. Thus, to account for the different effects of myosin-XVa deficiency in outer hair cells and inner hair cells, it has been suggested that the loss of fast adaptation in inner hair cells of shaker 2 mice is associated with an unusual hair bundle architecture in these cells [Stepanyan and Frolenkov, 2009].

As for the mechanism of slow adaptation, in the classical scheme the motor complex is located in series with the transduction channel and its spring and is continuously trying to "climb up" the stereocilium, changing the position of the upper end of the tip link, thus increasing tension. Following a positive stimulus, the motor complex "slides down", decreasing tension in the tip link and closing the channel [Gillespie and Muller, 2009]. However, analysis of the time course and pattern of myosin-Ic expression in inner and outer hair cell stereocilia [Schneider et al., 2006, Waguespack et al., 2007] poses several challenges to the motor model of adaptation [Peng et al., 2011]. Furthermore, a motor complex located at the upper end of the tip link is hard to reconcile with the localization of the mechanotransduction channel, and thus of the site of Ca^{2+} entry, at the lower end of the tip link [Beurg et al., 2009]. In order to resolve this conundrum, it has been proposed that Ca^{2+} entering through a transduction channel might affect the adaptation motor hooked up to the next tip link lower down the same stereocilium (for an explicative scheme, see Fig.5 of Ref. [Gillespie and Muller, 2009]). This implies that the tallest rows

of stereocilia, which do not admit Ca^{2+} through mechanotransduction channels, are not likely to present Ca^{2+} -dependent adaptation.

It is probably worth mentioning also that Ca^{2+} can influence mechanotransduction via cyclic adenosine monophosphate (cAMP), which has been shown to affect the response-displacement curve of the transducer [Ricci and Fettiplace, 1997]. This signaling pathway may involve cAMP produc tion by Ca^{2+}-calmodulin activated type I adenyl cyclase [Drescher et al., 1997], cAMP-induced activation of protein kinase A and phosphorylation of the mechanotransduction channel or the myosin motor [Fettiplace and Ricci, 2003].

After entering the stereocilia through mechanotransduction channels, Ca^{2+} is rapidly bound by endogenous Ca^{2+} chelators, present at millimolar concentration [Hackney et al., 2005], which restrict the distance Ca^{2+} diffuses to a few tens of nm from the mouth of the channel [Ricci et al., 1998]. Also mitochondria, conspicuously concentrated in a band beneath the cuticular plate (the cytoskeletal anchor for the stereociliary bundle) [Spicer et al., 1999, Mammano et al., 1999b], can act as large-capacity Ca^{2+} store [Beurg et al., 2010b]. In outer hair cells, the mitochondrial barrier may be bypassed by ATP-induced release of Ca^{2+} from a system of endoplasmic reticulum membranes located beneath the cuticular plate known as Hensen's body [Mammano et al., 1999b].

Ca^{2+} is eventually exported back to endolymph by plasma membrane Ca^{2+}-ATPase (PMCA) pumps, which are highly expressed in the hair bundle of vestibular and cochlear outer hair cells and, to a lesser extent, inner hair cells [Dumont et al., 2001]. The stereociliary PMCA can be sufficiently active to elicit a substantial membrane current during transduction [Yamoah et al., 1998, Apicella et al., 1997]. The pump isoform of the stereocilia is the PMCA2, encoded by the ATP2b2 gene [Noben-Trauth et al., 1997, Kozel et al., 1998, Street et al., 1998, Takahashi and Kitamura, 1999]. The extrusion task is performed by the w/a splicing isoform of PMCA2 [Hill et al., 2006, Grati et al., 2006]. Ablation of the ATP2b2 gene causes deafness and balance disorders in mice [Kozel et al., 1998], further more, various PMCA2 mutations have been linked to hereditary hearing loss in mice and humans. Some of the mutations described so far led to the truncation of the molecule and to its eventual disappearance from the stereocilia of the hair cell [Kozel et al., 1998, Takahashi and Kitamura, 1999, McCullough and Tempel, 2004]. Three of the described mutations were instead point mutations that did not compromise the reading frame of the gene and were, thus, compatible with the expression of the full length PMCA2w/a variant of the pump; they all affected residues that are highly conserved in all PMCA isoforms across species and in other P-type pumps [Street et al., 1998, Tsai et al., 2006, Spiden et al., 2008]. Recently, the Tommy mouse mutation was identified as a new PMCA2 pump mutant with progressive deafness from an ENU mutagenesis screen [Bortolozzi et al., 2010]. These mice show profound hearing impairment from P18, with significant differences in hearing thresholds between wild type and heterozygotes. Furthermore, immunofluorescence studies of the organ of Corti in homozygous Tommy mice showed a progressive degeneration of hair cells after P40 from the base of the cochlea (where high frequencies are detected) to its apex (low frequency region).

Due to the crucial role of Ca^{2+} at the endolymphatic pole of the hair cell for the performance of the mechanotransduction channel, a diminished Ca^{2+} removal from the stere-

ocilia is expected to affect the mechanotransduction currents. Indeed, pharmacological blockade [Beurg et al., 2010b], as well as mutation or knock out of the PMCA2 pump [Ficarella et al., 2007] have been reported to shift the current-displacement ($I-X$) curve in the positive direction and to reduce its slope considerably. Moreover, the only cochlear PMCA2 exposed to endolymph is that of the stereocilia [Dumont et al., 2001, Wood et al., 2004]. Thus if less Ca^{2+} is exported from the stereocilia , its concentration in the endolymph is expected to fall [Wood et al., 2004]. This may provide a clue as to why, in some cases, mutations in the gene of the PMCA2 pump potentiated the deafness phenotype induced by coexisting mutation of cadherin 23 [Ficarella et al., 2007, Schultz et al., 2005, Noben-Trauth et al., 2003].

1.3.2 Calcium regulation of synaptic transmission

As previously mentioned , mature hair cells respond to hair bundle deflection with graded changes in their membrane potential, which ultimately result in neurotransmitter release from the cell synaptic pole (see [Glowatzki et al., 2008] for review). In contrast, before the onset of hearing, inner hair cells do not generate graded sound-driven receptor potentials but fire spontaneous Ca^{2+}-driven action potentials [Johnson et al., 2011b, Marcotti et al., 2003a, Marcotti et al., 2003b]. These are prevented in mature inner hair cells by the expression of the rapidly activating large conductance Ca^{2+}-activated K^+ current [Kros et al., 1998, Marcotti et al., 2004] and the negatively activating delayed rectifier $I_{K,n}$, carried by KCNQ4 channels [Marcotti et al., 2003a] (see [Marcotti, 2012] for a review). The inner hair cells synapses are already functional in the pre-hearing period [Beutner and Moser, 2001], and glutamate release triggered by action potentials may be important for the refinement of the synaptic connections in the auditory pathway [Appler and Goodrich, 2011].

The hair cell synaptic machinery is unique in its genre, because of the special tasks it is required to accomplish. This is especially evident for the afferent synapse of cochlear inner hair cells, which must encode a wide range of external sound stimuli with the sub-millisecond temporal precision required for sound localization and phase locking; moreover, the constant presence of acoustic stimulation requires the prolonged maintenance of synaptic transmission [Fuchs, 2005]. The ability to produce both rapid and sustained neurotransmitter release is thought to be conferred to the hair cell synapse by the presence of the synaptic ribbon, a specialized electron-dense proteinaceous structure anchored at the synapse's active zone, where synaptic vesicle exocytosis occurs [Nouvian et al., 2006]. This organelle, also found in retinal photoreceptor and bipolar cells (see [Matthews and Fuchs, 2010] for a review), tethers ∼100-400 glutamate-containing synaptic vesicles through thin filaments [Lenzi et al., 1999, Fuchs et al., 2003]. Some of these vesicles (around 16-30) are kept in direct contact with the plasma membrane [Lenzi and von Gersdorff, 2001, Khimich et al., 2005] and it has been suggested that the ribbon may be important for synchronous multi-vesicular release [Khimich et al., 2005, Glowatzki and Fuchs, 2002, Keen and Hudspeth, 2006, Graydon et al., 2011].

Vesicle exocytosis is triggered by the influx of Ca^{2+} through class-D L-type Ca^{2+} channels ($Ca_V1.3$) clustered at each active zone [Platzer et al., 2000, Spassova et al., 2001, Brandt

et al., 2003] (∼80 per active zone in mouse inner hair cells [Brandt et al., 2005]), where, they operate in close proximity with Ca^{2+}-activated K^+ channels (BK channels) [Kros et al., 1998]. In mammalian inner hair cells and outer hair cells, the majority of the total Ca^{2+} current (>90%) is carried by $Ca_V1.3$ channels [Platzer et al., 2000, Michna et al., 2003]. It has been proposed that harmonin, a scaffolding protein that has been also implicated in mechanotrasduction at the level of the hair bundle [Boeda et al., 2002, Grillet et al., 2009], tags $Ca_V1.3$ channels for ubiquitination and may thus constrain the number of presynaptic $Ca_V1.3$ channels in inner hair cells [Gregory et al., 2011]. The biophysical properties of these channels make them particularly suitable for the demands of synaptic transmission in these cells. First, $Ca_V1.3$ channels activate at relatively hyperpolarized membrane potential, as negative as −70 mV in immature inner hair cells [Platzer et al., 2000, Zampini et al., 2010], indicating that they would be capable of generating both the spontaneous action potentials in immature inner hair cells and the fast synaptic response of mature hair cells [Marcotti et al., 2003b]. Second, they activate very rapidly (∼300-400 µs in gerbil basal inner hair cells) and show very little inactivation in mature hair cells [Johnson and Marcotti, 2008, Grant and Fuchs, 2008], a characteristic that is required for sustained release. The exocytosis of individual fusion-competent vesicles is mediated by the stochastic gating of one or few $Ca_V1.3$ channels located within a few nanometer from the release site and such "nanodomain control" of neurotransmitter has been proposed to permit temporally precise synaptic coding even for weak stimuli [Brandt et al., 2005].

Because $Ca_V1.3$ channels show strong Ca^{2+}-dependent inactivation when studied in heterologous expression systems [Koschak et al., 2001], it has been proposed that calmodulin-like Ca^{2+} binding protein (CaBP), which are expressed within the organ of Corti, may moderate the inactivation in cochlear inner hair cells by competing with calmodulin binding to the channel's C-terminus [Cui et al., 2007, Yang et al., 2006]. Recent work has suggested that Rab3-interacting molecule-2 (RIM2) proteins may represent another possible molecular mechanism capable of inhibiting Ca^{2+}- and voltage-dependent inactivation of $Ca_V1.3$ channels in inner hair cells [Gebhart et al., 2010].

Similarly to stereociliary Ca^{2+} , presynaptic Ca^{2+} domains are presumably spatiotemporally restricted by the presence of mobile, proteinaceous Ca^{2+} buffers calretinin, calbindin and parvalbumin, which have been found in a variety of cochlear and vestibular hair cells with concentration in the mM range [Hackney et al., 2005, Hackney et al., 2003]. However, discrepancies regarding both the amount and kinetic properties of such buffers in different hair cells suggest that their exact role and scope of function need to be analyzed further [Bortolozzi et al., 2008]. It has also been suggested that the restriction of the available presynaptic space due to the presence of the ribbon and its associated vesicles defines a small cytoplasmic volume where Ca^{2+} buffers are saturated, thus permitting fast and large Ca^{2+} rises near release sites beneath the synaptic ribbon [Graydon et al., 2011].

The stimulus-secretion coupling between the inward Ca^{2+} current and transmitter release has been investigated by measuring the increase in the hair cell membrane capacitance (ΔC_m) following depolarization-triggered Ca^{2+} entry [Brandt et al., 2005, Beutner

et al., 2001, Johnson et al., 2005, Johnson et al., 2008, Schnee et al., 2005]. In these studies, at least two kinetic components of exocytosis are commonly distinguished: a fast initial component, which saturates within a few milliseconds, and one or more slower components, triggered by prolonged (tens of ms to s in duration) depolarizing steps; for a summary of different studies on size and kinetics of synaptic release components in hair cells see [Nouvian et al., 2006]. The fast component is generally thought to represent the release of a ready releasable pool (RRP) of vesicles which might co-localize with Ca^{2+} channels [Moser and Beutner, 2000, Spassova et al., 2004, Rutherford and Roberts, 2006]. However, data establishing a direct link between vesicle location and release pools are limited [Nouvian et al., 2006].

Transmitter release evoked by membrane depolarization over the physiological voltage range (between the resting potential and $\sim -20mV$ [Glowatzki et al., 2008]) shows a linear dependence on Ca^{2+} influx , at least in high frequency inner hair cells [Brandt et al., 2005, Johnson et al., 2005, Schnee et al., 2005, Goutman and Glowatzki, 2007]. This linear relationship, which extends to the postsynaptic current [Keen and Hudspeth, 2006, Goutman and Glowatzki, 2007], is believed to allow the synapse to respond efficiently to both small and large stimuli, thus broadening the hair cell's dynamic range. Transmitter release shows a higher order (3^{rd}-5^{th} power) Ca^{2+}-dependance when the hair cell is depolarized to positive holding potentials [Goutman and Glowatzki, 2007] or when exocytosis is triggered by Ca^{2+} uncaging (7 µM to 110 µM) [Beutner et al., 2001]. Recently, using real-time capacitance measurements to identify saturable pools of vesicles, a superlinear release component requiring recruitment of vesicles to release sites has been identified, leading to the suggestion that Ca^{2+}-dependent vesicle trafficking is responsible for this movement, which is required for hair cell synapses to maintain high rates of sustained vesicle fusion [Schnee et al., 2011].

The identification of the molecular composition of the synaptic machinery of the hair cell remains a major challenge. The hair cell synapse lacks the most common protein involved in exocytosis, for example complexins, synapsins and synaptophysins [Safieddine and Wenthold, 1999, Uthaiah and Hudspeth, 2010, Strenzke et al., 2009]; moreover, even though neuronal SNARE proteins are expressed in inner hair cells, they may not be required for vesicle fusion at the inner hair cell ribbon synapse [Nouvian et al., 2011]. A major gap in our understanding of the components of the synaptic ribbon relates to the identification of the Ca^{2+} sensor. Synaptotagmins (Syt) I-II are the conventional Ca^{2+}-sensing proteins at neuronal synapses [Sudhof, 2004], but their role at the hair cell ribbon synapse is debated. Though earlier studies suggested that Syt I-II were not present in mature inner hair cells [Safieddine and Wenthold, 1999], more recent work has shown that they are transiently expressed in the cochlea [Beurg et al., 2010a, Johnson et al., 2010, Reisinger et al., 2011]. However these studies came to different conclusions about Syt I-II importance for inner hair cell synaptic transmission, since some of them suggest their involvement (Syt1: [Beurg et al., 2010a, Johnson et al., 2010], Syt II: [Johnson et al., 2010]) while others exclude it (Syt1: [Reisinger et al., 2011]. Syt II: [Beurg et al., 2010a, Reisinger et al., 2011]). The observation that otoferlin deficient mice ($Otof^{-/-}$) are profoundly deaf [Yasunaga et al., 1999], and show impaired synaptic development and

lack of exocytosis [Roux et al., 2006] prompted the proposal that otoferlin is the major Ca^{2+} sensor of synaptic vesicle fusion in cochlear hair cells [Roux et al., 2006,Beurg et al., 2008]. However, even though recent evidence has shown that otoferlin may be involved in synaptic vesicle replenishment [Pangrsic et al., 2010], its role as the Ca^{2+} sensor for exocytosis remains indetermined. Indeed, otoferlin is not found in inner hair cells of a hypothyroid rat model, even though those inner hair cells exhibited Ca^{2+}-dependent exocytois [Johnson et al., 2010,Brandt et al., 2007]. Moreover, another study showed that Ca^{2+}-evoked exocytosis in the first postnatal days (P0-P4) is both otoferlin- and Syt-independent [Beurg et al., 2010a]. Finally, the transition from a nonlinear to a linear order of exocytotic Ca^{2+}-dependance observed before and after the onset of hearing doesn't correlate with the qualitatively similar distribution of otoferlin found in immature and mature inner hair cells [Johnson et al., 2008, Johnson et al., 2009], and seems to depend on another molecular factor, which has been recentely identified as Synaptotagmin IV, an unconventional synaptotagmin [Johnson et al., 2010].

Besides Ca^{2+} influx through voltage-gated Ca^{2+} channels of the basolateral plasma membrane, two other mechanisms, both implicated in the efferent control of hair cell function [Bruce et al., 2000, Bulankina and Moser, 2012], may promote an increase of intracellular free Ca^{2+} concentration ($[Ca^{2+}]_c$) at the basal pole of the hair cell.

The first mechanism is Ca^{2+} entry through $\alpha 9\alpha 10$ nicotinic acetylcholine receptors (nAChR) [Vetter et al., 2007, Plazas et al., 2005], which activates, via calmodulin, a hyperpolarizing small conductance potassium current (SK, for review, see [Adelman et al., 2012]). The hyperpolarizing SK current (i) is required for sustaining the action potential activity and modulating action potential frequency when activated by ACh in immature inner hair cells [Marcotti et al., 2004,Johnson et al., 2007,Glowatzki and Fuchs, 2000] and (ii) mediates fast Ca^{2+} -dependent decrease of axial stiffness in outer hair cells [Oliver et al., 2000, Frolenkov et al., 2000].

The second (interrelated) mechanism is calcium-induced calcium release (CICR), an autocatalytic mechanism whereby $[Ca^{2+}]_c$ elevation induces Ca^{2+} release from internal stores through channels such as inositol-1, 4,5-trisphosphate (IP_3) receptors (IP_3Rs) or ryanodine receptors (RyRs) [Berridge et al., 2003]. CICR has been investigated in mammalian inner hair cells [Kennedy and Meech, 2002], outer hair cells [Frolenkov et al., 2000, Sridhar et al., 1997, Dallos et al., 1997, Evans et al., 2000, Frolenkov et al., 2003, Frolenkov, 2006] as well as in vestibular hair cells [Lelli et al., 2003]. In particular, in inner hair cells, Ca^{2+} release from intracellular store has been found to modulate the fast outward Ca^{2+} activated K^+ current (BK) [Marcotti et al., 2004,Beurg et al., 2005], thus suggesting that RyRs and BK channels are functionally coupled and act to suppress fast neurotransmission [Beurg et al., 2005].

1.3.3 Calcium signaling in cochlear non-sensory cells

As mentioned above, cochlear non-sensory cells form vast syncytia coupled by gap junction channels that, in the mammalian cochlea, are formed primarily by connexin26 and connexin30 protein subunits [Lautermann et al., 1999, Lautermann et al., 1998], respectively encoded by DNFB1 genes GJB2 and GJB6 (reviewed in refs. [Nickel and

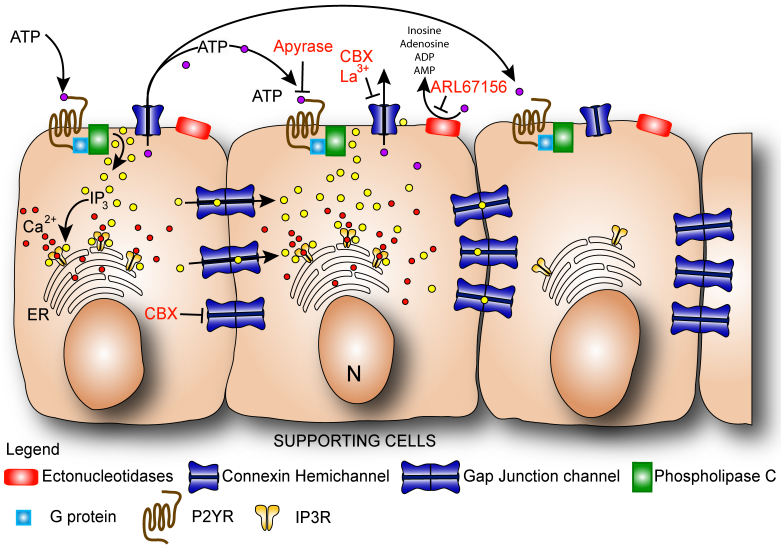

Figure 1.7: Scheme of the molecular mechanisms underlying Ca^{2+} signaling in non-sensory cells of the cochlea. The drawing shows ATP release through connexin hemichannels. P_2Y receptors (P_2YR), a family of G protein-coupled purinoceptors, are stimulated by ATP, ADP, UTP, UDP and UDP-glucose; IP_3R (inositol trisphosphate receptor) is a membrane glycoprotein complex; IP_3Rs are Ca^{2+} channels in the endoplasmic reticulum (ER) that are activated by inositol trisphosphate (IP_3); FFA (flufenamic acid) and NFA (niflumic acid) are non-specific inhibitors of connexin hemichannels. CBX (carbenoxolone) blocks both hemichannels and gap junction channels. ATP degradation by ectonucleotidases terminates signaling. ARL67156, 6-N,N-Diethyl-D-β,γ-dibromomethyleneA is a selective inhibitor of ectoATPases. Apyrase is an enzyme that catalyzes the hydrolysis of ATP to yield AMP and inorganic phosphate. La^{3+} is a blocker of connexin hemichannels that does not affect gap junction channels when applied extracellularly to cochlear cultures. (Figure from Ref. [Majumder et al., 2010])

Forge, 2008, Martinez et al., 2009]). The fact that DFNB1 is the most common form of inherited deafness in Caucasian populations highlights the importance of connexins for hearing (reviewed in ref. [Hilgert et al., 2009]).

While the exact function of connexins expressed by non–sensory cells of the inner ear remains unclear, it is important to mention that they also form unpaired connexons, i.e. non−junctional connexin hemichannels [Bennett et al., 2003, Goodenough and Paul, 2003, Evans et al., 2006]. Experiments performed with a combination of genetic interference in four different mouse lines and ATP biosensors [Huang et al., 2007] apposed to cochlear non−sensory cells indicate that connexin26 and connexin30 protein subunits form functional hemichannels, which can be detected at the endolymphatic surface of the sensory epithelium with CELAb antibodies [Clair et al., 2008], and release ATP into endolymph under physiological conditions (Figure 1.7) [Anselmi et al., 2008, Majumder et al., 2010]. ATP release had been previously proposed on the ground of experiments in which mechanical stimulation was applied by gently pipetting (once per 3–4 s with a 20 µl pipette) a solution containing glass beads (with a diameter of 30-50 µm) over a cochlear explant for a 15-min period [Zhao et al., 2005].

The binding of extracellular ATP to G–protein coupled P_2Y_2 and P_2Y_4 receptors, also expressed on the endolymphatic surface of the developing sensory epithelium, activates phospholipase–C dependent generation of IP_3 [Beltramello et al., 2005, Gale et al., 2004, Piazza et al., 2007]. While gap junction channels allow IP_3 diffusion through these coupled cells, IP_3 binding to its receptors (IP_3R) promotes Ca^{2+} release from the endoplasmic reticulum raising the cytosolic free Ca^{2+} concentration ($[Ca^{2+}]_c$, Figure 1.7). The probability of connexin hemichannel opening is a bell–shaped function of the $[Ca^{2+}]_c$, peaking at ∼500 nM [De Vuyst et al., 2006]. This is a key feature that enables the propagation of Ca^{2+} signals as regenerative and coordinated intercellular Ca^{2+} waves, with peak amplitude of ∼500 nM, sustained by ATP–induced ATP–release [Mammano et al., 2007, Beltramello et al., 2005, Anselmi et al., 2008, Majumder et al., 2010, Gale et al., 2004, Piazza et al., 2007]. Mitochondria function as spatial Ca^{2+} buffers and play a significant role in regulating the spatio–temporal properties of these intercellular Ca^{2+} waves [Mann et al., 2009].

This was demonstrated by blocking mitochondrial Ca^{2+} uptake by dissipating the mitochondrial membrane potential using the protonophore carbonyl cyanide m–chlorophenylhydrazone (CCCP) and oligomycin, an inhibitor of oxidative phosphorylation, or using Ru360, an inhibitor of the mitochondrial Ca^{2+} uniporter, which enhanced the peak amplitude and duration of ATP–induced transients. The numerous roles played by extracellular ATP in the adult cochlea are reviewed in ref. [Housley et al., 2009]; the rest of this chapter focuses on some critical signalling events that occur during maturation of cochlear tissue.

Rhythms are ubiquitous at all levels of biological organization. At the cellular level, they involve biochemical oscillations that modulate the concentration of key metabolic substrates and second messengers. Among these, rhythmic variations in the $[Ca^{2+}]_c$ have been found in a variety of cells and shown to arise spontaneously or after stimulation by hormones or neurotrasmitters.

In non–sensory cells of the lesser epithelial ridge, ATP–dependent $[Ca^{2+}]_c$ oscillations occur (i) as consequence of intercellular Ca^{2+} wave propagation, (ii) sustained ATP delivery in the submicromolar range or (iii) during pharmacological inhibition of ectonucleotidases, a manipulation which highlights the tonic release of ATP from these cells [Anselmi et al., 2008] and their sensitivity to ATP degradation by ectonucleotidases [Vlajkovic et al., 2002].

In rat cochlear explants [Tritsch et al., 2007, Tritsch and Bergles, 2010], as well as in mouse organotypic cochlear cultures [Schutz et al., 2010], $[Ca^{2+}]_c$ transients due to release of ATP in rhythmic bursts have been reported also for a class of non–sensory cells of the greater epithelial ridge (first described by Kölliker) which transiently populate the sensory epithelium from spiral limbus to inner hair cell [Hinojosa, 1977, Kamiya et al., 2001]. These periodic Ca^{2+} signals can be blocked by apyrase, as shown for the propagation of intercellular Ca^{2+} waves in the lesser epithelial ridge. Furthermore, the frequency of spontaneous $[Ca^{2+}]_c$ transients is significantly decreased by purinergic receptor antagonists PPADS (50 µM) and suramin (150 µM), the gap junction channel inhibitor carbenoxolone (100 µM) as well as flufenamic acid (50 µM), a bona–fide inhibitor of connexin hemichannels.

Both the propagation range of intercellular Ca^{2+} waves in the lesser epithelial ridge and the frequency of spontaneous $[Ca^{2+}]_c$ transient in the greater epithelial ridge increase when the extracellular free Ca^{2+} concentration ($[Ca^{2+}]_o$) is decreased [Anselmi et al., 2008, Tritsch et al., 2007, Tritsch and Bergles, 2010], and this manipulation is known to increase the open probability of connexin hemichannels [Muller et al., 2002, Gomez-Hernandez et al., 2003, Saez et al., 2005, Gonzalez et al., 2007]. Finally, focal UV photolysis of a caged intracellular IP_3 precursor in the greater epithelial ridge evokes Ca^{2+} transients similar to those that arise spontaneously in this region [Majumder et al., 2010]. Thus it seems reasonable to hypothesize that release of ATP through connexin hemichannels activates similar IP_3 receptor–dependent signal transduction cascades in non–sensory cells of the lesser and the greater epithelial ridge.

These findings are particularly interesting if viewed from the perspective that connexin dysfunction may ensue in a deafness phenotype through a bidirectional link to impaired ATP–dependent Ca^{2+} signaling in the develop ing cochlea. This tenet is exemplified by a study of hearing loss based on the substitution of an evolutionarily conserved threonine by a methionine residue at position 5 near the N–terminus of connexin30 (connexin30 T5M) [Grifa et al., 1999]. In connexin30(T5M/T5M) knock in mice, obtained by homologous recombination in mouse embryonic stem cells, expression of the mutated connexin30 T5M protein is under the control of the endogenous connexin30 promoter [Schutz et al., 2010]. When probed by auditory brainstem record ings, connexin30(T5M/T5M) mice exhibit a mild, but significant increase in their hearing thresholds of about 15 dB at all frequencies. Western blot analysis of adult inner ear tissue shows significantly down–regulated expression levels of connexin26 and connexin30. In the developing cochlea, electrical coupling, probed by dual patch–clamp recordings, is normal; however, transfer of the fluorescent tracer calcein between cochlear non–sensory cells is reduced, as is the intercellular Ca^{2+} signaling due to spontaneous

ATP release from connexin hemichannels [Schutz et al., 2010]. Previous studies had noted that ATP–dependent Ca^{2+} oscillations in non–sensory cells of the cochlear feed–back on connexin expression and participate in the coordinated regulation of connexin26 and connexin30 through NF–kB [Ortolano and Pasquale, 2008, Crispino et al., 2011] (nuclear factor kappa–light–chain–enhancer of activated B cells). Of notice, these articles also show that gene delivery with recombinant *bovine adeno associated virus* (BAAV) vectors restores connexin expression and rescue intercellular coupling and Ca^{2+} signaling in cochlear organotypic cultures from mice with defective expression of connexin26 and connexin30 [Ortolano and Pasquale, 2008, Crispino et al., 2011]. A widely held hypothesis is that information is encoded mainly by the frequency of $[Ca^{2+}]_c$ oscilla tions [Dolmetsch et al., 1998, Li et al., 1998], however, a possible role of amplitudes and duration in signal transduction has been discussed [Dolmetsch et al., 1997, Prank et al., 2000]. It has also been argued that amplitude modulation and frequency modulation differentially regulate distinct targets [Berridge, 1997]. Note that NF–kB is just one of the several Ca^{2+}-dependent transcription factors used by non–excitable cells [Mellstrom et al., 2008].

2 Aims of this work

In this thesis work we investigated the biophysical properties of intercellular coupling in non-sensory cell networks of the developing organ of Corti, and the functional consequences of connexin mutations implicated in genetic deafness. Part of this work was also dedicated to the design and construction of a confocal fluorescence imaging apparatus and to the development of image processing software used for data analysis. We combined large scale optical recordings, single cell electrophysiology and computer simulations with the specific aim to

1. quantify the degree of electrical intercellular coupling provided by connexin26 and connexin30 in the developing mouse cochlea using a novel technique the development of which was integral part of this thesis work;

2. quantify the reduction in the degree of intercellular coupling in two different transgenic mice (connexin30($-/-$) and connexin30(T5M/T5M));

3. characterize ATP- and IP_3- dependent intracellular Ca^{2+} signaling in cochlear non-sensory cells and its relationship with connexin expression and function ;

4. formulate a minimal mathematical model of intracellular Ca^{2+} oscillations and intercellular Ca^{2+} waves in strict and quantitative adherence to experimental data;

5. investigate the relationship between spontaneous Ca^{2+} transients of cochlear non-sensory cells and the spontaneous electrical activity of immature cochlear inner hair cells;

3 General methods

3.1 Animal handling

Animal handling was approved by the Ethical Committee of Padua University (Comitato Etico di Ateneo per la Sperimentazione Animale, C.E.A.S.A.) project n. 54/2009, protocol n. 51731.

3.2 Reagents and drugs

Vf2.1.Cl [Miller et al., 2012] was provided by Roger Y. Tsien (University of California, San Diego). Carbenoxolone (CBX), pluronic F–127, Hanks' balanced salt solutions (HBSS) and the salts used to prepare solutions were purchased from Sigma–Aldrich. Calcium dyes Fluo-4 AM and Fura-2 AM, lipofectamine, Dulbecco's modified Eagle's medium (DMEM/F12), amino acids, vitamins and fetal bovine serum (FBS) were purchased from Life Technologies. Cell Tak was purchased from Becton Dickinson.

3.3 Cochlear organotypic cultures

Cochleae were dissected from P5 mouse pups, where the day of birth is P0, in ice−cold Hepes buffered (10 mM, pH 7.2) HBSS, placed onto glass coverslips coated with 185 µg/ml of Cell Tak and incu- bated overnight at 37°C in DMEM/F12 supplemented with FBS 5%.

3.4 HeLa cells

A clone of HeLa cells essentially devoid of connexins was provided by Klaus Willecke (University of Bonn, Germany) and cultured according to standard procedures. Twenty four hours after plating, a lipofectamine transfection system was used to transiently transfect these communication–incompetent HeLa cells with hCx26–CFP, a previously described human connexin26 construct tagged with the cyan fluorescent protein (CFP) at its carboxyl terminal end [Beltramello et al., 2005].

3.5 Electrophysiology from cochlear non-sensory cells and HeLa cells

All experiments were performed at room temperature (22–25°C). Cochlear or HeLa cell cultures were transferred to the stage of an upright wide–field fluorescence microscope (BX51, Olympus) and continually superfused with EXM, an extracellular medium containing (in mM): NaCl 138, KCl 5, $CaCl_2$ 2, NaH_2PO_4 0.3, KH_2PO_4 0.4, Hepes−NaOH 10, d−glucose 6 (pH 7.2, 300 mOsm). Glass capillaries for patch clamp recordings were formed on a vertical puller (PP–83, Narishige, Japan) from 1.5−mm outer diameter borosilicate glass (G85150T–4, Warner Instruments) and filled with an intracellular solution containing (in mM): KCl 134, NaCl 4, $MgCl_2$ 1, HEPES 20, EGTA 10 (adjusted to pH 7.3 with KOH, 290 mOsm) and filtered through 0.22 µm pores (Millipore). Pipette resistances were 3–4 MΩ when immersed in the EXM bath. For whole−cell patch clamp recordings performed on pairs of cochlear non-sensory cells, cell 1 was maintained under voltage clamp conditions with a patch clamp amplifier (Model 2400, AM Systems) while cell 2 was kept under current clamp conditions with a second amplifier (EPC−7, HeKa). Current and voltage were filtered at 3 kHz by an 8 pole Bessel filter and sampled at 20 kHz using a standard laboratory interface (Digidata 1440A, Molecular Devices) controlled by the PClamp 10 software (Molecular Devices).

3.6 Voltage imaging and immunofluorescence

To visualize hCx26–CFP, transfected HeLa cells were illuminated by light from a 385 nm LED (M385L2, Thorlabs) passing through a D390/70X filter (Chroma) and directed onto the sample through a 440 dclp dichromatic mirror (Chroma) while CFP emission was selected by an ET480/40M filter (Chroma). For voltage imaging, cochlear or HeLa cell cultures were incubated for 15 min at 37°C in EXM supplemented with Vf2.1.Cl (200 nM) and pluronic F–127 (0.1% w/v), thereafter cultures were continually superfused with EXM.

Vf2.1.Cl fluorescence was excited by light from a 470 nm LED (M470L2, Thorlabs) passing through a BP460–480 filter (Olympus) and directed onto the sample through a 515 dcxr dichromatic mirror (Chroma) while Vf2.1.Cl fluorescence emission was selected by an ET535/30M filter (Chroma). All fluorescence images were formed by a 60× water immersion objective (NA 1.0, Fluor, Nikon) and projected on a scientific–grade CCD camera (SensiCam; PCO AG) controlled by software developed in the laboratory. Image sequences of Vf2.1.Cl fluorescence were acquired continuously at 10 frames per second with 100 ms exposure time. To synchronize image acquisition and electrical recordings, we sampled the 5 V pulse (FVAL) that signals active exposure of the CCD camera [Mammano et al., 1999a]. Vf2.1.Cl signals were measured as relative changes of fluorescence emission intensity ($\Delta F/F_0$), where F_0 is prestimulus fluorescence, F is fluorescence at time t and $\Delta F = F - F_0$. Miller et al. reported that Vf2.1.Cl and other PeT–based voltage indicators have a slower rate of bleachingand are less toxic than the FRET–based dyes [Miller et al., 2012]. We did not make a direct comparison between these two classes

of indicators. However, in our hands patch clamp recordings from cochlear non–sensory cells in Vf2.1.Cl loaded cultures were stable for tens of minutes during continuous illumination with the LED used to excite dye's fluorescence. In addition, we did not notice any visible sign of cellular degeneration.

3.7 Ratiometric calcium imaging

Cochlear cultures were incubated for 40 min at 37° in DMEM, supplemented with fura–2 AM (16 µM). The incubation medium contained also pluronic F–127 (0.1%, w/v), and sulphinpyrazone (250 µM) to prevent dye sequestration and secretion [Di Virgilio, 1989]. Cultures were then transferred on the stage of an upright microscope (BX51, Olympus) and perfused in EXM for 20 min at 2 ml/min to allow for de−esterification. For recording, EXM was substituted by ECM, a medium obtained by replacing 2 mM Ca^{2+} in EXM with an endolymph-like concentration of Ca^{2+} (20 µM). Fura–2 fluorescence was excited using alternatively two light emitting diodes (LEDs, center wavelengths 365 nm and a 385 nm, M365L and M385L, Thorlabs) passing through a FF01-360/12-2 and FF01-387-11 filter respectively (Semrock, Rochester, NY, USA) and directed onto the sample through a dichromatic mirror (T400LP, Chroma, Rockingham, VT). Fluorescence emission was selected by a BA495-540HQ filter (Olympus, Tokyo, Japan) to form fluorescence images on a scientific–grade CCD camera using a 60× water immersion objective (NA 1.0, Fluor, Nikon).

Image sequences were acquired using software developed in the laboratory, stored on disk and processed off–line using the Matlab 7.0 software package (The MathWorks, Inc., Natick, MA, USA). Signals were measured as dye emission ratio changes, $\Delta R = R(t) - R(0)$, where t is time and $R(t)$ is emission intensity excited at 365 nm divided by the intensity excited at 385 nm, and $R(0)$ indicates pre−stimulus ratio.

To directly compare fluorescence measurements to Ca^{2+} concentrations computed with computer simulations, we converted fluorescence intensity ratios R to cytosolic Ca^{2+} concentration values ($[Ca^{2+}]_c$) by the following equation [Grynkiewicz et al., 1985]

$$[Ca^{2+}]_c = K_D \cdot \frac{R - R_{min}}{R_{max-R_{min}}} \cdot \frac{F_{min}}{F_{max}} \tag{3.1}$$

where

- $K_D = 287.3$ nM is the Fura-2 dissociation constant at 25°C [Larsson et al., 1999]
- R_{min} and R_{max} are ratio values in Ca^{2+} free conditions and in saturating Ca^{2+} conditions respectively
- F_{min}/F_{max} is the ratio of the fluorescence intensity after excitation at 385 nm in free and saturating Ca^{2+} conditions respectively.

R_{max} and F_{max} were measured by perfusing cochlear cultures with an extracellular solution containing 10 µM ionomycin and 5 mM Ca^{2+} for 2 minutes. R_{min} and F_{min} were

measured after perfusion with a solution containing 100 µM EGTA and 10 µM ionomycin for 30 minutes. The overall $[Ca^{2+}]_c$ of the cell was computed by averaging R values on a region of interest centered on it.

For ATP stimulation experiments, ATP dissolved in ECM was applied by pressure using glass micro-capillaries (puff pipettes) that were pulled to a tip of 2−10 µm on a vertical puller, similarly to patch clamp electrodes (PP80, Narishige) and placed near the target cell. Pressure was applied at the back of the pipette by delivering a transistor-transistor logic (TTL) pulse of carefully controlled duration to a Pneumatic PicoPump (PV800, World Precision Instruments) under software control. All cells tested responded to ATP, whereas no response was detected when ATP (or other P_2YR agonists) was omitted from the solution used to fill the puff pipette, indicating that accidental mechanical activation of the cells was negligible.

3.8 Statistical analysis

Means are quoted ± standard error of the mean (s.e.m.) and p–values are indicated by letter P. Statistical comparisons were made using the Mann–Whitney U test [Mann and Whitney, 1947] and $p < 0.05$ was selected as the criterion for statistical significance.

3.9 Photostimulation with caged IP3

Cochlear cultures were incubated for 30 min at 37° in DMEM supplemented with the ca dye fluo–4 AM (16 µM), caged IP_3 AM (5 µM), pluronic F–127 (0.1%, w/v), and sulphinpyrazone (250 µM) and thereafter perfused in EXM for 10 min at 2 ml/min to allow for de−esterification. Fluorescence emission was selected by a ET535/30M filter (Chroma, Rockingham, VT), centred around a 535 nm wavelength, to form fluorescence images on a scientific– grade CCD camera (SensiCam; PCO AG) using a 20× water immersion objective (NA 0.95, LumPlanFl, Olympus) connected to a microscope (BX51, Olympus) and illuminated by a collimated 470 nm light emitting diode (M470L2, Thorlabs) directed onto the sample through a dichromatic mirror (505 dcxr, Chroma, Rockingham, VT, USA). For focal photostimulation with caged IP_3, the output of a TTL−controlled semiconductor lased module (20 mW, 379 nm, part number FBB–375–020– FS–FS–1–1, RGBLase LLC, CA, USA) was injected into a UV permissive fibre optic cable (multimode step index 0.22 N.A., 105 µm core, part number AFS105/125YCUSTOM, Thorlabs GmbH, Dachau, Germany). Fibre output was projected onto the specimen plane by an aspheric condenser lens (20 mm effective focal length, part number ACL2520, Thorlabs) and the re−collimated beam was directed onto a dichromatic mirror (400 dclp, Chroma) placed at 45° just above the objective lens of the microscope. By carefully adjusting the position of the fiber in front of the aspheric lens we projected a sharp image of the illuminated fiber core (spot) onto the specimen focal plane selected by the (infinity corrected) objective lens. Under these conditions, the fiber optic diameter determined accurately the laser irradiated area, which encompassed one to few cells. Baseline (pre–stimulus) fluorescence emission (F_0) was recorded for 2 s, thereafter a UV laser pulse of 170 ms was

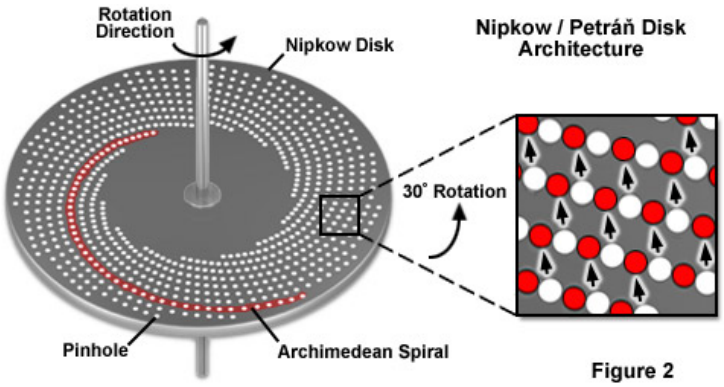

Figure 3.1: Schematic drawing of a Nipkow disk used for confocal microscopy.[From `http://zeiss-campus.magnet.fsu.edu/articles/spinningdisk/introduction.html`]

applied to release IP_3 and fluorescence emission was monitored for up to 60 sec. Signals were measured as relative changes of fluorescence emission intensity ($\Delta F/F_0$), where F is fluorescence at post–stimulus time t and $\Delta F = F - F_0$.

3.10 Microscope design

Spontaneous Ca^{2+} signals in cochlear non-sensory cells were recorded using a custom made spinning disk confocal microscope, whose design and development was part of the work performed during this thesis work.

Confocal microscopy is an optical technique in which the sample is illuminated point-by-point with a finely focused spot. Point wise illumination improves contrast in the lateral direction. For ordinary single-photon confocal microscopy, spatial filtering through a pinhole located in a plane conjugated with the objective focal plane improves contrast further, reduces axial blurring and enables optical-sectioning. This is particularly important in thick samples, where, compared to wide field microscopy, confocal microscopy shows a dramatic improvement in axial resolution thanks to the ability of this technique to reject the out of focus background [Pawley, 2006]. A spinning-disk confocal microscope, tipically uses a rotating Nipkow disk with thousands of pinholes arranged in an Archimedes spiral (Figure 3.1). The disk lies in a plane that is optically conjugated with that of the specimen (object plane). Illumination light passes through the pinholes whose images are projected onto the object plane where they trace concentric arcs across the sample as the disk revolves; fluorescence light emitted by the specimen returns along the same path through the objective lens and the pinholes, and is projected through a relay lens onto the detector (tipically a CCD or a sCMOS 2D sensor) which also sits in a plane conjugated with the object plane. The whole field of view is scanned in this way during the time interval required to form a (confocal) image onto the detector. The spinning disk confocal microscope parallelizes the illumination and detection processes and therefore is intrinsically faster and less prone to photobleaching than the single point

Figure 3.2: Olympus DSU confocal slit disk.

laser scanning microscope as light from the excitation source is distributed over multiple foci rather than a single one.

For cost reasons, we opted for a cheaper version based on the Olympus striped disk in which pinholes are replaced by two orthogonal Ronchi ruling patterns (Figure 3.2). The microscope, whose optical scheme is shown in Figure 3.3 consisted of three parts:

1 - Fluorescence illumination system. fluorescence excitation was produced by light emitted from a custom built illumination system comprising an array of four high power LEDs (center wavelengths: 365 nm, 385 nm, 470 nm, 490 nm). Light from each LED was passed through a narrow band interference filter; the LEDs were activated in sync with the acquisition camera by a programmable microcontroller (Arduino Mega 2560, Smart Projects, Italy) connected to a computer.

2 - Spinning disk After reflection off a dichromatic mirror (515 dcxr, Chroma), excita-

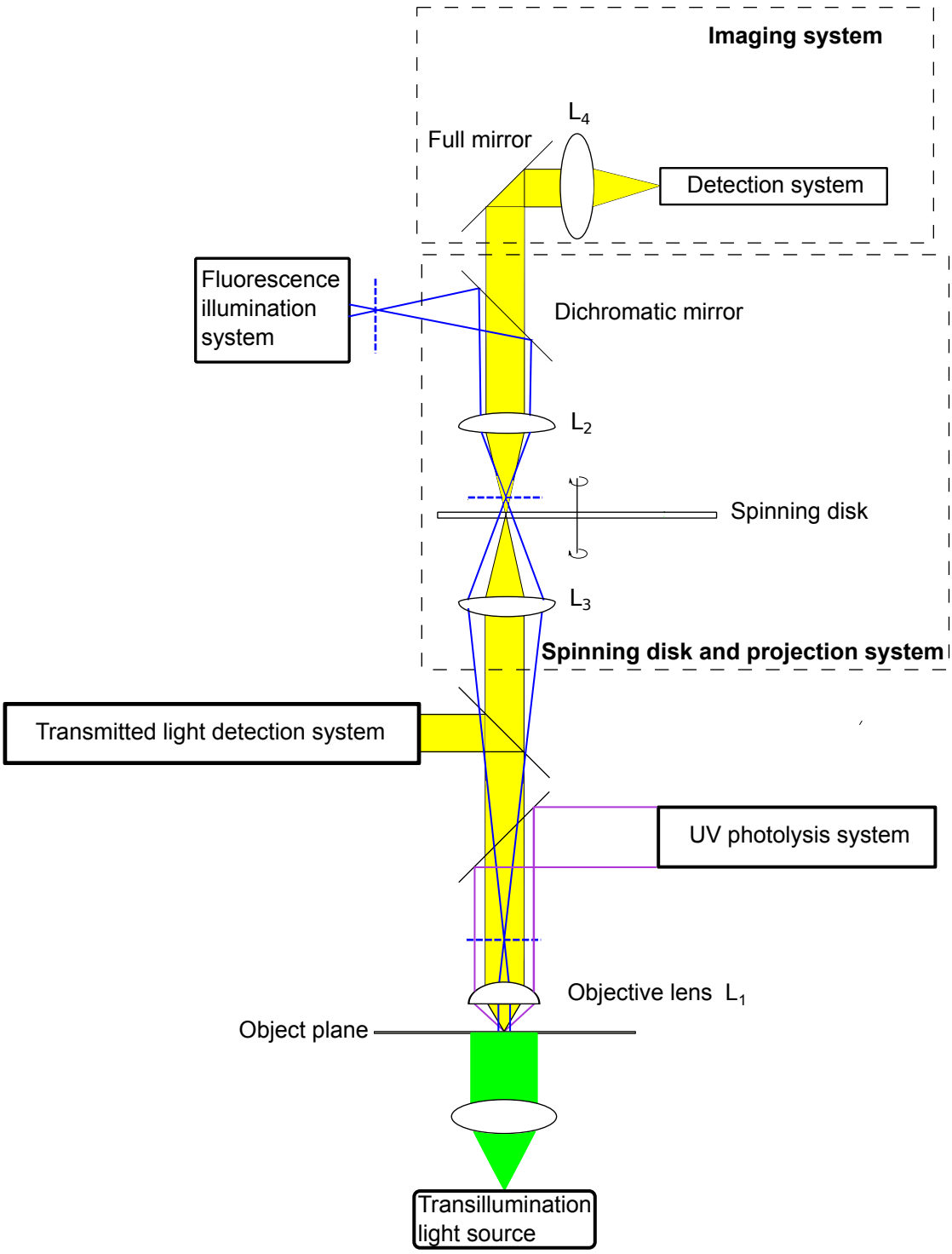

Figure 3.3: Scheme of the confocal microscope. See main text for a full description

tion light was fed to a unit gain keplerian telescope formed by two identical UV permissible achromatic doublets (L_2 and L_3). An x-y-z precision manipulator was used to place the slit disk in the focal plane shared by these two doublets, which is also a primary image plane for the entire microscope. The slit disk was spun by a DC motor up to a speed of 7200 rpm. To avoid transmitting vibrations to the optical table supporting the microscope, the disk, the DC motor and the x-y-z manipulator attached to it were suspended on a horizontal beam connected to the frame of the Faraday cage that encased the entire system and was mechanically uncoupled from the rest of the microscope.

3 - Imaging system Emitted light collected by the objective was spatially filtered through the slit disk, traversed the illumination dichroic and an emission filter and was finally focused onto a sCMOS detector (PCO.edge, PCO, Germany) by a projection lens (L_4, Thorlabs). The detector was located in a plane optically conjugated both with the spinning disk and the object plane.

To test the optical sectioning capabilities of the microscope, we imaged fluorescent beads (15 µm diameter, Figure 3.4A) while stepping the objective in 2 µm increments along its optical axis (z direction) with a piezoelectric actuator. We then measured the average fluorescence intensity collected by the sCMOS sensor within a region of interest with a diameter of 15 µm centered on the bead. Figure 3.4B plots this average signal as a function of defocus. The full width at half maximum of the two intensity vs. defocus curves were 37 µm when the disk was excluded from the optical path and 12 µm when the disk was inserted.

3.11 Simultaneous recording of spontaneous action potentials in immature inner hair cells and spontaneous calcium transients in cochlear non-sensory cells of the GER

Apical cochlear coils from mice of either sex were studied in acutely dissected organs of Corti from P4 to P6. Cochleae were dissected in an extracellular solution containing (in mM): NaCl 135, KCl 5.8, $CaCl_2$ 1.3, $MgCl_2$ 0.9, NaH_2PO_4 0.7, Hepes 10, pyruvate 2, amino acids and vitamins. Sodium pyruvate, MEM amino acids solution (50X, without L-Glutamine) and MEM vitamins solution (100X) were added from concentrates (Fisher Scientific, UK). The pH was adjusted to 7.5 (osmolality $\sim$ 308 mmol kg^{-1}).

Explants were incubated for 30 min at 37° in DMEM supplemented with Fluo–4 AM (16 µM) pluronic F–127 (0.1%, w/v), and sulphinpyrazone (250 µM) and then perfused for 20 minutes for de-esterification in the extracellular solution .

The pipette solution used for cell-attached recordings contained (in mM) 140 NaCl, 5.8 KCl, 1.3 $CaCl_2$, 0.9 $MgCl_2$, 0.7 NaH_2PO_4, 5.6 d-glucose, 10 HEPES- NaOH (pH 7.5). Patch pipettes were made from soda glass capillaries (Harvard Apparatus) and coated with surf wax (SexWax, Mr. Zoggs) to minimize the fast transient due to the patch

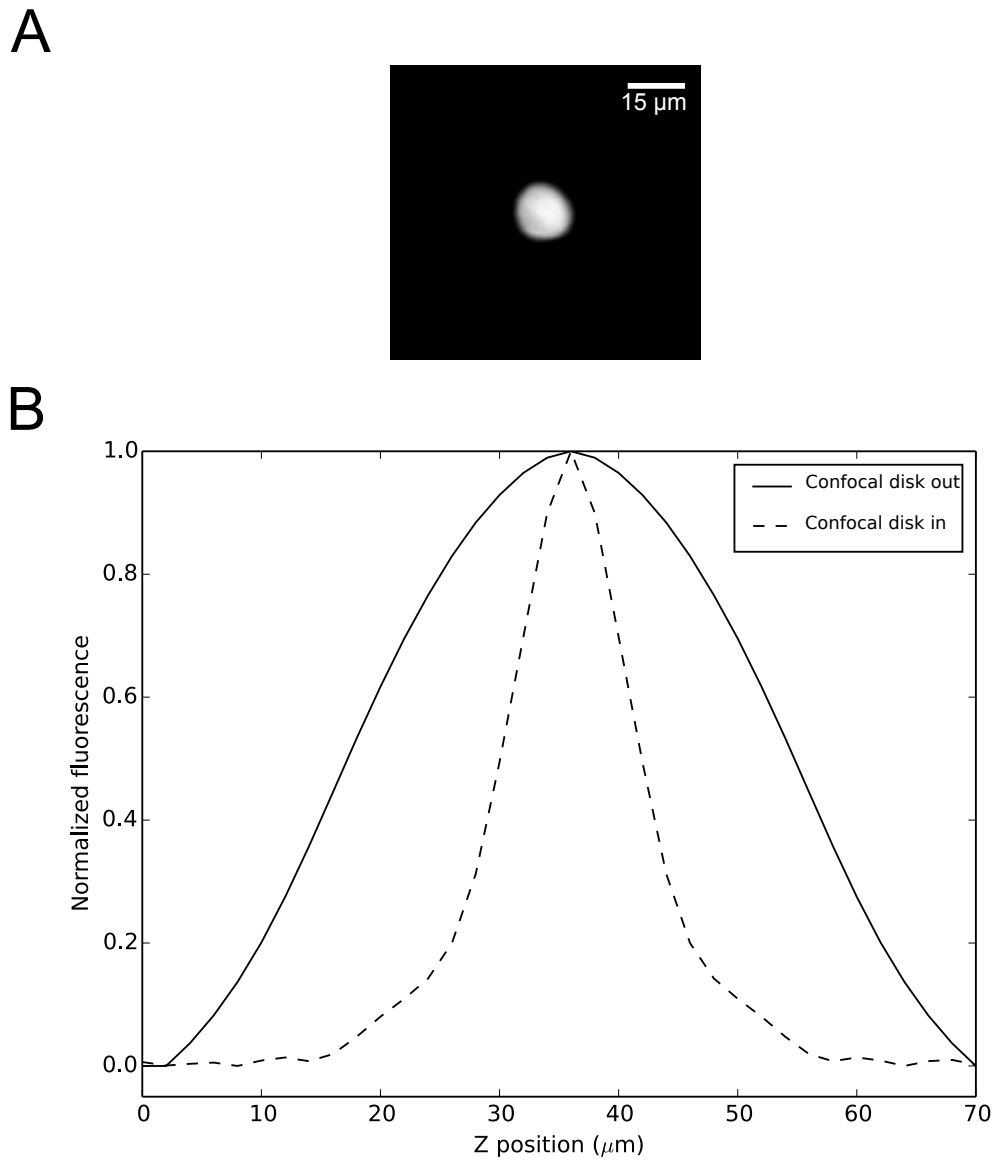

Figure 3.4: Optical sectioning capabilities of the confocal microscope. See main text for a full description.

pipette capacitance. Experiments were performed at near body temperature (35–37 °C) and with 1.3 mM Ca^{2+} and 5.8 mM K^{+} in the extracellular solution, concentrations similar to those of perilymph, to mimic normal physiological conditions as best as possible. Electrophysiology recordings were performed using an EPC−7, (HeKa) amplifier. Current and voltage were filtered at 2.5 kHz by an 8 pole Bessel filter and sampled at 5 kHz.

Fluo-4 fluorescence was excited using the 460 nm LED and its emission was filtered through a 535/43M bandpass interference filter (Edmund). Images were acquired at 10 frames per second and synchronized to electrophysiological recordings as described above (see section 3.6).

4 A voltage sensitive dye assessment of electrical coupling in cell networks of the inner ear

4.1 Introduction

The most widely used approach to monitor intercellular communication employs optical methods to track the movement of tracer molecules between neighboring cells. However, the sensitivity of this technique depends on the junctional permeability of the tracer employed, which varies significantly with the size of the permeant molecule and the type of gap junction channels. Sensitivity can be increased by prolonging the loading time or by employing smaller tracer molecules (e.g. serotonin [Hou et al., 2013]). Here, we used cochlear organotypic cultures to unravel the potential of Vf2.1.Cl, a member of the novel VoltageFluor (VF) family of fluorescent sensors [Miller et al., 2012]. VF dyes detect voltage changes by modulation of photo–induced electron transfer (PeT) from an electron donor through a synthetic molecular wire to a fluorophore. They have large, linear, turn–on fluorescence responses to depolarizing steps (20–27% fluorescence change per 100 mV), fast kinetics ($\tau << 140$ µs) and negligible capacitative loading. We exploited the Vf2.1.Cl voltage sensitive dye [Miller et al., 2012] to probe dynamically the extent of gap junction coupling by a combination of single cell electrophysiology, large scale optical recordings and digital phase–sensitive detector of fluorescence signals. Our method is readily applicable to a variety of cellular systems, as it requires only a patch–clamp amplifier to inject sinusoidal electrical signals at fixed frequency and amplitude in a single cell and a fluorescence microscope to track optically the VF dye response at the frequency of the stimulus throughout the network.

4.2 Results

4.2.1 In situ calibration of the Vf2.1Cl voltage sensitive dye

Organotypic cultures of cochlear explants from postnatal mice permit to investigate the patho–physiology of gap–junction–mediated intercellular signaling in a readily accessible whole–organ context [Gale et al., 2004,Beltramello et al., 2005,Piazza et al., 2007,Anselmi et al., 2008, Majumder et al., 2010, Mammano, 2013]. In order to calibrate the voltage response of the fluorescent sensor in our experimental conditions (see Methods), we loaded organotypic cultures from wild type mice, euthanized at postnatal day 5 (P5), with Vf2.1.Cl. We then performed paired whole–cell patch clamp recordings from cochlear

non−sensory cells of the lesser epithelial ridge. We stepped the voltage V_0 of the patch clamp amplifier connected to one cell (cell 1, Figure 4.1A) in 10 mV increments from the zero current potential (-61 ± 2 mV, $n = 15$ cells) while monitoring the membrane potential (V_m) (Figure 4.1B, red trace) of a nearby cell (cell 2, Figure 4.1A) maintained under current–clamp conditions with a second amplifier. At the same time, we measured Vf2.1.Cl fluorescence emission (F) from cell 2 (Figure 4.1B, blue trace). Data in Figure 4.1B,C highlight a linear relationship between the change in membrane potential (ΔV_m) and the corresponding fractional change ($\Delta F/F_0$) in Vf2.1.Cl fluorescence emission. Note that both $\Delta F/F_0$ and ΔV_m were detected from cell 2. The correlation coefficient between $\Delta F/F_0$ and ΔV_m was R = 0.98 ($n = 5$ paired recordings in 3 cultures) and a linear fit to the data (Figure 4.1C, solid line) yielded a responsivity (slope) m = 0.23 $\pm$ 0.03 $\Delta F/F_0$ /mV (i.e. 23 $\pm$ 3% per 100 mV). Both ΔV_m and $\Delta F/F_0$ responses were suppressed after incubating the culture for 20 minutes in 100 µM carbenoxolone (CBX, Figure 4.1D), a non−selective blocker of gap junction channels [Verselis and Srinivas, 2013]. Based on this calibration, we estimated optically the voltage step in cell 1 (ΔV_1) corresponding to a given voltage command ΔV_0 delivered by the patch clamp amplifier. On average, $\Delta V_0 = 70$ mV yielded a $\Delta V_1 = 22 \pm 4$ mV ($n = 5$) in wild type cultures. We then derived the access resistance of the patch pipette connected to cell 1 as $R_a = \Delta(V_0 - V1)/\Delta I$, where $\Delta I = 6.8 \pm 1.1$ nA ($n = 5$) is the current step measured by the amplifier. The value we obtained, Ra = 7.8 $\pm$ 0.9 MΩ($n = 5$), is in excellent agreement with the estimate provided by the membrane test of the patch clamp software, $R_{a,(patch)} = 7.5 \pm 1.2$ MΩ($n = 5$).

4.2.2 A digital phase-sensitive detector of Vf2.1Cl signals visualizes and quantifies network connectivity

Paired electrophysiological recordings, such as those in Figure 4.1, have excellent time resolution but provide extremely limited spatial information regarding network connectivity. The main goal of the present study was to visualize rapidly network connectivity using large−scale optical recordings of Vf2.1.Cl florescence in different preparations and experimental conditions. The calibration procedure reported in Figure 4.1 yielded maximal fluorescence changes $\Delta F/F_0$ in cell 2, close to cell 1, which rarely exceeded 10%. Electrical signals spreading passively through a resistive network are expected to attenuate rapidly with distance from the source (i.e. cell 1) and fluctuations due to photon shot noise hamper their detection [Davies et al., 2013]. We sought to overcome these limitations by the following procedure. We loaded cochlear organotypic cultures from P5 mice with the Vf2.1.Cl dye and delivered a sinusoidal voltage command, also named carrier wave (frequency $\nu = 0.5$ Hz, amplitude 35 mV) to the patch clamp amplifier connected to one cell of the network (cell 1, Figure 4.2A). In wild type cultures, this stimulation elicited instantly sinusoidal optical signals of Vf2.1.Cl fluorescence at the frequency ν of the carrier wave (reference frequency) in virtually all cells of the network within the field of view. We then used the off−line digital phase–sensitive detector (also known as lock–in amplifier) described in Section 4.3 to extract Vf2.1.Cl signal amplitude $A(x, y)$ at each network location (x, y) at the reference frequency (Figure 4.2B). This method works

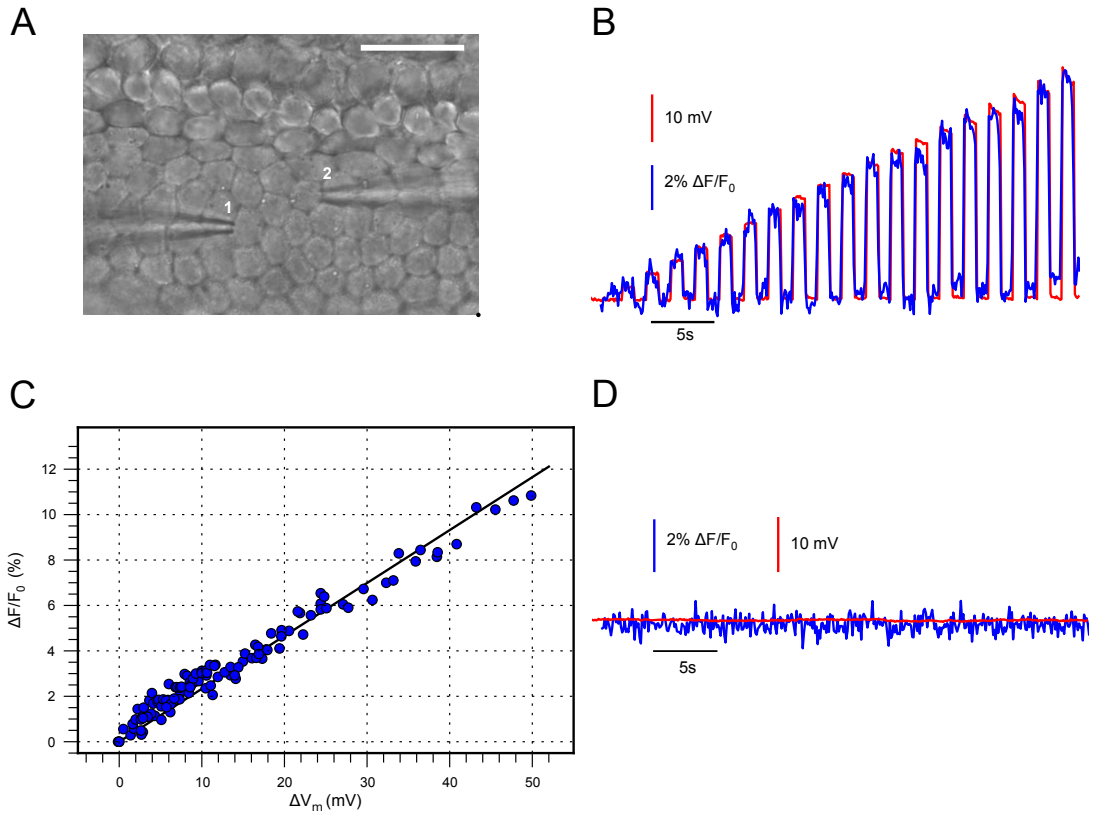

Figure 4.1: Calibration of Vf2.1Cl voltage responses by paired patch clamp recordings in cochlear organotypic cultures. (A) Differential interference contrast (DIC) image showing two patch clamp pipettes, each one sealed to a non−sensory cell of the lesser epithelial ridge; scale bar, 25 µm. (B) Representative traces showing simultaneous membrane potential (red) and Vf2.1.Cl fluorescence (blue) from cell 2, in the neighborhood of the stimulated cell (cell 1); the black trace (top) represents the waveform of the stimulus delivered by the patch clamp amplifier connected to cell 1. (C) Fractional fluorescence signal change ($\Delta F/F_0$) vs. membrane potential change ΔV_m (both signals are from cell 2); dots are individual measurements from $n = 5$ cells in 3 cultures; the straight line is a linear fit to the data. (D) Both voltage and fluorescence responses of cell 2 were suppressed after incubating the culture for 20 minutes in 100 µM carbenoxolone (CBX).

because noise at frequencies other than ν is rejected and does not affect the measurement [Cova et al., 1979]. Throughout this article, relative amplitude refers to $A(x, y)/A_1$ where A_1 is signal amplitude at the reference frequency in the stimulated cell. At each point (x, y), relative amplitude values remained stable for tens of seconds during carrier wave delivery to cell 1, but decreased rapidly with distance from this cell (Figure 4.2C and D). At the single pixel level, the standard deviation σ of the signal $A(x, y)$ returned by the digital phase–sensitive detector scaled correctly as the square root of the number N of integration cycles (Figure 4.2E). Note that $\sigma \simeq 2.2$ mV at $N = 1$ and $\sigma \simeq 0.5$ mV at $N = 25$; reaching sub–mV sensitivity required $N \geq 5$.

To estimate cell network extension, we computed $A(x, y)$ by integrating Vf2.1.Cl signals over $N = 5$ carrier wave cycles (Figure 4.3). This approach permitted us to discriminate rapidly (10 s per recording) network connectivity of wild type cultures (Figure 4.3A, top left) from that of genetically modified connexin30(T5M/T5M) (top right) and connexin30(−/−) (bottom left) cultures [Schutz et al., 2010]. Incubating wild type cultures for 20 minutes in 100 µM CBX confined the Vf2.1.Cl signal to the stimulated cell (bottom right), indicative of junctional conductance (g_j) collapse over the entire network.

For statistical comparison, we increased the precision of these steady–state measurements by integrating Vf2.1.Cl signals over $N = 25$ carrier wave cycles (50 s per recording) and measured the culture area where $A(x, y)$ exceeded an arbitrary threshold value corresponding to $2\sigma \approx 1.0$ mV (suprathreshold area; pooled results are summarized in Figure 4.3B). Compared to wild type cultures, suprathreshold areas in connexin30(T5M/T5M) and connexin30(−/−) cultures were significantly shifted towards lower values (P = 0.03 and P = 0.006, respectively; Mann–Whitney U test; n = 5 cultures for each genotype). In wild type cultures, the lower quartile, the median, and upper quartile of suprathreshold area values were respectively: 17230, 18430, 18970 µm^2; the corresponding values in connexin30(T5M/T5M) cultures were: 10730, 13550, 15100 µm^2; finally, in connexin30(−/−) cultures, they were: 2730, 3550, 5300 µm^2.

4.2.3 A simple resistive network model accounts for the spatial dependance of Vf2.1Cl signals

To gain further insight into the spatial dependence of the data shown in Figure 4.3, we modeled the cell network as a collection of nodes (individual non–sensory cells) forming an hexagonal mesh that reflects the anatomy [Lagostena et al., 2001]. In this model, nodes were coupled by resistive links with identical junctional conductance g_j . Each node was also connected to ground by a resistor with conductance g_m representing cell membrane (Figure 4.4). We pooled data from $n = 5$ cultures for each genotype at equal distances from the stimulated cell along the coiling axis of the cochlea and plotted the result versus this distance. Finally, we obtained least–square fits to these averaged data using the network model with g_j as the only free parameter. The results were: $g_j = 206$ nS for wild type, 177 nS for connexin30(T5M/T5M) and 19 nS for connexin30(−/−) cultures.

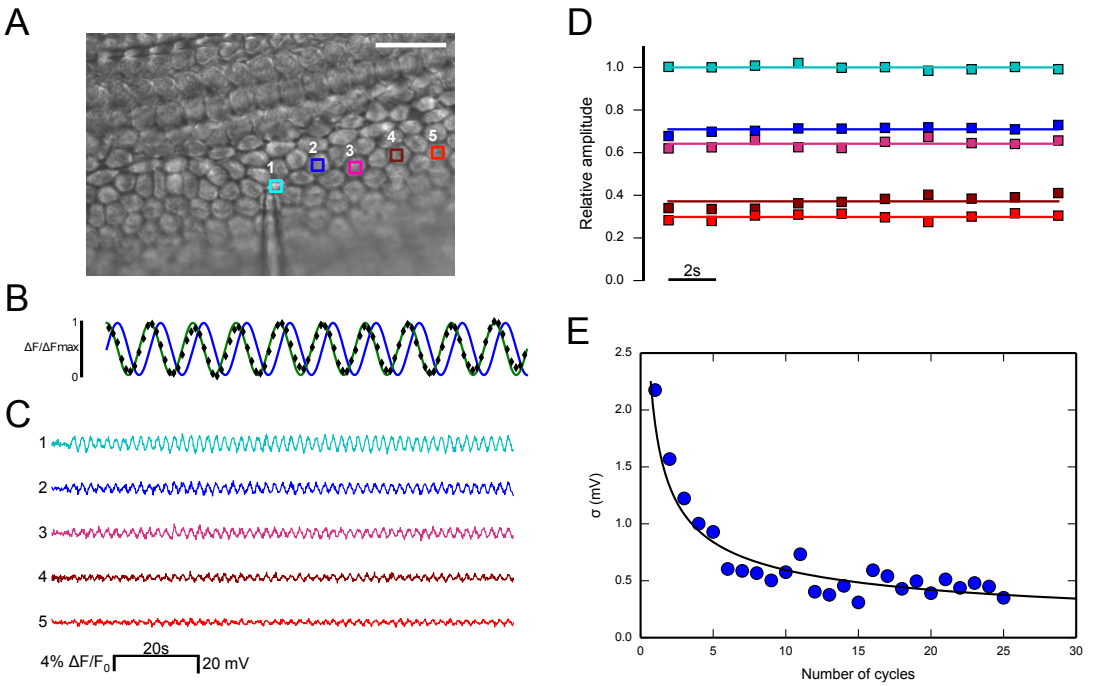

Figure 4.2: Illustrating phase-sensitive detection of Vf2.1Cl fluorescence responses. (A) DIC image showing a single patch clamp pipette sealed to a non−sensory cell of the lesser epithelial ridge (cell 1, zero current potential −66 mV); scale bar, 25 µm. (B) Black diamonds: normalized optical signals from a specific cell network location; green trace: unit amplitude carrier wave delivered to cell 1; blue trace: its phase–shifted counterpart used in the computation of signal amplitude (see Section 4.3). (C) Calibrated optical responses from the five regions of interest (ROIs) shown in (A) during a typical stimulation protocol. A low order polynomial fit was subtracted to the raw traces to compensate for the effects of photobleaching (see Section 4.3). (D) Relative amplitude signals derived by integrating traces shown in (C) over a single carrier wave cycle ($N = 1$). (E) The standard deviation σ of the single pixel amplitude signal $A(x, y)$ is plotted against the number N of integration cycles (see Section 4.3); the black solid line is a least-square fit to the data with the function $\sigma_1/\sqrt{N_1}$ where $\sigma_1 = 1.9$ mV.

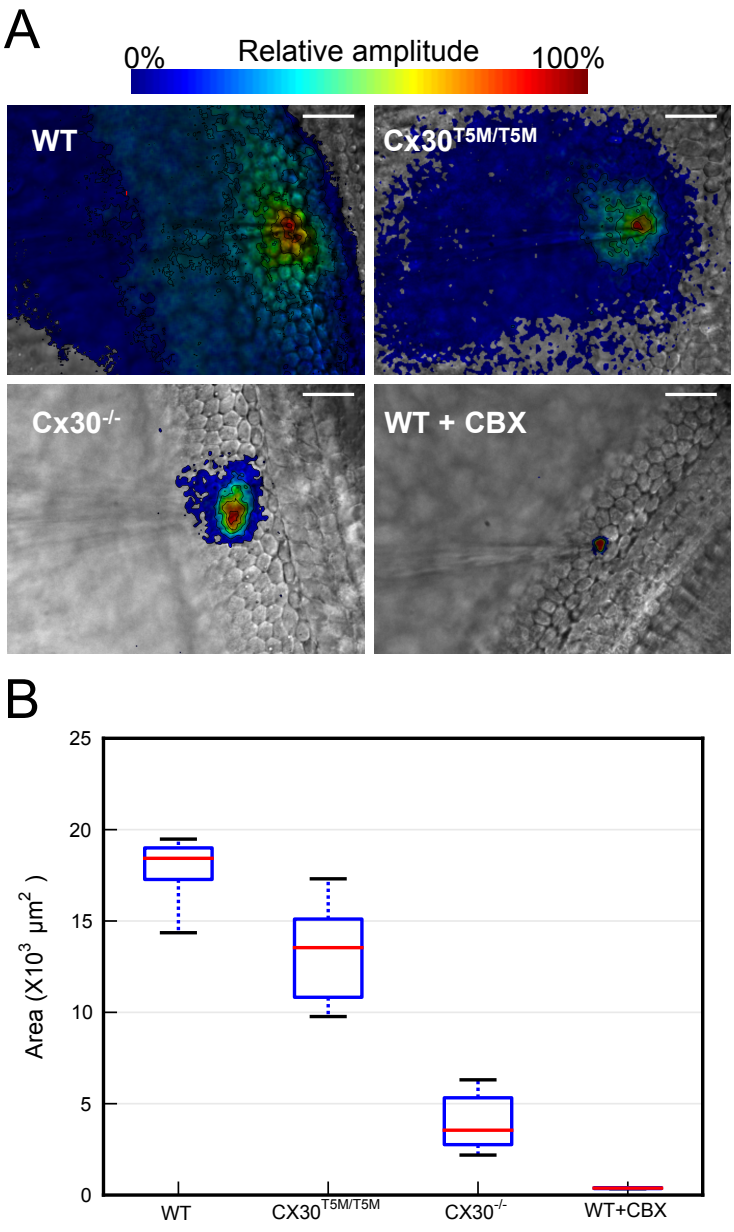

Figure 4.3: Direct readout of network connectivity by large-scale optical recordings of Vf2.1Cl fluorescence responses to a 0.5 Hz, 35 mV carrier wave. (A) Representative false–color images showing the spatial distribution of Vf2.1.Cl relative amplitude signals in cultures from P5 wtype (top left), connexin30(T5M/T5M) (top right) and connexin30(−/−) (bottom left) mice; the bottom right image refers to a wild type culture in which gap junction channels were blocked by 20 min incubation with CBX (100 µM); in this image, the area with a residual relative amplitude signal (226 μm^2) is very close to the average area of a single cell in this part of the culture (210 ± 7 μm^2 , $n = 10$ cells); scale bars, 25 µm. (B) Suprathreshold area distributions shown in box plot form; see main text for details.

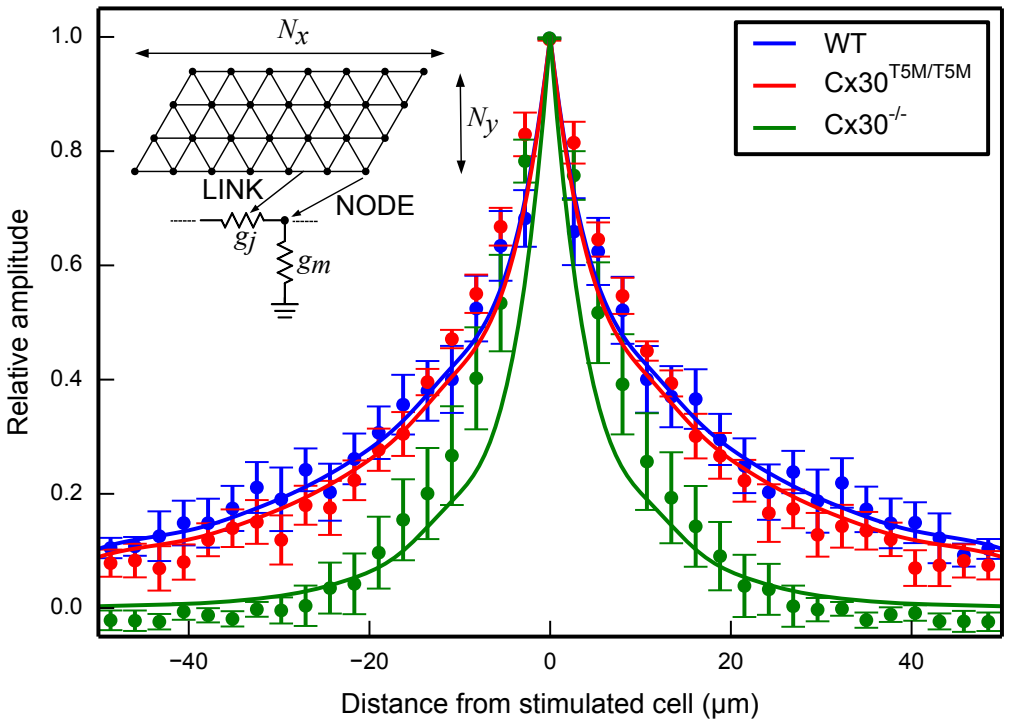

Figure 4.4: Data fit by a simple resistive network model that reflects the anatomy. The inset shows model scheme. Simulations were performed using the ngspice software (`http://ngspice.sourceforge.net`). $N_x = 45$ and $N_y = 15$ indicate the number of rows and columns in the grid, respectively. Each node represents one cell and each link represents a resistive connection between adjacent nodes. The patch pipette connected to cell 1 was simulated as a variable voltage source connected to one node of the grid through an access resistance $R_a = 7.8$ MΩ(not shown). A single value for membrane conductance ($g_m = 8.3$ nS) and junctional conductance (g_j) were used throughout the network. g_j was left as the only free parameter in the simulations and its value was derived using a maximum–likelihood algorithm.

4.2.4 Application to network dynamics

In patho–physiological conditions, gap junction networks are dynamically regulated by a variety of mechanisms that govern connexin channel permeability and gating [Goodenough and Paul, 2009, Hernandez et al., 2007, Harris, 2007, Beltramello et al., 2005, Bukauskas and Verselis, 2004]. Our next goal was to track dynamical changes in cell network connectivity by applying a digital phase–sensitive detector to Vf2.1.Cl signals. For this series of recordings, we limited time integration to $N = 4$ carrier wave cycles while transiently superfusing cochlear cultures with an extracellular medium saturated with 100% CO_2 to produce carbonic acid (H_2CO_3). In its non−dissociated form H_2CO_3 is membrane permeable and causes a rapid and reversible closure of gap junction channels [Hernandez et al., 2007, Bukauskas and Verselis, 2004]. This manipulation led to a reduction in the number of cells coupled to the stimulated cell, accompanied by a transient increase in Vf2.1.Cl fluorescence in the neighborhood of this cell (Figure 4.5A, B). To mimic the time course of the events shown in Figure 4.5A, B, we simply assumed that the g_j of the network model represented in Figure 4.4 undergoes a time−dependent exponential decrease from 206 nS to 2 nS with a time constant of 7 s (Figure 4.5C).

4.2.5 Application to immortalized cell lines

A number of gap junction communication studies are performed in expression systems and/or immortalized cell lines. To demonstrate the applicability of the method highlighted above to this important area of research, we used a clone of HeLa cells virtually devoid of connexins (see Methods, Chapter 3) that were either left untreated (HeLa parental) or transiently transfected with a construct expressing human connexin26 fused in tandem with a cyan fluorescent protein (CFP) reporter (hCx26–CFP) [Beltramello et al., 2005]. These chimerical proteins localized to the plasma membrane at regions of contact between adjacent cells and also formed distinct fluorescent puncta in the cytoplasm, as previously described [Beltramello et al., 2005, Beltramello et al., 2003, Bicego et al., 2006]. Confluent HeLa cell cultures were loaded with the Vf2.1.Cl dye and subjected to the same patch–clamp protocol used in organotypic cochlear cultures. In HeLa parental cultures, the Vf2.1.Cl signal remained confined to the stimulated cell (Figure 4.6A). In transfected cultures, the Vf2.1.Cl signal displayed variable degrees of cell–to–cell spreading, reflecting the number of transfected cells connected to the stimulated cell by hCx26–CFP gap junction channels (Figure 4.6B, C and D).

4.3 Imaging methods and phase-sensitive detection of Vf2.1.Cl fluorescence signals

Vf2.1.Cl fluorescence image sequences were stored on disk and processed off–line using the Matlab R2011a software package (The MathWorks, Inc.) as described hereafter. Following electrical stimulation of cell 1 with a carrier wave at frequency ν, each image was preprocessed by applying a 3–by–3 mean spatial filter to reduce acquisition noise.

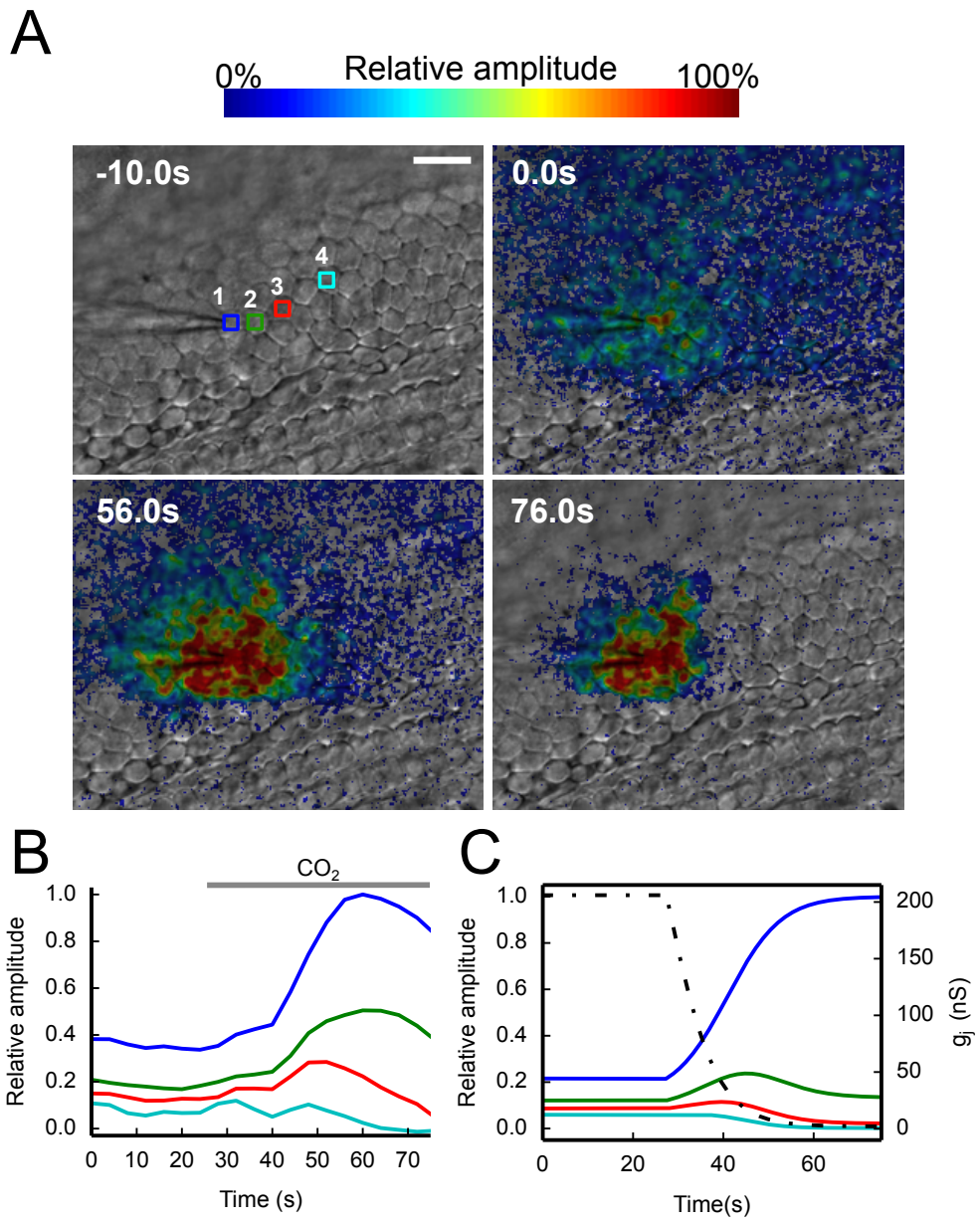

Figure 4.5: Effects of cell uncoupling by CO_2. (A) Four selected frames from the same image sequence showing the progressive reduction of the number of cells coupled to the stimulated cell before and during exposure to 100% CO_2; the top left image was captured 10.0 s before the delivery of the carrier wave stimulus to cell 1; CO_2 delivery started at 25 s and was maintained thereafter; scale bar, 25 µm. (B) Time course of pixel averages from the color−coded ROIs shown in (A). (C) Numerical simulation of the electrical uncoupling process; the effect was mimicked by rapidly decreasing the value of junctional conductance g_j (black dashed line) in the network model of Figure 4.4 from an initial value of 206 nS to 2 nS.

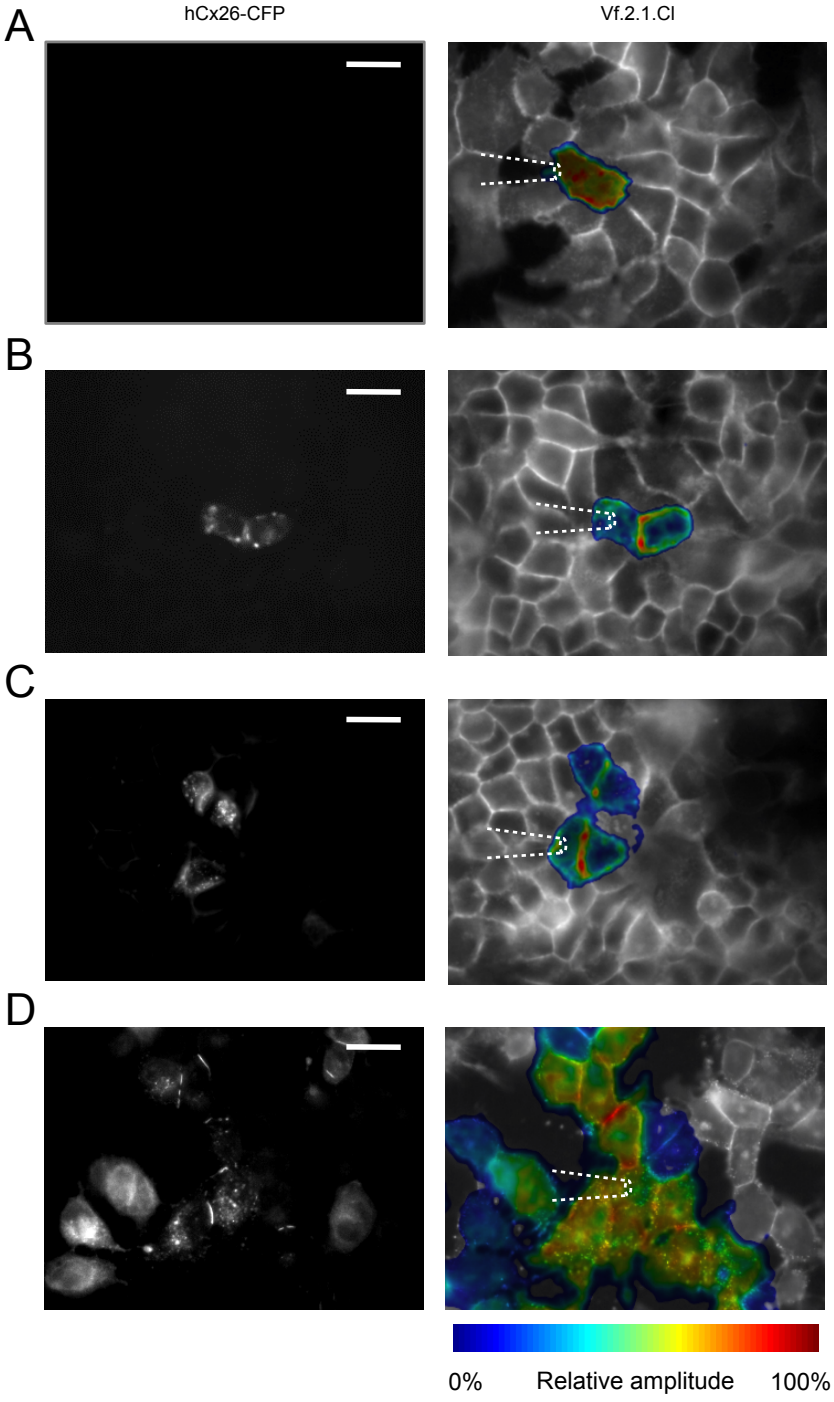

Figure 4.6: Optical readout of network connectivity in HeLa cells loaded with Vf2.1.Cl. (A) HeLa parental cells. (B, C, D) Transiently transfected HeLa cells showing increasing amounts of interconnectivity provided by hCx26–CFP gap junction channels; images of CFP fluorescence emission from chimerical proteins are shown at left, the corresponding Vf2.1.Cl relative amplitude data at right (integration cycles $N = 25$); scale bars, 25 µm.

To correct for photobleaching, we first estimated its time course by performing a low order polynomial fit to the $(\Delta F/F_0)(t;x,y)$ data at each pixel location (x,y); the fitting function $P(t;x,y)$ was then subtracted from the $(\Delta F/F_0)(t;x,y)$ signal, yielding an effectively high–pass filtered trace

$$f(t;x,y) = \frac{\Delta F(t;x,y)}{F_0(x,y)} - P(t;x,y) \tag{4.1}$$

The purpose of using a phase–sensitive detector is to extract the signal amplitude $A(x,y)$ from the preprocessed single pixel signal

$$f(t;x,y) = A(x,y)\cos(2\pi\nu t - \theta) \tag{4.2}$$

where θ is a constant phase delay [Cova et al., 1979]. We performed the extraction procedure in two steps:

Step 1: Demodulation $f(t,x;y)$ was multiplied by two orthogonal reference signals

$$V_1^{ref}(t) = \cos(2\pi\nu t) \tag{4.3}$$

$$V_2^{ref}(t) = \sin(2\pi\nu t) \tag{4.4}$$

(see Figure 4.2B) yielding two output signals of the form

$$f_1(t;x,y) = V_1^{ref}(t)\cdot f(t;x,y) = A(x,y)\cos(2\pi\nu t - \theta)\cos(2\pi\nu t) \tag{4.5}$$

$$f_2(t;x,y) = V_2^{ref}(t)\cdot f(t;x,y) = A(x,y)\cos(2\pi\nu t - \theta)\sin(2\pi\nu t) \tag{4.6}$$

Considering the trigonometric identities

$$\cos(a)\cos(b) = \frac{1}{2}\left[\cos(a-b) + \cos(a+b)\right] \tag{4.7}$$

$$\cos(a)\sin(b) = \frac{1}{2}\left[\sin(a+b) - \sin(a-b)\right] \tag{4.8}$$

the two output signals can be written as

$$f_1(t;x,y) = \frac{1}{2}A(x,y)\left[\cos(\theta) + \cos(2\pi(2\nu)t - \theta)\right] \tag{4.9}$$

$$f_2(t;x,y) = \frac{1}{2}A(x,y)\left[\sin(2\pi(2\nu)t - \theta) + \sin(\theta)\right] \tag{4.10}$$

and are seen to consist of a DC signal proportional to the amplitude $A(x,y)$ of the original function $f(t;x,y)$ and a time-dependent component with frequency 2ν.

Step 2: Amplitude estimation The time-dependent component was filtered out by time integration of $f_1(t;x,y)$ and $f_2(t;x,y)$. In the absence of noise, integration over a single carrier wave cycle would yield the DC components of $f_1(t;x,y)$ and $f_2(t;x,y)$:

$$a_1(x,y) = \frac{1}{2}A(x,y)\cos(\theta) \tag{4.11}$$

$$a_2(x,y) = \frac{1}{2}A(x,y)\sin(\theta) \tag{4.12}$$

In practice, integration is better performed over a number N of cycles to reduce the contributions from various noise sources (see Figure 4.2E). Finally, the amplitude of f(t;x,y) was computed as

$$A(x,y) = 2\sqrt{[a_1(x,y)]^2 + [a_2(x,y)]^2} \tag{4.13}$$

The reference level $A(x,y) = 0$ was set by applying the above algorithm to the pre-stimulus trace (i.e. to the trace segment that preceded cell 1 stimulation by the carrier wave).

4.4 Discussion

We report here the application of the novel Vf2.1.Cl fluorescent sensor [Miller et al., 2012] to voltage imaging in cell networks coupled by gap junction channels. We focused our attention on non−sensory cell networks of the developing cochlea and used organotypic cultures from P5 mice as model system. Our in situ calibration yielded an estimated responsivity of 23 ± 3 % $\Delta F/F_0$ per 100 mV change of the cell membrane potential V_m (Figure 4.1), in substantial agreement with measurements performed in HEK293 cells (26% per 100 mV) [Miller et al., 2012]. The limited dispersion of the data in Figure 4.1C, which were acquired under different F_0 conditions, indicates that the responsivity is fairly independent of the loading conditions. However, F_0 does affect the signal−to−noise ratio, which is ultimately dictated by fluctuations in the number of collected photons (see, e.g. Ref. [Davies et al., 2013]), and consequently also the sensitivity of the measurement.

The Vf2.1.Cl signal tracks the membrane potential with no detectable delay [Miller et al., 2012], a highly desirable feature that distinguishes this dye from the substantially slower voltage sensors based on fluorescent proteins. The use of these proteins is also hindered by the necessity of transfecting/transducing target cells with a suitable expression vector [Jin et al., 2012]. In contrast, Vf2.1.Cl loads readily (15 min) and our use of a digital phase–sensitive detector (see Section 4.3 and Figure 4.2) allowed us to rapidly map cellular connectivity over vast network areas (Figures 4.3, 4.4, 4.5 and 4.6). With our methodology, the time required for data collection is a multiple of the carrier wave period (2 s in our conditions). Increasing the integration interval slows down the acquisition (i.e. it reduces the temporal resolution of dynamical measurements such as those

presented in Figure 4.5) but reduces fluctuations (Figure 4.2E) and thus increases both sensitivity and precision (defined as the degree to which repeated measurements under unchanged conditions show the same result).

By integrating the Vf2.1.Cl signal over $N = 5$ carrier wave cycles (10 s), we detected intercellular connectivity down to (at least) 10^{th} order cells (i.e. to cells that were separated from the stimulated cells by a linear sequence of 10 adjacent neighbors), in wild type cultures. For comparison, microinjection experiments with fluorescent tracers that permeate cochlear gap junction channels (e.g. calcein, a relatively large permeant tracer that barely fits into the pore of connexin26 channels [Zonta et al., 2013]) require typically 4 minutes to allow dye transfer to 3^{rd} or 4^{th} th order cells (e.g., see Supplementary Figure 6 of ref. [Anselmi et al., 2008]). Comparable time intervals are necessary to assay gap junction communication by fluorescence recovery after photobleaching (gap–FRAP) [Wade et al., 1986] (see, e.g. Figure 5 of ref. [Ortolano and Pasquale, 2008]).

The exact stoichiometry of cochlear gap junction channels in terms of connexin26 and connexin30 subunits is not known. Single channel currents from HeLa cells overexpressing either connexin26 or connexin30 homomeric channels yielded respectively values of 115 pS and 160 pS for the unitary conductance γ [Beltramello et al., 2005, Bicego et al., 2006]. A study in HeLa cells co–transfected with the cDNA of both proteins, and thus presumably forming heteromeric/heterotypic channels, reported γ values in a comparable range of 110–150 pS [Yum et al., 2007]. The junctional conductance $g_j = 206$ nS we obtained by fitting wild type culture data in Figure 4.3 with the resistive network model of Figure 4.4 suggests that cochlear non−sensory cells are already well coupled at P5, by as many as $N_{open} = g_j/\gamma = 1300$ to 1800 open channels per cell pair. It must be noted that cochlear organotypic cultures used for this study were obtained from the basal turn of the cochlea of P5 mice. Studies performed with the gap-FRAP assay using the fluorescent tracer calcein in P5 mice revealed a base-to-apex gradient of dye coupling, with a 30% reduction in apical compared to basal supporting cells [Schutz et al., 2010]. Hence, we estimate that the number of channels coupling neighboring non-sensory cells in the apical part of the cochlea is 910 to 1260 open channels per cell pair.

An older study in isolated pairs of supporting cells of the adult guinea pig organ of Corti reported that junctional conductance may exceed non−junctional conductance by three orders of magnitude and, at least in some cell pairs, g_j was as large as 1 µS [Santos-Sacchi, 1991] corresponding to $N_{open} \simeq 10^4$. We are not aware of structural investigations performed in the developing cochlea. However, Forge et al. [Forge et al., 2003] noted that gap junction plaques in the supporting cells of the mature cochlea are "enormous" and they often occupy a major fraction of the plasma membrane between two adjacent cells (from 25% to almost 100% in pillar cells). From their freeze fracture studies, Forge et al. concluded that plaques containing about 10^4 channels are not rare and some may even contain 10^5 channels, such as those coupling inner pillar cells in the longitudinal direction. Thus our g_j estimate is not in contrast with the proposal that only about 10% of channels within a plaque are in the open state [Bukauskas et al., 2000, Palacios-Prado et al., 2009, Palacios-Prado et al., 2010].

Data in Figure 4.3 show a 27% and 80% reduction in the median suprathreshold area

respectively for connexin30(T5M/T5M) and connexin30(−/−) cultures relative to wild type cultures. Our resistive network model suggests that these reduced areas correspond to a g_j decrease of 14% and 91% for connexin30(T5M/T5M) and connexin30(−/−) cultures, respectively. We previously reported massive down–regulation of connexin26 in the developing organ of Corti of connexin30(−/−) mice [Ortolano and Pasquale, 2008]. Connexin26 is similarly reduced, to 10% of the wild type level, in the cochlea of adult connexin30(−/−) mice. These findings complement and extend our prior work [Schutz et al., 2010], which highlighted a significant reduction in the level of dye coupling in connexin30(T5M/T5M) cultures, whereas dye coupling was absent in connexin30(−/−) cultures. We also showed that adult connexin30(T5M/T5M) mice, when probed by auditory brainstem recordings, exhibit a mild but significant increase in their hearing thresholds, of about 15 dB at all frequencies [Schutz et al., 2010]. By contrast, connexin30(−/−) mice are profoundly deaf [Schutz et al., 2010, Teubner, 2003]. The present experiments and our previous work confirm cochlear organotypic cultures as an attractive test ground to explore the intricacies of connexin expression regulation and function. In addition, our findings support the notion that connexin30(−/−) mice are a model for humans in which large deletions in the DFNB1 locus lead to down–regulation of both GJB6 and GJB2 and to profound deafness [del Castillo and del Castillo, 2011].

It is well known that electrical conductance and permeability to solutes other than small inorganic ions are not directly related [Harris, 2007, Beltramello et al., 2005, Goldberg et al., 1999]. Even the junctional permeability to fluorescent probes may not be directly related to electrical coupling [Schutz et al., 2010, Ek-Vitorin et al., 2006]. We believe that the methodology described in the present article may help clarifying this complex relationship when used in combination with other complementary techniques, particularly those that (i) provide a direct estimate of the unitary permeability to signaling molecules [Hernandez et al., 2007] and (ii) aid data interpretation by the use of Molecular Dynamics [Zonta et al., 2013].

5 ATP-dependent calcium signaling in non-sensory cells of the developing cochlea: experiments and simulations

5.1 Introduction

As mentioned before, ATP-mediated Ca^{2+} signals propagate in a coordinated fashion as intercellular Ca^{2+} waves across non-sensory cells (supporting and epithelial cells) of the polarized neuro-epithelium that lines the developing cochlear duct [Gale et al., 2004, Piazza et al., 2007, Majumder et al., 2010]. ATP–dependent oscillations of the cytosolic Ca^{2+} concentration ($[Ca^{2+}]_c$) in cochlear non–sensory cells occur as a consequence of intercellular Ca^{2+} wave propagation or due to sustained ATP stimulation in the submicromolar range (reviewd in [Mammano, 2013]).

It has long been known that intracellular Ca^{2+} oscillations in non-excitable cells, such as cochlear non-sensory cells, arise from the interplay between Ca^{2+}-permeable channels in the endoplasmic reticulum (ER), that release Ca^{2+} into the cytosol, and Ca^{2+} pumps and exchangers that remove Ca^{2+} from the cytosol either by re-uptaking it into the ER or by exporting it through the cell plasma membrane [Berridge and Galione, 1988, Tsien and Tsien, 1990].

Part of this thesis work was devoted to the development of a minimal mathematical model of intracellular Ca^{2+} oscillations and intercellular Ca^{2+} waves in strict and quantitative adherence to experimental data. This study was based on previous work conducted in the laboratory as well as on a new set of experiments performed in organotypic cultures of apical cochlear coils obtained from mice at postnatal day 5 (P5).

5.2 Computational Methods

A schematic representation of the model is shown in Figure 5.1. Letters J and K, both expressed in µM/s, indicate fluxes through channels/pumps and rate of production/degradation, respectively. The model is composed of three main building blocks, namely: the Ca^{2+} subsystem, the IP_3 subsystem and the ATP subsystem, which are detailed below.

5.2.1 Calcium regulation: the two-variable Li-Rinzel model

Intracellular calcium levels can be modulated by a large variety of mechanisms, which include Ca^{2+} influx from the extracellular space or release from various intracellular

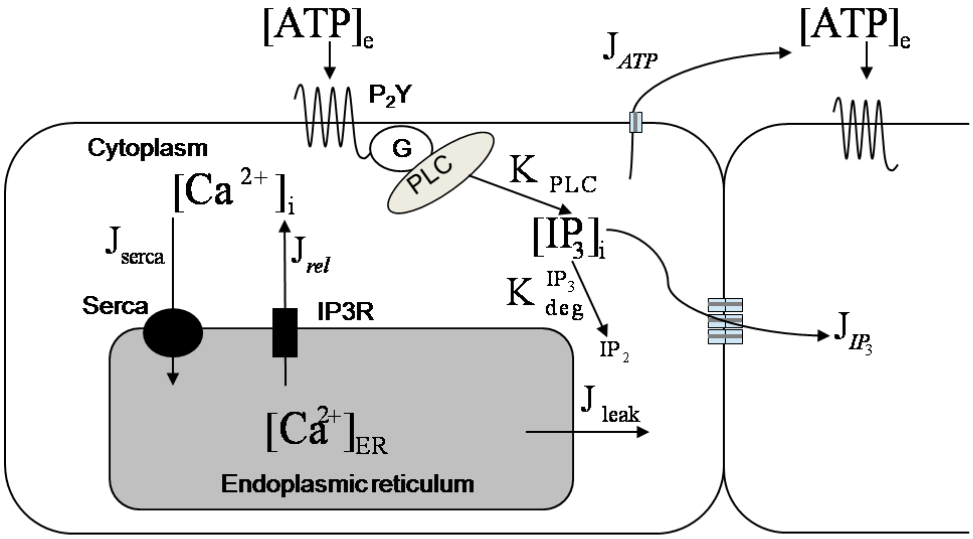

Figure 5.1: Schematic representation of the mathematical model of Ca^{2+} dynamics in cochlear non-sensory cells. See chapter 5.2 for details.

stores (such as the endoplasmic/sarcoplasmic reticulum and mitochondria). In our model, we considered IP_3-dependent Ca^{2+} induced Ca^{2+} release (CICR) from the ER as the only mechanism responsible for the observed changes of the $[Ca^{2+}]_c$, akin to similar models of Ca^{2+} dynamics in non-excitable cells [De Young and Keizer, 1992, De Pittà et al., 2009, Agulhon et al., 2008]. Model parameters are summarized in Table 5.1. Treating the whole cell cytoplasm as a *well stirred* compartment, the continuity equation for Ca^{2+} reads:

$$\frac{d[Ca^{2+}]_c}{dt} = J_{rel} + J_{leak} - J_{serca} \tag{5.1}$$

where:

- J_{rel} is the rate of change of $[Ca^{2+}]_c$ due to the (IP_3-dependent) Ca^{2+} release from the ER through IP_3 receptors (IP_3Rs)
- J_{leak} is the rate of (IP_3-independent) Ca^{2+} leakage from the ER
- J_{serca} is the rate of Ca^{2+} clearance due to uptake into the ER by sarco/endoplasmic reticulum Ca^{2+}-ATPase (SERCA pumps).

Experimental data show that $[Ca^{2+}]_c$ oscillations in cochlear non-sensory cells persist for tens of minutes even in the absence of extracellular Ca^{2+} [Gale et al., 2004, Piazza et al., 2007]. We thus neglected Ca^{2+} exchange through the plasma membrane, reducing our model to a *close cell* compartment in which the total intracellular free Ca^{2+} concentration ($[Ca^{2+}]_{tot}$) is constant. We also neglected other intercellular compartments other

than the ER. Consequently, the Ca^{2+} concentration in the ER ($[Ca^{2+}]_{ER}$) is linked to that of the cytosol by the conservation equation:

$$\alpha \cdot [Ca^{2+}]_{ER} = [Ca^{2+}]_{TOT} - [Ca^{2+}]_c \tag{5.2}$$

where α denotes the ratio of ER to cytosol volume.

We described the SERCA pump rate as a Hill function of $[Ca^{2+}]_c$ with exponent 2:

$$J_{serca} = v_{serca} \frac{([Ca^{2+}]_c)^2}{([Ca^{2+}]_c)^2 + (k_{serca})^2} \tag{5.3}$$

where v_{serca} is the maximum rate of the pump and k_{serca} its Ca^{2+} affinity [Lytton et al., 1992].

The leakage rate was assumed to be proportional to the concentration difference between the ER and the cytosol:

$$J_{leak} = r_{leak}([Ca^{2+}]_{ER} - [Ca^{2+}]_c) \tag{5.4}$$

The rate of Ca^{2+} release through IP_3R was described by the following equation:

$$J_{rel} = r_{rel} P_{IP_3R} \cdot \left([Ca^{2+}]_{ER} - [Ca^{2+}]_c\right) \tag{5.5}$$

where r_{rel} is the maximum rate of release and P_{IP_3R}, the open probability of the IP_3R, is given by

$$P_{IP_3R} = m_\infty^3 n_\infty^3 [h(t)]^3 \tag{5.6}$$

m, n and h (with values comprized between 0 and 1) are the three adimensional variables of the DeYoung-Keizer model [De Young and Keizer, 1992] which, respectively, account for IP_3 binding, activation by Ca^{2+} and inactivation by Ca^{2+} of the IP_3R. In the Li-Rinzel reduction of the DeYoung-Keizer model [Li and Rinzel, 1994], which we adopted here, IP_3 binding and activation by Ca^{2+} are assumed to happen on a faster time scale than Ca^{2+} inactivation. Consequently m and n are assumed in instantaneous equilibrium (hence the ∞ subscript in equation 5.6) and to obey a Hill function of the intracellular IP_3 concentration ($[IP_3]_c$) with affinity d_1 and $[Ca^{2+}]_c$ with affinity d_5, respectively:

$$m_\infty = \frac{[IP_3]_c}{[IP_3]_c + d_1} \tag{5.7}$$

$$n_\infty = \frac{[Ca^{2+}]_c}{[Ca^{2+}]_c + d_5} \tag{5.8}$$

Finally, the time-dependent, Hodgjkin and Huxley-like variable h is a solution to the differential equation

$$\frac{dh}{dt} = \frac{h_\infty - h}{\tau_h} \tag{5.9}$$

where

$$\tau_h = \frac{1}{a_2(Q_2 + [Ca^{2+}]_c)} \tag{5.10}$$

$$h_\infty = \frac{Q_2}{Q_2 + [Ca^{2+}]_c} \tag{5.11}$$

$$Q_2 = d_2 \frac{[IP_3]_c + d_1}{[IP_3]_c + d_3} \tag{5.12}$$

The parameters d_1, d_3, d_5 and the power of 3 in equation 5.6 were chosen by DeYoung and Keizer [De Young and Keizer, 1992] in order to fit the steady-state open probability of the IP_3R measured experimentally by Bezprozvanny et al. [Bezprozvanny et al., 1991].

In summary, the balance of cytosolic Ca^{2+} is dictated by equation 5.9 and the following equation:

$$\begin{aligned} \frac{d[Ca^{2+}]_c}{dt} =& (r_{rel} \cdot m_\infty^3 n_\infty^3 [h(t)]^3 + r_{leak}) \left([Ca^{2+}]_{ER} - [Ca^{2+}]_c\right) \\ & - v_{serca} \frac{([Ca^{2+}]_c)^2}{([Ca^{2+}]_c)^2 + (k_{serca})^2} \end{aligned} \tag{5.13}$$

5.2.2 IP3 regulation

The dynamics of IP_3 was described by the equation

$$\frac{d[IP_3]_c}{dt} = K_{PLC} - K_{deg}^{IP_3} + J_{GJ}^{IP_3} \tag{5.14}$$

where:

- K_{PLC} indicates the rate of IP_3 production due to phospholipase-C activity;
- $K_{deg}^{IP_3}$ indicates IP_3 degradation;
- $J_{GJ}^{IP_3}$ is the rate of change of $[IP_3]_c$ due to the intercellular flux from adjacent cells through gap junction channels.

A detailed mathematical description of agonist-dependent IP_3 production is provided in ref. [Lemon et al., 2003]. To limit the number of variables in our model, we assumed K_{PLC} to be a Hill function of the extracellular concentration of ATP ($[ATP]_e$)

$$K_{PLC} = v_{PLC} \frac{([ATP]_e)^{n_{PLC}}}{([ATP]_e)^{n_{PLC}} + (k_{PLC})^{n_{PLC}}} \tag{5.15}$$

where v_{PLC}, n_{PLC} and k_{PLC} are empirically fitted parameters (see Figure 5.5B and Table 5.1).

Following Sneyd et al. [Sneyd et al., 1995], we modeled IP_3 degradation as a linear function of $[IP_3]_c$:

$$K_{deg}^{IP_3} = r_{deg}^{IP_3} [IP_3]_c \tag{5.16}$$

The flux of IP_3 between each pair of neighboring cells was assumed to be proportional to the difference of $[IP_3]_c$ between them:

$$J_{GJ}^{IP_3} = k_j \cdot \sum_{<i>} ([IP_3]_{c,i} - [IP_3]_c) \tag{5.17}$$

where $\sum_{<i>}$ indicates the sum over all nearest neighboring cells and $[IP_3]_{c,i}$ indicates the cytosolic IP_3 concentration in the i-th neighbor [Hofer et al., 2001]. The IP_3 junctional transfer rate

$$k_j = p_u \frac{N_{ch}}{V} \tag{5.18}$$

depends on the number of channels, N_{ch}, their unitary permeability to IP_3, p_u, and the volume of the cell, V [Hernandez et al., 2007].

5.2.3 ATP release to and diffusion through the extracellular space

Experimental data indicate that a key component of Ca^{2+} signaling in cochlear non-sensory cells is extracellular ATP which is released through connexin hemichannels at the endolymphatic surface of the sensory epithelium and is degraded by ectonucleotidases [Mammano, 2013]. To incorporate the effects of ATP in our model, we used the following reaction diffusion equation:

$$\frac{\partial [ATP]_e}{\partial t} = D\nabla^2 [ATP]_e + J_{ATP} - K_{deg}^{ATP} \tag{5.19}$$

The first term on the right hand side describes ATP diffusion in the extracellular space (D is the diffusion coefficient of ATP in the extracellular medium and ∇^2 is the laplacian operator in space); J_{ATP} represents the ATP efflux through connexin hemichannels and K_{deg}^{ATP} represents the rate of ATP degradation by ectonucleotidases.

Akin to equation 5.16, we modeled ATP degradation rate as a linear function of $[ATP]_e$:

$$K_{deg}^{ATP} = r_{deg}^{ATP} [ATP]_e \tag{5.20}$$

J_{ATP} was assumed to be proportional to the hemichannels open probability, P_{HC}, according to the equation:

$$J_{ATP} = v_{HC} P_{HC} \tag{5.21}$$

To account for the experimentally determined bell-shaped dependence of P_{HC} on $[Ca^{2+}]_c$ (Figure 5.3) [De Vuyst et al., 2006], we formulated the four-state model described in Figure 5.2. Each state is indicated as $S_{i,j}$, where $i = 0, 1$ indicates Ca^{2+} binding to a putative activating site and $j = 0, 1$ indicates Ca^{2+} binding to a putative inactivating site. We also assumed that the rate of Ca^{2+} binding to the activating site is independent of whether or not Ca^{2+} is present at the inactivating site and vice versa (4 rate constants). The channel is open if Ca^{2+} is bound to the activating site and not bound to the inactivating site (state $S_{1,0}$). Thus, denoting with $x_{i,j}$ the fraction of channel

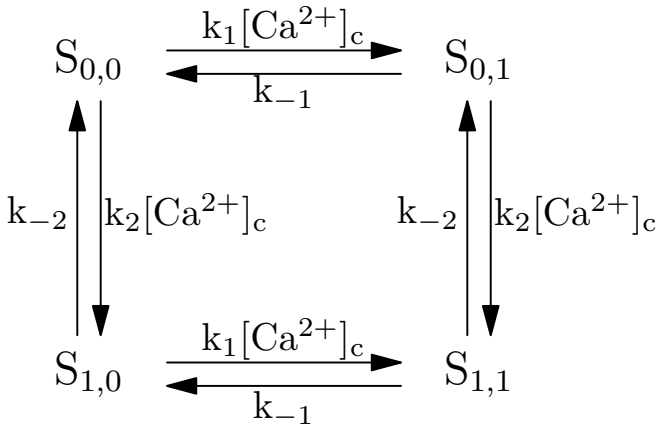

Figure 5.2: State diagram of the hemichannel model. See text for details.

subunits in the state $S_{i,j}$, the scheme in Figure 5.2 is equivalent to the following set of equations

$$\frac{dx_{0,0}}{dt} = -k_1[Ca^{2+}]_c \cdot x_{0,0} + k_{-1} \cdot x_{0,1} - k_2[Ca^{2+}]_c \cdot x_{0,0} + k_{-2} \cdot x_{1,0} \tag{5.22}$$

$$\frac{dx_{1,0}}{dt} = -k_1[Ca^{2+}]_c \cdot x_{1,0} + k_{-1} \cdot x_{1,1} + k_2[Ca^{2+}]_c \cdot x_{0,0} - k_{-2} \cdot x_{1,0} \tag{5.23}$$

$$\frac{dx_{0,1}}{dt} = k_1[Ca^{2+}]_c \cdot x_{0,0} - k_{-1} \cdot x_{0,1} - k_2[Ca^{2+}]_c \cdot x_{0,1} + k_{-2} \cdot x_{1,1} \tag{5.24}$$

$$x_{1,1} = 1 - (x_{0,0} + x_{1,0} + x_{0,1}) \tag{5.25}$$

and the open probability is given by

$$P_{HC} = \beta \cdot (x_{1,0})^{\gamma} \tag{5.26}$$

where β is a normalization constant. Values for the other parameters in equations 5.22-5.26 (Table 5.1) were selected by fitting the data of DeVuyst et al. [De Vuyst et al., 2006], see Figure 5.3.

We solved the above set of time-dependent ordinary differential equations iteratively using Euler's method [Butcher, 2008] with time step $\Delta t_{\text{ord}} = 1$ ms. The partial differential equation 5.19 was solved on a bidimensional grid with spacing $\Delta x = \Delta y = 1$ µm using the Crank-Nicholson algorithm [Crank and Nicolson, 1996] with time step $\Delta t_{\text{part}} = 10$ µs.

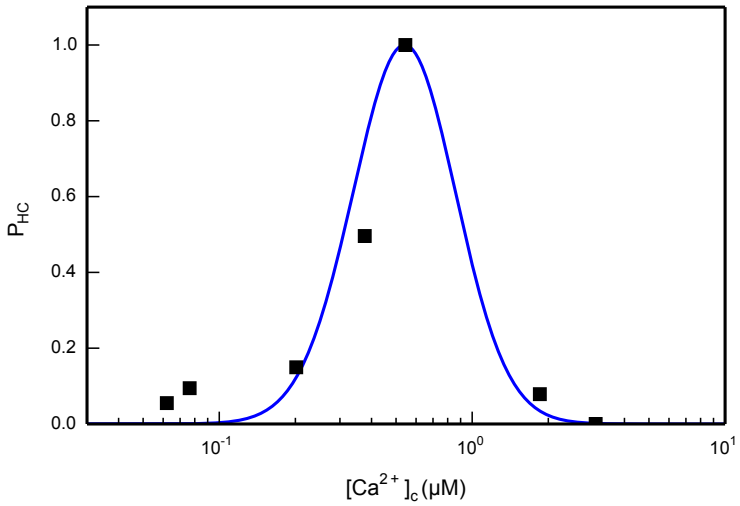

Figure 5.3: Hemichannel open probability as a function of $[Ca^{2+}]_c$. Black squares : data from [De Vuyst et al., 2006]; blue solid line: model fit (equations 5.22−5.26)

5.3 Results

5.3.1 ATP-dependent calcium oscillations in cochlear non-sensory cells can be described by a class 1 mathematical model

Ca^{2+} oscillations may or may not require oscillations of the cytosolic IP_3 concentration. Accordingly, models of Ca^{2+} dynamics have been grouped into two broad families, named Class 1 and Class 2 by Sneyd et al. [Sneyd et al., 2006]. In Class 1 models, Ca^{2+} oscillations derive solely from the properties of the IP_3R, and in particular from the bell-shaped dependence of the channel open probability on Ca^{2+} [Bezprozvanny et al., 1991]. In these models, $[Ca^{2+}]_c$ oscillations may occur at constant $[IP_3]_c$. In Class 2 models, Ca^{2+} oscillations are driven by $[IP_3]_c$ oscillations due to Ca^{2+} modulation of IP_3 levels through feedback regulation of IP_3 degradation or production [Sneyd et al., 2006].

To determine the type of mathematical model that best represents oscillatory phenomena in cochlear non-sensory cells, we adopted the protocol designed by Sneyd et al. [Sneyd et al., 2006] whereby $[Ca^{2+}]_c$ oscillations are elicited by agonist application followed by photostimulation with caged IP_3 to increase the $[IP_3]_c$ at a specific time point. If $[Ca^{2+}]_c$ oscillations do not depend on IP_3 oscillations (class 1 models) an increase in the oscillation frequency is expected. Conversely, if Ca^{2+} coscillations depend on IP_3 oscillations, a delay in the occurrence of the peak after the flash is expected [Sneyd et al., 2006]. To implement this protocol, we co-loaded cochlear organotypic cultures with Fluo-4 and caged IP_3 (see Chapter 3.9) and pressure-applied ATP (200 nM) from a glass microcapillary positioned above the sensory epithelium while imaging Fluo-4 fluores-

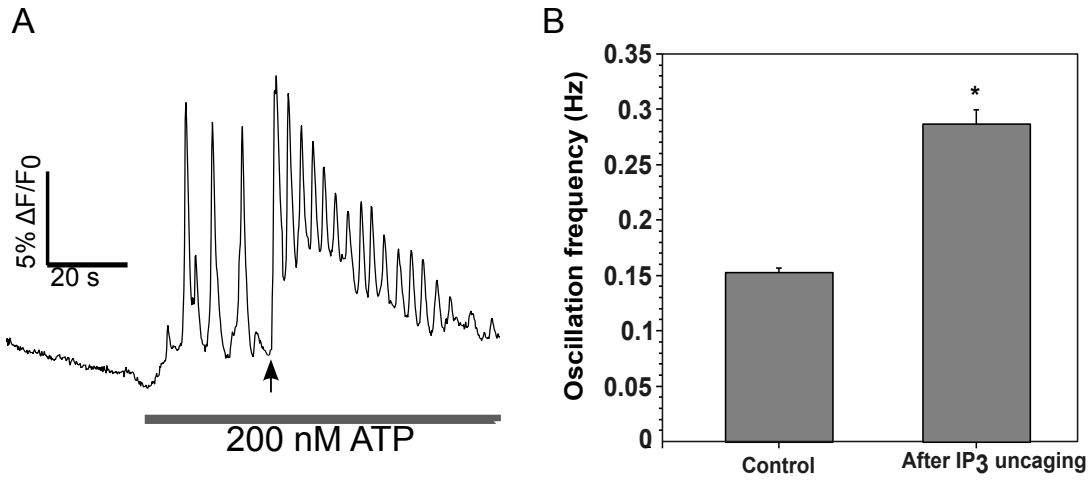

Figure 5.4: Determination of the type of mathematical model. (A) Representative trace from one cell during the application of the protocol detailed in 5.3.1. ATP (200 nM) was applied after a baseline of 20 s for all the duration of the experiment. The black arrow indicates IP_3 photoactivation by a pulse of UV light. (B) Summary of the results. An 88% increase in the mean oscillation frequency was detected after photoactivation of caged IP_3.

cence using a wide-field microscope. This procedure reliably elicited $[Ca^{2+}]_c$ oscillations, as previously reported [Majumder et al., 2010]. After a suitable time interval (40 s after starting ATP application), we activated a 365 nm light emitting diode (LED) for 400 ms to stimulate all cells in the field of view by the uncaging of IP_3 (Figure 5.4A). Following IP_3 photoactivation, we consistently detected a significant ($P<0.001$, Mann-Whitney U test) nearly two-fold increase in the frequency of $[Ca^{2+}]_c$ oscillations (Figure 5.4B, $n = 29$ cells in 3 cultures). Consistent with this result, no delay was observed in the occurrence of the first peak after photoactivation. Altogheter ,these data indicate that ATP-dependent $[Ca^{2+}]_c$ oscillations in cochlear non-sensory cells can be described by a Class 1 model [Sneyd et al., 2006].

5.3.2 Intracellular calcium oscillations are governed by a Hopf-type bifurcation

The model components we selected based on the results highlighted above, and our prior work, are summarized schematically in Figure 5.1 and described in detail in the Computational Methods section (Chapter 5.2). To fine tune model parameters, we performed a set of experiments in apical cochlear cultures from P5 mice loaded with the ratiometric Ca^{2+} reporter Fura-2.

Consistent with previous reports [Gale et al., 2004, Piazza et al., 2007], $[Ca^{2+}]_c$ oscillations were evoked only within a limited range of ATP concentration. Specifically, Ca^{2+} responses, although detectable, failed to exhibit an oscillatory character at $[ATP]_e <$

10 nM. Damped oscillations were detected between approximately 20 nM and 50 nM $[ATP]_e$. $[Ca^{2+}]_c$ oscillations could be reliably elicited in 9 out of 9 organotypic cultures between 50 nM and 1 µM $[ATP]_e$. Above this level, oscillations displayed a damped or overdamped character.

We obtained what appears a satisfactory match between experimental data and model responses (Figure 5.5A) using the set of parameter values reported in Table 5.1. We then constructed ATP dose-response curves both for the peak ATP-evoked Ca^{2+} response and for the peak-to-peak amplitude of $[Ca^{2+}]_c$ oscillations and used the model to fit experimental data (Figure 5.5B). Altogheter, these results indicate that model components represented in Figure 5.1 account for the observed behaviour with a satisfactory degree of precision.

Although only a discrete set of $[ATP]_e$ values can be tested experimentally (in a finite time), the mathematical model allowed us to explore ATP-dependent Ca^{2+} responses *in silico* over a continuum of values comprised between 1 nM and 5 µM. This analysis showed that the appearance and disappearance of $[Ca^{2+}]_c$ oscillations in a certain $[ATP]_e$ range are governed by what are technically known as supercritical Hopf bifurcations [Strogatz, 2000] (Figure 5.6) occurring at about 178 nM and 1.59 µM $[ATP]_e$.

5.3.3 The mathematical model also accounts for intercellular calcium wave propagation

As mentioned in Chapter 1.3.3, a critical component of Ca^{2+} wave propagation through the syncytium of cochlear non-sensory cells is ATP release through connexin hemichannels located at the endolimphatic surface of the epithelium. The other critical component is the cell-to-cell diffusion of IP_3, which depends on (a) the unitary permeability p_u of gap junction channels to this second messenger and (b) the number of channels (N_{ch}) that couple adjacent cell pairs.

To directly compare propagation experiments to computer simulations, we reconstructed cell network topology by laser scanning confocal imaging of actin filaments stained with Texas Red conjugated phalloidin, highlighting cell boundaries (Figure 5.7).

In a first set of experiments, we evoked radially propagating intercellular Ca^{2+} waves by focal photoactivation of caged IP_3 in cochlear cultures co-loaded with the AM ester forms of this compound and of Fluo-4 (see Methods). We applied a brief (170 ms), focalized pulse of UV light which elicited the (non-regenerative) spreading of oscillatory Ca^{2+} signals (Figure 5.9). The size of the irradiated area was estimated by measuring the dimensions of the spot carved by the focused laser into a thin film of black ink deposited on a microscope coverslip located at the front focal plane of the objective. On average, this area comprized a central cell and its six nearest neighbors (Ca^{2+} signal generators), from which radial Ca^{2+} waves propagated to 18 ± 1 cells of the culture (n=4 experiments in 3 cultures).

We then simulated the experimental conditions by imposing an increase of $[IP_3]_c$ in a group of neighboring cells (5 µM in one cell and 0.7 µM in its nearest neighbors). As previously done for the experiments, we evaluated the number of cells (N_{cells}) whose

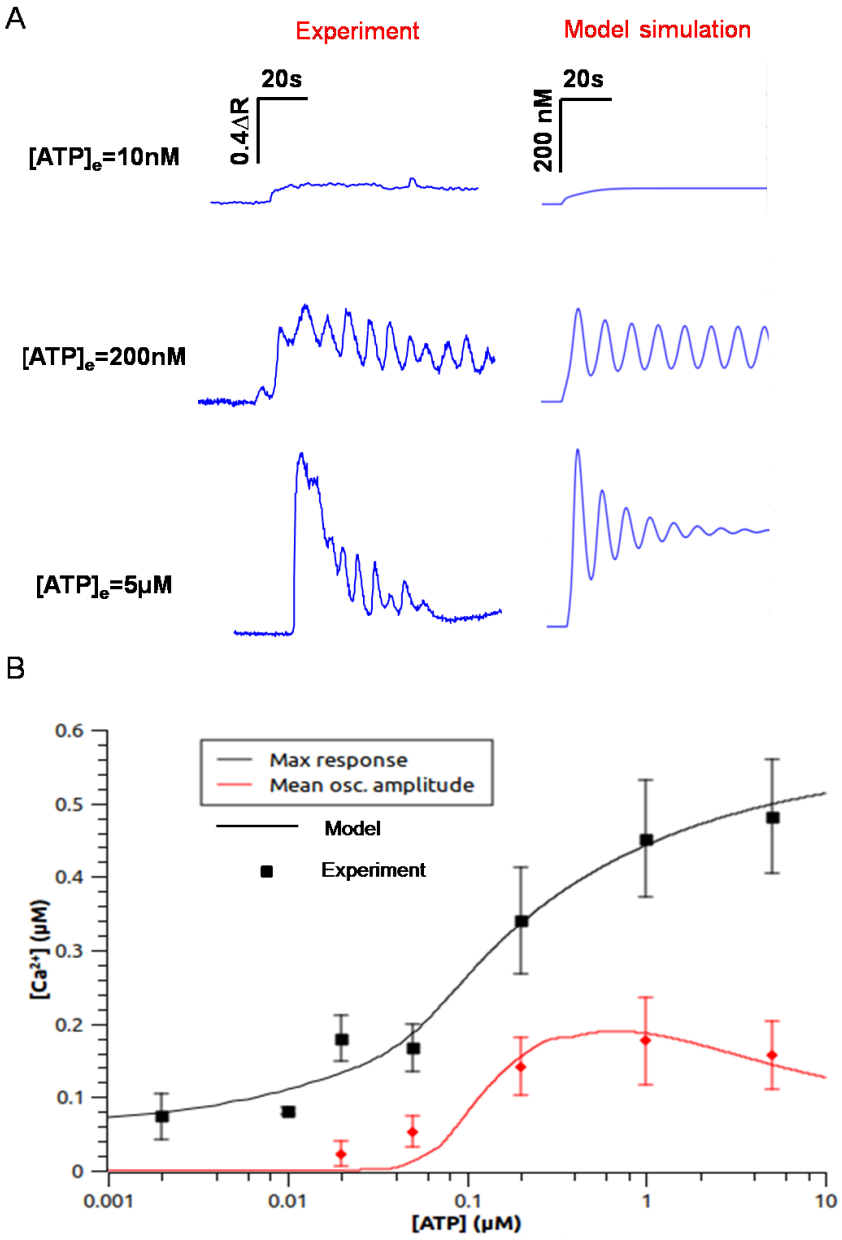

Figure 5.5: Setting of model intracellular parameters. (A) Side-by-side comparison between representative traces recorded from individual non-sensory cells and model simulations for three different concentrations of ATP. (B) The model successfully reproduced the peak of ATP-induced Ca^{2+} response (black line) and the mean oscillation amplitude (red line). Each data point represents the average response of at least 30 non-sensory cells in 3 different cultures.

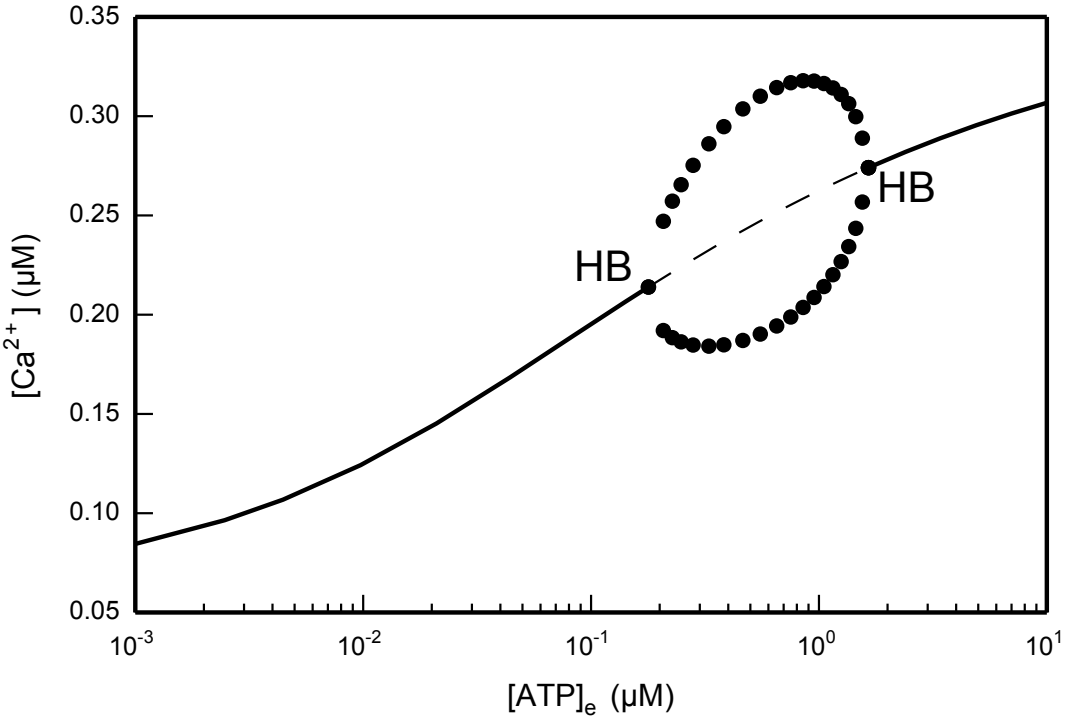

Figure 5.6: Bifurcation diagram of the model. The solid and the dashed lines indicate stable and unstable solutions of the system of differential equations, respectively. Circles indicate the amplitude of steady state oscillations. The appearance and disappearance of $[Ca^{2+}]_c$ oscillations are determined by two supercritical Hopf bifurcations (HB) at $[ATP]_e = 0.178$ µM and $[ATP]_e = 1.59$ µM

intracellullar $[Ca^{2+}]_c$ reached an arbitrary threshold value of 10% of the peak value in the flashed cell.

In the model, N_{cells} depended on the junctional conductance k_j and, therefore, on the number of gap junction channels, N_{ch}, coupling each pair of neighboring cells (see equations 5.17 and 5.18). The model reproduced the propagation range of the experiments assuming a unitary permeability to IP_3 $p_u = 72 \cdot 10^{-3}$ µm^3·s^{-1} [Hernandez et al., 2007], a cell volume $V = 3900$ µm^3 and $N_{ch} = 935$ (Figure 5.8). Of notice, this number of channels is compatible with the one estimated in our voltage imaging experiments (see Chapter 4).

Ca^{2+} waves can also be triggered by focal application of brief ATP puffs (4 µM, 50 ms) from a glass microcapillary placed in close proximity to a non-sensory cell. In this case, waves propagate radially over distances in excess of 150 µm, with a speed of 13 to 17 µm/s [Gale et al., 2004, Piazza et al., 2007]. Focal application of ATP was reproduced in the computational model by setting the ATP concentration value to 4 µM in a focal

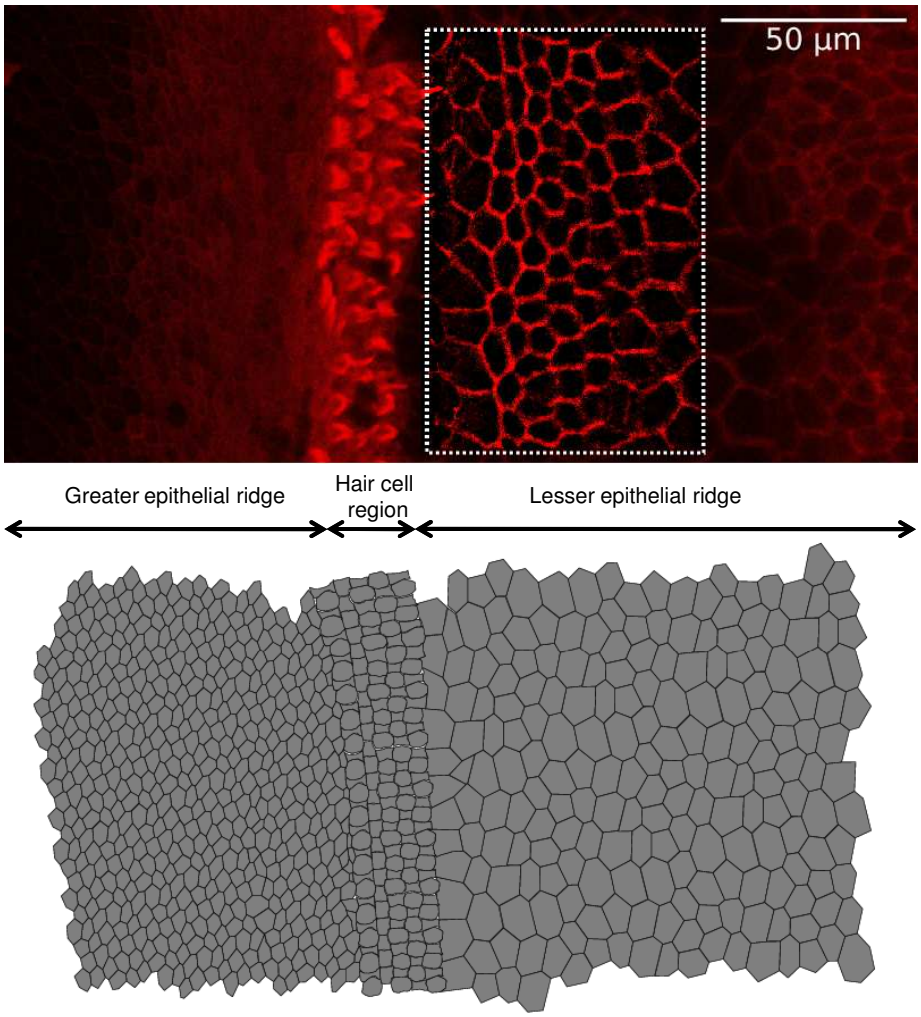

Figure 5.7: Construction of a realistic tissue morphology. We built a realistic tissue morphology starting from a confocal fluorescence image of a cochlear organotypic culture where actin filaments were stained with Texas Red conjugated phalloidin (top figure), highliting cell boundaries. Contrast was enhanced by application of an unsharp mask filter and an edge detection algorithm. Bottom figure shows the digitally reconstructed epithelium; the set of differential equations of the model (see chapter 5.2) was solved iteratively for all the cells and intercellular diffusion of IP_3 was computed for each pair of neighboring cells.

spot of 2 µm diameter for 50 ms. The propagation speed of the ensuing Ca^{2+} waves depended mainly on three model parameters: the number of gap junction channels between

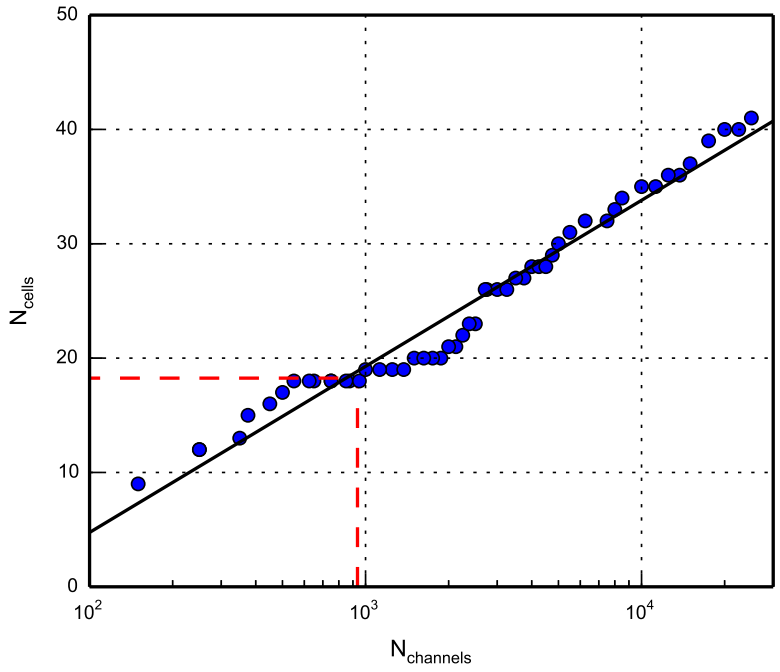

Figure 5.8: Estimation of the number of gap junction channels coupling each pair of non-sensory cells. Number of cells involved in the propagation of Ca^{2+} signals after photolitic release of IP_3 (see text for details) plotted as a function of the number N_{ch} of gap junction channels coupling each pair of non-sensory cells. The straight line through the model data points is a fit with a function $f(x) = A\log(x/B)$ where $A = 6.31$ and $B = 47.08$, The red dashed line indicates the average number of cells invaded by the Ca^{2+} signal computed from experiments, which could be reproduced by the model assuming $N_{ch} = 935$, in accord with the value determined in voltage imaging experiments (chapter 4)

neighboring cells, N_{ch}, the maximal rate of ATP release through connexin hemichannels, v_{HC}, and the ATP degradation rate by ectonucleotidases, r_{deg}^{ATP}. For the latter, data in the literature is lacking; therefore, we assumed a value in the same physiological range of other models [Warren et al., 2010, Zuo et al., 2008] (see table 5.1).

As noted previously [Gale et al., 2004], a regenerative mechanism is necessary in order to account for the constant propagation speed and the propagation range of these Ca^{2+} waves, which cannot be reproduced by a simple diffusion model from a point source (Figure 5.10A) as proposed in ref. [Arcuino et al., 2002]. The regenerative mechanism depends on ATP release through connexin hemichannel and cell-to-cell diffusion of IP_3 [Anselmi et al., 2008]. As one would expect, the propagation speed estimated by the model was an increasing function of v_{HC}; experiments could be reproduced by a

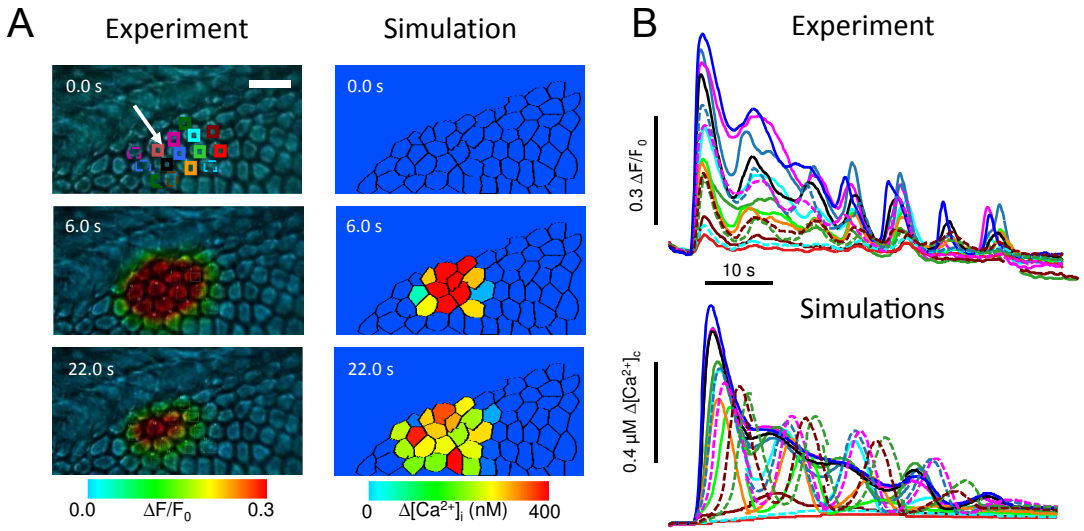

Figure 5.9: Focal photoactivation of caged IP_3. Comparison between experiments and simulations. (A) Cochlear cultures were loaded with the photoactivatable precursor of IP_3 and the propagation of Ca^{2+} signals between adiacent cells, and the insurgence of Ca^{2+} oscillations, was elicited by flashing a single cell, indicated by the white arrow, with a brief pulse of UV light. In the simulations, photolitic release of IP_3 was reproduced by increasing the value of the intracellular IP_3 concentration. (B) Time course of Ca^{2+} signals in experiments (top) and simulations (bottom) from the regions of interest shown in (A)

range of parameter values, ranging from ~ 600 µM/s to ~ 1500 µM/s (Figure 5.11).

Impairing IP_3 diffusion by setting $N_{ch} = 0$ reduced the propagation speed by 17% (Figure 5.10B), indicating that the major contributor to the long range propagation of intercellular Ca^{2+} waves in cochlear non-sensory cells is ATP release through connexin hemichannels. A side-by-side comparison between experiments and simulations is shown in Figure 5.12.

5.4 Discussion

The minimal mathematical model we present here capture the essential biochemical features of ATP- ant IP_3- dependent Ca^{2+} signaling in cochlear non-sensory cells, namely:

i the dose-response relationship between $[ATP]_e$ and $[Ca^{2+}]_c$

ii the range of values of $[ATP]_e$ which evokes $[Ca^{2+}]_c$ oscillations in non-sensory cells

iii Speed and propagation range of intercellular Ca^{2+} waves

To keep the model as simple as possible, thus minimizing the number of unknown parameters, we neglected several regulatory processes, such as Ca^{2+} modulation of IP_3

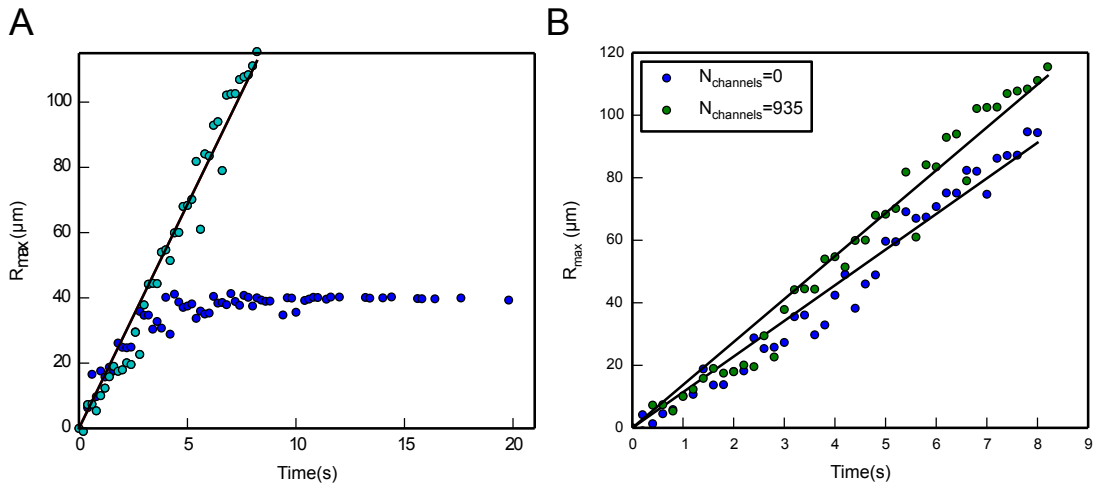

Figure 5.10: Contribution of ATP release and intercellular IP_3 propagation to the speed of ATP evoked Ca^{2+} waves. (A) Comparison between regenerative and non-regenerative mechanisms of Ca^{2+} wave propagation. Simulation of Ca^{2+} waves triggered by focal application of ATP with (cyan circles) and without (blue circles) ATP release from connexin hemichannels; the maximal radius of the wave R_{max} is plotted against the time since its onset. $v_{HC} = 600$ µM/s for the regenerative case and $v_{HC} = 0$ µM/s for the non-regenerative case. The constant speed and the propagation range of this kind of Ca^{2+} waves found in experiments [Gale et al., 2004, Piazza et al., 2007] cannot be reproduced by the simple diffusion of ATP from a point source. (B) The contribution of the intercellular diffusion of IP_3 through gap junction channels to the long range propagation of Ca^{2+} waves triggered by focal ATP application was evaluated by setting $N_{ch} = 0$ in the model; a 17% reduction of the Ca^{2+} wave speed (13.7 µm/s vs. 11.4 µm/s) was found in these conditions. $v_{HC} = 600$ µM/s

levels either through feedback regulation of IP_3 degradation or production (PLC-δ, PLC-β and PLC-γ isoenzymes, all present in cochlear non-sensory cells [Okamura et al., 2001], use Ca^{2+} as a cofactor [Fukami, 2002]). It must be noted, however, that in Class 1 models, as the one developed here, Ca^{2+} regulation of IP_3 is not required for $[Ca^{2+}]_c$ oscillations [Sneyd et al., 2006], which instead arise from the kinetics of the IP_3R. In this Class of models, Ca^{2+} can both increase and decrease the IP_3R open probability, thus Ca^{2+} oscillations are caused by sequential positive and negative feedback of Ca^{2+} on the IP_3R [De Young and Keizer, 1992, Li and Rinzel, 1994]. One important consequence is that $[Ca^{2+}]_c$ oscillations can occur at constant IP_3 values [Sneyd et al., 2006].

The physiological intracellular signals controlling hemichannel opening are currently not known. Leybaert and collaborators showed that IP_3 and downstream signals can activate hemichannel opening [Leybaert et al., 2003]; furthermore, DeVuyst et al. demonstrated that an increase of cytoplasmic calcium concentration is sufficient to trigger hemichannel opening in ECV304 cells expressing connexin32, and that the hemichannel open probability has a bell shaped relationship with $[Ca^{2+}]_c$ [De Vuyst et al., 2006]. Our

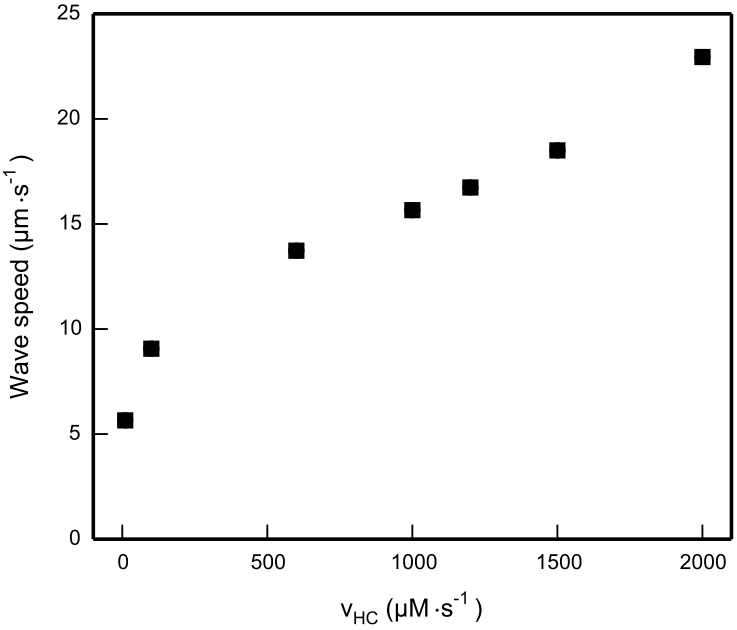

Figure 5.11: Relationship between the speed of Ca^{2+} waves triggered by focal application of ATP and the hemichannel maximal release rate. In the model, v_{HC} controls the propagation speed of Ca^{2+} waves triggered by focal application of ATP. A value of this parameter in the range $600 - 1500$ µM$\cdot s^{-1}$ could account for the wave speed observed in experiments (13 to 17 µm/s).

hemichannel model (Figure 5.2 and Figure 5.3), although oversimplified, captures these experimental results. It must be noted that a bell shaped dependence on $[Ca^{2+}]_c$ has been demonstrated for connexin32 [De Vuyst et al., 2006] and connexin43 [De Vuyst et al., 2009]; whether this mechanism occurs for connexin26 and connexin30 is currenty unknown.

In scientific fields as diverse as fluid mechanics, electronics, chemistry and theoretical ecology, performing a local bifurcation analysis (i.e. the analysis of a system of ordinary differential equations under variation of one or more parameters) is often a powerful way to predict what kind of behaviour (equilibrium, cycling) occurs. Indeed, bistability is a phenomenon common to many biological systems (see for example [Fukai et al., 2000, Fussmann, 2000, Ozbudak et al., 2004]). We show here that the appearance and disappearance of ATP-evoked Ca^{2+} oscillations in cochlear supporting cells are mathematically represented by a Hopf-type bifurcations (Figure 5.6). Interestingly, the high degree of coupling provided by gap junction channels may eventually lead to synchronization of Ca^{2+} oscillations in a vast number of cells. This might have broad implications for the encoding of information and intercellular communication.

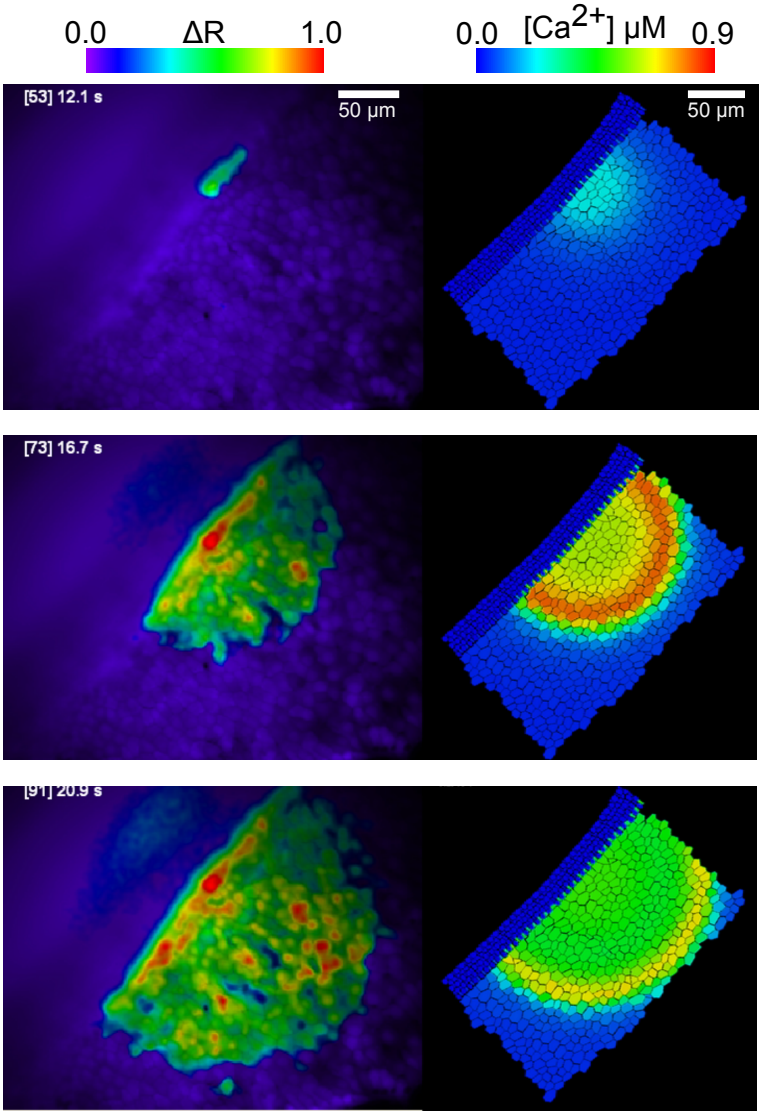

Figure 5.12: Side-by-side comparison between experiments (left column) and simulations (right column). In the simulation v_{HC} was set to 1000 µM/s

We also used our model to investigate the intercellular spreading of Ca^{2+} signals in cochlear non-sensory cells. One of the key parameters in this contest is the unitary permeability p_u for IP_3. However, the p_u for connexin26 and connexin30 heterotypic channels is not known, therefore we used that of homotypic connexin26 channels previously measured in HeLa cells [Hernandez et al., 2007]. Using voltage imaging, we estimated that non-sensory cells in the apical coil of the cochlea are coupled by 910 to 1260 open channels per cell pair (see Chapter 4). We think that it is a remarkable outcome of this thesis work

that this value is consistent with the one determined by a completely different approach ($N_{ch} = 935$) to account for the propagation range of Ca^{2+} signals evoked by photolitic release of IP_3 (Figure 5.8).

Two mechanisms are responsible for the intercellular spreading of Ca^{2+} signals in cochlear non-sensory cells: a) IP_3 diffusion through gap junction channels and b) ATP release from connexin hemichannels. One important prediction of the model is the relative contribution of this two mechanisms in the long range propagation of Ca^{2+} waves elicited by focal ATP release. In the past, these phenomena have been proposed as a mechanism to sense noise damage in the inner ear [Gale et al., 2004]. Pharmacological isolation of the two components is difficult to achieve, since no specific blocker of gap junction channels or hemichannels is known. In our model, IP_3 propagation through gap junction channels accounted for the 17% of the wave speed (Figure 5.10B). Conversely, blocking ATP release through connexin hemichannels by setting $v_{HC} = 0$ resulted in Ca^{2+} waves that remained confined in an area of ~ 40 µm diameter (Figure 5.10A). Thus, the model predicts that ATP release through connexin hemichannels is the primary mechanism responsible for the long range propagation of Ca^{2+} signals in the developing cochlea. By binding to P2Y receptors on neighboring cells, the released ATP activates PLC-dependent IP_3 production. This in turn promotes Ca^{2+} release from intracellular stores raising the cytosolic Ca^{2+} concentration up to 500 nM, which increases the hemichannel open probability, fostering further ATP-dependent ATP release in a self-regenerative cascade of biochemical reactions.

Table 5.1: Model parameters

Parameter	Unit	Description	Value	Reference
		Li-Rinzel model		
r_{rel}	s^{-1}	Maximal rate of Ca^{2+} release	1.11	[Li and Rinzel, 1994]
r_{leak}	s^{-1}	Maximal rate of Ca^{2+} leak	0.02035	[Li and Rinzel, 1994]
v_{serca}	$\mu M \cdot s^{-1}$	Maximal rate of SERCA pumps	0.9	[Li and Rinzel, 1994]
k_{serca}	μM	Ca^{2+} affinity of SERCA pumps	0.111	fitted, Fig. 5.5B
d_1	μM	IP_3 dissociation constant for the IP_3R	0.13	[Li and Rinzel, 1994]
d_2	μM	Ca^{2+} inactivation dissociation constant for the IP_3R	1.049	[Li and Rinzel, 1994]
d_3	μM	IP_3 dissociation constant for the IP_3R	0.9434	[Li and Rinzel, 1994]
d_5	μM	Ca^{2+} activation dissociation constant for the IP_3R	0.08234	[Li and Rinzel, 1994]
a_2	s^{-1}	IP_3R binding rate for Ca^{2+} inhibition	0.2	[Li and Rinzel, 1994]
α	-	Ratio between cytosol and ER volume	0.185	[Li and Rinzel, 1994]
$[Ca^{2+}]_{TOT}$	μM	Total free Ca^{2+} concentration referred to the cytosol volume	2	[Li and Rinzel, 1994]
		IP_3 subsystem		
v_{PLC}	$\mu M \cdot s^{-1}$	Maximal rate of IP_3 production by PLC	1	fitted, Fig. 5.5
k_{PLC}	μM	ATP dissociation constant	0.047155	fitted, Fig. 5.5
n_{PLC}	–	Hill exponent for ATP-dependent IP_3 production	0.3	fitted, Fig. 5.5
$r_{deg}^{IP_3}$	s^{-1}	Rate of IP_3 degradation	1.42	fitted, Fig. 5.5
p_u	$\mu m^3 \cdot s^{-1}$	Unitary IP_3 permeability of gap junction channels	72×10^{-3}	[Hernandez et al., 2007]
V	μm^3	Cell volume	3900	
N_{ch}	-	Number of channels between two adjacent supporting cells	935	fitted, Fig. 5.8
		ATP subsystem		
r_{deg}^{ATP}	s^{-1}	Rate of ATP degradation	0.01	[Zuo et al., 2008]
v_{HC}	$\mu M \cdot s^{-1}$	ATP maximal production rate	$0 - 2000$	see text
D	$\mu m^2 \cdot s^{-1}$	ATP diffusion coefficient	363	[Hubley et al., 1996]
k_1	$\mu M^{-1} \cdot s^{-1}$	hemichannel model constant	8.9	fitted, Fig. 5.3
k_2	$\mu M^{-1} \cdot s^{-1}$	hemichannel model constant	5.0	fitted, Fig. 5.3
k_{-1}	s^{-1}	hemichannel model constant	5.8	fitted, Fig. 5.3
k_{-2}	s^{-1}	hemichannel model constant	3.2	fitted, Fig. 5.3
γ	-	hemichannel model constant	9	fitted, Fig. 5.3

6 Ongoing work: spontaneous activity in sensory and non-sensory cells of the developing cochlea

6.1 Introduction

It is well established that immature inner hair cells (IHCs) transiently generate Ca^{2+} action potentials (APs) before the onset of hearing (at around postnatal day 12 in most rodents) [Marcotti, 2012]. The periodic increase in intracellular Ca^{2+} associated with this firing activity in immature IHCs, which is known to regulate gene expression in other cells (particularly neurons), is thought to control the maturation of the mammalian cochlea and therefore it is crucial for sound acquisition [Kros et al., 1998, Kandler et al., 2009]. The evidence that signaling from non-sensory cells could directly influence IHC firing activity, and so cochlear development, has generated a lot of interest within the hearing community with several recent publications [Tritsch et al., 2007, Tritsch and Bergles, 2010, Johnson et al., 2011b, Johnson et al., 2012]. However, the specific contribution of ATP on IHC electrical activity is still hotly debated. Some studies have proposed that waves of ATP from cochlear non-sensory cells transiently depolarize immature IHCs causing them to generate action potentials (AP origin mechanism) [Tritsch et al., 2007, Tritsch and Bergles, 2010]. By synchronizing the output of neighboring IHCs, this ATP–mediated firing activity in IHCs is proposed to play a specific role in the postnatal refinement of synaptic connections to/from the brain [Tritsch et al., 2007, Tritsch and Bergles, 2010]. Other recent studies have instead shown that: a) Ca^{2+} APs are intrinsically generated by IHCs; b) endogenous ATP modulates the frequency and/or pattern of IHC intrinsic electrical activity (AP modulating mechanism) [Johnson et al., 2011b, Johnson et al., 2012].

In order to define how connexins influence sensory hair cell function via ATP-dependent Ca^{2+} signaling, we complemented single-cell electrophysiological recordings (performed by Dr. Stewart Johnon and Prof. Walter Marcotti, University of Sheffield, UK) with non-invasive large scale optical imaging using the confocal microscopy system developed in our laboratory and described in detail in section 3.10, which enables data collection from vast population of cells at high spatial and temporal resolution.

6.2 Preliminary results

In order to validate whether ATP release by non-sensory cells is required for the origin (AP origin mechanism) or modulation (AP modulating mechanism) of AP activity in IHCs, we performed simultaneous Ca^{2+} imaging from cochlear non-sensory cells and extracellular recordings in the cell–attached mode under voltage–clamp from IHCs (Figure 6.1A). Cell-attached patch clamp recording has the advantage, compared to the more classical whole–cell technique, of preserving the intracellular milieu including the endogenous Ca^{2+} buffers. These recordings tend to be more stable and long–lasting (>10min), which is essential when investigating the frequency and pattern of action potential activity. For these experiments, the patch pipette contained extracellular solution, instead of the normal K^+–based intracellular solution, and the pipette potential was set to 0 mV.

Cochlear explants were obtained from mice during the first postnatal week, loaded with the Ca^{2+} dye Fluo-4 acetoxymethyl ester (16 µM, see Chapter 3) and maintained at 37°C in a perilymph–like extracellular solution (1.3 mM Ca^{2+} and 5.8 mM K^+) throughout the experiment.

In these conditions, we detected action potentials from IHCs even in the absence of detectable Ca^{2+} waves in nearby non-sensory cells (Figure 6.1B and 6.2A), therefore confirming that spontaneous activity is intrinsically generated in IHCs during development [Johnson et al., 2011b]. Furthermore, we found an increase in the frequency of action potentials in IHCs during spontaneous Ca^{2+} activity in supporting cells (Figure 6.2B).

We performed cross correlation analysis between the Ca^{2+} signals detected from a region of interest of ~ 700 µm^s in the proximity of the patched cell and the firing rate of the IHC (see Chapter 3.11). We found a significative increase of the frequency of action potentials in IHCs during spontaneous Ca^{2+} activity in supporting cells (frequency of APs correlated to Ca^{2+} signals: 5.5 ± 0.09 Hz, n=1500 events; frequency of APs uncorrelated to Ca^{2+} signals: 3.4 ± 0.12 Hz, n=589 events, $P<0.001$, Mann-Whitney U test.), which suggests that endogenous ATP has a modulating effect on IHC intrinsic electrical activity (AP modulating mechanism) [Johnson et al., 2011b, Johnson et al., 2012].

6.3 Discussion and future perspectives

Overall, these preliminary data support the hypothesis that inner hair cells are intrinsically active during development and calcium waves in non-sensory cells are not required to trigger calcium APs in inner hair cells [Johnson et al., 2011b]; however, calcium waves may modulate AP firing rate in inner hair cell. This suggests that extracellular ATP could be involved in setting the different pattern of AP activity along the cochlea, a role currently ascribed only to the inhibitory efferent system [Johnson et al., 2011b] .

We already have evidence that alteration in Ca^{2+} signaling due to impairment of the PLC- and IP_3- dependent cascade described in this thesis ensues in defects of hearing acquisition [Schutz et al., 2010, Rodriguez et al., 2012]. Investigating the physiological

mechanisms that link Ca^{2+} signaling in non-sensory cells to IHC function and development will be essential to understand the pathophysiology of DFNB1 and, in a broader perspective, to uncover critical determinants of cochlear development and hearing acquisition.

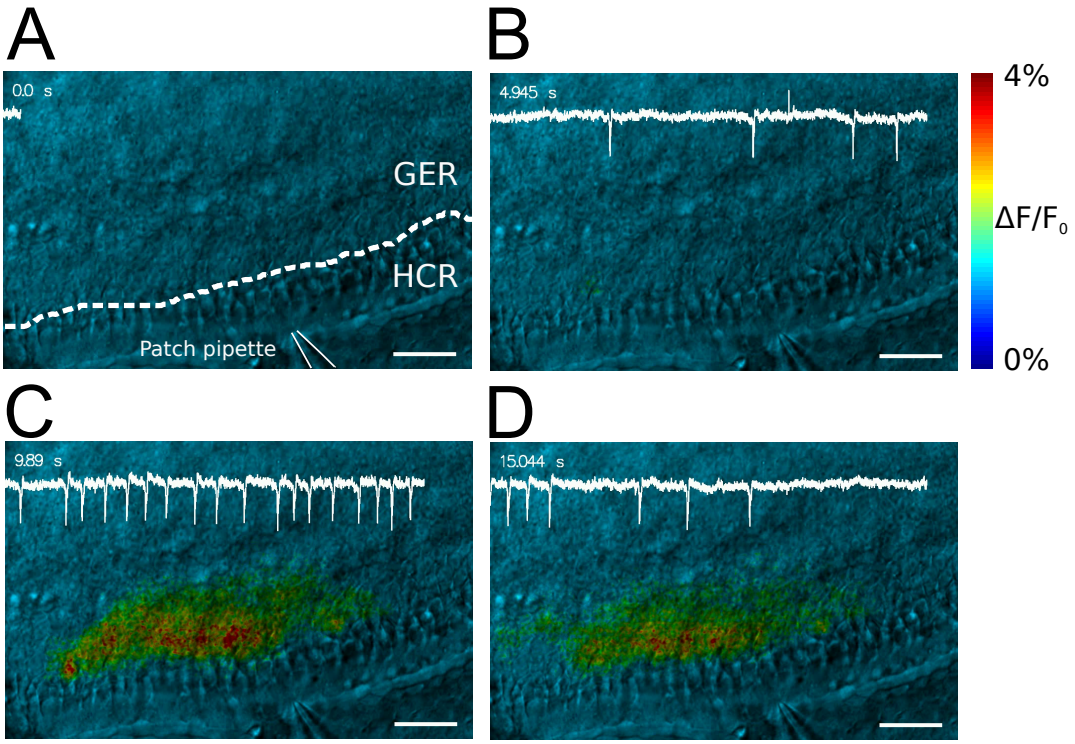

Figure 6.1: Simultaneous recording of inner hair cell and non-sensory cells spontaneous activity. Four selected frames from the same image sequence. (A) The IHC was approached with the patch pipette from the outer hair cell side, in order to avoid the disruption of the epithelium in the non-sensory cell region. The IHC exhibited basal spontaneous electrical activity (white trace) (B) whose frequency increased when a Ca^{2+} wave was detected in nearby non-sensory cells (C). (D) The firing rate decreased towards baseline values at the end of the Ca^{2+} signal. GER: greater epithelial ridge; HCR: hair cell region. Scale bar: 25 µm

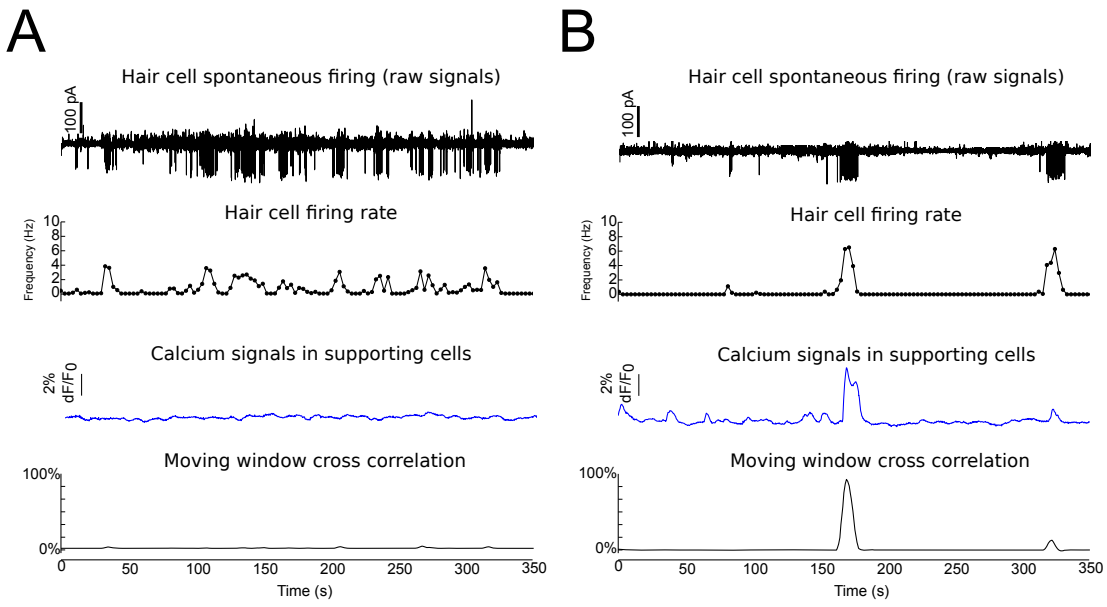

Figure 6.2: Cross-correlation analysis. (A) Representative trace from one recording in which the IHC exhibited spontaneous electrical activity, while no spontaneous Ca^{2+} activity was detected in neighboring supporting cells. (B) Recording from one IHC whose electrical activity exhibited a high degree of correlation with spontaneous Ca^{2+} signals in nearby cochlear non-sensory cells.

Bibliography

[Adelman et al., 2012] Adelman, J. P., Maylie, J., and Sah, P. (2012). Small-conductance Ca2+-activated K+channels: form and function. *Annu Rev Physiol*, 74:245–269.

[Agulhon et al., 2008] Agulhon, C., Petravicz, J., McMullen, A. B., Sweger, E. J., Minton, S. K., Taves, S. R., Casper, K. B., Fiacco, T. A., and McCarthy, K. D. (2008). What Is the Role of Astrocyte Calcium in Neurophysiology? *Neuron*, 59(6):932–946.

[Ahmad et al., 2003] Ahmad, S., Chen, S., Sun, J., and Lin, X. (2003). Connexins 26 and 30 are co-assembled to form gap junctions in the cochlea of mice. *Biochem Biophys Res Commun*, 307:362–368.

[Ahmed et al., 2003] Ahmed, Z. M., Riazuddin, S., Ahmad, J., Bernstein, S. L., Guo, Y., Sabar, M. F., Sieving, P., Griffith, A. J., Friedman, T. B., Belyantseva, I. A., and Wilcox, E. R. (2003). PCDH15 is expressed in the neurosensory epithelium of the eye and ear and mutant alleles are responsible for both USH1F and DFNB23. *Hum Mol Genet*, 12:3215–3223.

[Alagramam et al., 2011] Alagramam, K. N., Goodyear, R. J., Geng, R., Furness, D. N., van Aken, A. F., Marcotti, W., Kros, C. J., and Richardson, G. P. (2011). Mutations in protocadherin 15 and cadherin 23 affect tip links and mechanotransduction in mammalian sensory hair cells. *PLoS One*, 6:e19183.

[Anselmi et al., 2008] Anselmi, F., Hernandez, V. H., Crispino, G., Seydel, A., Ortolano, S., Roper, S. D., Kessaris, N., Richardson, W., Rickheit, G., Filippov, M. a., Monyer, H., and Mammano, F. (2008). ATP release through connexin hemichannels and gap junction transfer of second messengers propagate Ca2+ signals across the inner ear. *Proc Natl Acad Sci USA*, 105(48):18770–18775.

[Apicella et al., 1997] Apicella, S., Chen, S., Bing, R., Penniston, J. T., Llinas, R., and Hillman, D. E. (1997). Plasmalemmal ATPase calcium pump localizes to inner and outer hair bundles. *Neuroscience*, 79:1145–1151.

[Appler and Goodrich, 2011] Appler, J. M. and Goodrich, L. V. (2011). Connecting the ear to the brain: Molecular mechanisms of auditory circuit assembly. *Prog Neurobiol*, 93:488–508.

[Arcuino et al., 2002] Arcuino, G., Lin, J. H., Takano, T., Liu, C., Jiang, L., Gao, Q., Kang, J., and Nedergaard, M. (2002). Intercellular calcium signaling mediated by point-source burst release of ATP. *Proc. Natl. Acad. Sci.*, 99(15):9840.

[Ashmore, 2008] Ashmore, J. (2008). Cochlear outer hair cell motility. *Physiol Rev*, 88:173–210.

[Ashmore, 2011] Ashmore, J. (2011). Pushing the envelope of sound. *Neuron*, 70:1021–1022.

[Assad et al., 1991] Assad, J. A., Shepherd, G. M., and Corey, D. P. (1991). Tip-link integrity and mechanical transduction in vertebrate hair cells. *Neuron*, 7:985–994.

[Beltramello et al., 2003] Beltramello, M., Bicego, M., Piazza, V., Ciubotaru, C. D., Mammano, F., and D'Andrea, P. (2003). Permeability and gating properties of human connexins 26 and 30 expressed in HeLa cells. *Biochem Biophys Res Commun*, 305:1024–1033.

[Beltramello et al., 2005] Beltramello, M., Piazza, V., Bukauskas, F. F., Pozzan, T., and Mammano, F. (2005). Impaired permeability to Ins(1,4,5)P3 in a mutant connexin underlies recessive hereditary deafness. *Nat Cell Biol*, 7:63–69.

[Belyantseva et al., 2003] Belyantseva, I. A., Boger, E. T., and Friedman, T. B. (2003). Myosin XVa localizes to the tips of inner ear sensory cell stereocilia and is essential for staircase formation of the hair bundle. *Proc Natl Acad Sci U S A*, 100:13958–13963.

[Bennett et al., 2003] Bennett, M. V., Contreras, J. E., Bukauskas, F. F., and Sáez, J. C. (2003). New roles for astrocytes: gap junction hemichannels have something to communicate. *Trends Neurosci.*, 26(11):610–617.

[Berridge and Galione, 1988] Berridge, M. and Galione, A. (1988). Cytosolic calcium oscillators. *FASEB J*, 2(15):3074–3082.

[Berridge, 1997] Berridge, M. J. (1997). The AM and FM of calcium signalling. *Nature*, 386:759–760.

[Berridge et al., 2003] Berridge, M. J., Bootman, M. D., and Roderick, H. L. (2003). Calcium signalling: dynamics, homeostasis and remodelling. *Nat Rev Mol Cell Biol*, 4:517–529.

[Beurg et al., 2009] Beurg, M., Fettiplace, R., Nam, J.-H. H., and Ricci, A. J. (2009). Localization of inner hair cell mechanotransducer channels using high-speed calcium imaging. *Nat Neurosci*, 12(5):553–558.

[Beurg et al., 2005] Beurg, M., Hafidi, A., Skinner, L. J., Ruel, J., Nouvian, R., Henaff, M., Puel, J. L., Aran, J. M., and Dulon, D. (2005). Ryanodine receptors and BK channels act as a presynaptic depressor of neurotransmission in cochlear inner hair cells. *Eur J Neurosci*, 22:1109–1119.

[Beurg et al., 2010a] Beurg, M., Michalski, N., Safieddine, S., Bouleau, Y., Schneggenburger, R., Chapman, E. R., Petit, C., and Dulon, D. (2010a). Control of exocytosis by synaptotagmins and otoferlin in auditory hair cells. *J Neurosci*, 30:13281–13290.

[Beurg et al., 2010b] Beurg, M., Nam, J. H., Chen, Q., and Fettiplace, R. (2010b). Calcium balance and mechanotransduction in rat cochlear hair cells. *J Neurophysiol*, 104(1):18–34.

[Beurg et al., 2008] Beurg, M., Safieddine, S., Roux, I., Bouleau, Y., Petit, C., and Dulon, D. (2008). Calcium- and otoferlin-dependent exocytosis by immature outer hair cells. *J Neurosci*, 28(8):1798–1803.

[Beutner and Moser, 2001] Beutner, D. and Moser, T. (2001). The presynaptic function of mouse cochlear inner hair cells during development of hearing. *J. Neurosci.*, 21(13):4593.

[Beutner et al., 2001] Beutner, D., Voets, T., Neher, E., and Moser, T. (2001). Calcium dependence of exocytosis and endocytosis at the cochlear inner hair cell afferent synapse. *Neuron*, 29(3):681–690.

[Bezprozvanny et al., 1991] Bezprozvanny, I., Watras, J., and Ehrlich, B. E. (1991). Bell-shaped calcium-response curves of Ins (1, 4, 5) P3-and calcium-gated channels from endoplasmic reticulum of cerebellum. *Nature*, 351(6329):751–754.

[Bicego et al., 2006] Bicego, M., Beltramello, M., Melchionda, S., Carella, M., Piazza, V., Zelante, L., Bukauskas, F. F., Arslan, E., Cama, E., and Pantano, S. (2006). Pathogenetic role of the deafness-related M34T mutation of Cx26. *Hum Mol Genet*, 15:2569–2587.

[Boeda et al., 2002] Boeda, B., El-Amraoui, A., Bahloul, A., Goodyear, R., Daviet, L., Blanchard, S., Perfettini, I., Fath, K. R., Shorte, S., and Reiners, J. (2002). Myosin VIIa, harmonin and cadherin 23, three Usher I gene products that cooperate to shape the sensory hair cell bundle. *EMBO J*, 21:6689–6699.

[Boettger et al., 2002] Boettger, T., Hubner, C. A., Maier, H., Rust, M. B., Beck, F. X., and Jentsch, T. J. (2002). Deafness and renal tubular acidosis in mice lacking the K-Cl co-transporter Kcc4. *Nature*, 416(6883):874–878.

[Bolz et al., 2001] Bolz, H., von Brederlow, B., Ramirez, A., Bryda, E. C., Kutsche, K., Nothwang, H. G., Seeliger, M., del CSCM, Vila, M. C., and Molina, O. P. (2001). Mutation of CDH23, encoding a new member of the cadherin gene family, causes Usher syndrome type 1D. *Nat Genet*, 27:108–112.

[Bork et al., 2001] Bork, J. M., Peters, L. M., Riazuddin, S., Bernstein, S. L., Ahmed, Z. M., Ness, S. L., Polomeno, R., Ramesh, A., Schloss, M., and Srisailpathy, C. R. (2001). Usher syndrome 1D and nonsyndromic autosomal recessive deafness DFNB12 are caused by allelic mutations of the novel cadherin-like gene CDH23. *Am J Hum Genet*, 68:26–37.

[Bortolozzi et al., 2010] Bortolozzi, M., Brini, M., Parkinson, N., Crispino, G., Scimemi, P., De Siati, R. D., Di Leva, F., Parker, A., Ortolano, S., Arslan, E., Brown, S. D.,

Carafoli, E., and Mammano, F. (2010). The novel PMCA2 pump mutation Tommy impairs cytosolic calcium clearance in hair cells and links to deafness in mice. *J. Biol. Chem.*, 285(48):37693–37703.

[Bortolozzi et al., 2008] Bortolozzi, M., Lelli, A., and Mammano, F. (2008). Calcium microdomains at presynaptic active zones of vertebrate hair cells unmasked by stochastic deconvolution. *Cell Calcium*, 44(2):158–168.

[Bosher and Warren, 1978] Bosher, S. K. and Warren, R. L. (1978). Very low calcium content of cochlear endolymph, an extracellular fluid. *Nature*, 273(5661):377–378.

[Brandt et al., 2005] Brandt, A., Khimich, D., and Moser, T. (2005). Few CaV1.3 channels regulate the exocytosis of a synaptic vesicle at the hair cell ribbon synapse. *J Neurosci*, 25:11577–11585.

[Brandt et al., 2003] Brandt, A., Striessnig, J., and Moser, T. (2003). CaV1. 3 channels are essential for development and presynaptic activity of cochlear inner hair cells. *J. Neurosci.*, 23(34):10832.

[Brandt et al., 2007] Brandt, N., Kuhn, S., Munkner, S., Braig, C., Winter, H., Blin, N., Vonthein, R., Knipper, M., and Engel, J. (2007). Thyroid hormone deficiency affects postnatal spiking activity and expression of Ca2+ and K+channels in rodent inner hair cells. *J Neurosci*, 27:3174–3186.

[Bruce et al., 2000] Bruce, L. L., Christensen, M. A., and Warr, W. B. (2000). Postnatal development of efferent synapses in the rat cochlea. *J Comp Neurol*, 423:532–548.

[Bruzzone et al., 2003] Bruzzone, R., Veronesi, V., Gomes, D., Bicego, M., Duval, N., Marlin, S., Petit, C., D'Andrea, P., and White, T. W. (2003). Loss-of-function and residual channel activity of connexin26 mutations associated with non-syndromic deafness. *FEBS Lett*, 533:79–88.

[Bukauskas et al., 2000] Bukauskas, F. F., Jordan, K., Bukauskiene, A., Bennett, M. V., Lampe, P. D., Laird, D. W., and Verselis, V. K. (2000). Clustering of connexin 43-enhanced green fluorescent protein gap junction channels and functional coupling in living cells. *Proc Natl Acad Sci USA*, 97:2556–2561.

[Bukauskas and Verselis, 2004] Bukauskas, F. F. and Verselis, V. K. (2004). Gap junction channel gating. *Biochim Biophys Acta*, 1662:42–60.

[Bulankina and Moser, 2012] Bulankina, A. V. and Moser, T. (2012). Neural circuit development in the Mammalian cochlea. *Physiol.*, 27:100–112.

[Burgess et al., 1997] Burgess, B. J., Adams, J. C., and Nadol Jr., J. B. (1997). Morphologic evidence for innervation of Deiters' and Hensen's cells in the guinea pig. *Hear Res*, 108(1-2):74–82.

[Butcher, 2008] Butcher, J. C. (2008). *Numerical Methods for Ordinary Differential Equations*. Wiley.

[Ceriani and Mammano, 2012] Ceriani, F. and Mammano, F. (2012). Calcium signaling in the cochlea - Molecular mechanisms and physiopathological implications. *Cell Commun. Signal.*, 10(1):20.

[Ceriani and Mammano, 2013] Ceriani, F. and Mammano, F. (2013). A rapid and sensitive assay of intercellular coupling by voltage imaging of gap junction networks. *Cell Commun. Signal.*, 11(1):78.

[Chang et al., 2008] Chang, Q., Tang, W., Ahmad, S., Zhou, B., and Lin, X. (2008). Gap junction mediated intercellular metabolite transfer in the cochlea is compromised in connexin30 null mice. *PLoS One*, 3:e4088.

[Cheung and Corey, 2006] Cheung, E. L. and Corey, D. P. (2006). Ca2+ changes the force sensitivity of the hair-cell transduction channel. *Biophys J*, 90:124–139.

[Clair et al., 2008] Clair, C., Combettes, L., Pierre, F., Sansonetti, P., and Tran Van Nhieu, G. (2008). Extracellular-loop peptide antibodies reveal a predominant hemichannel organization of connexins in polarized intestinal cells. *Exp Cell Res*, 314:1250–1265.

[Cohen-Salmon et al., 2005] Cohen-Salmon, M., del Castillo, F. J., and Petit, C. (2005). Connexins Responsiblbe for Hereditary Deafness - The Tale Unfolds. *Gap Junctions Dev. Dis.*, pages 111–134.

[Cohen-Salmon et al., 2002] Cohen-Salmon, M., Ott, T., Michel, V., Hardelin, J. P., Perfettini, I., Eybalin, M., Wu, T., Marcus, D. C., Wangemann, P., Willecke, K., and Others (2002). Targeted ablation of connexin26 in the inner ear epithelial gap junction network causes hearing impairment and cell death. *Curr. Biol.*, 12(13):1106–1111.

[Cohen-Salmon et al., 2007] Cohen-Salmon, M., Regnault, B., Cayet, N., Caille, D., Demuth, K., Hardelin, J. P., Janel, N., Meda, P., and Petit, C. (2007). Connexin30 deficiency causes instrastrial fluid-blood barrier disruption within the cochlear stria vascularis. *Proc Natl Acad Sci U S A*, 104:6229–6234.

[Corey and Hudspeth, 1983] Corey, D. and Hudspeth, A. (1983). Kinetics of the receptor current in bullfrog saccular hair cells. *J. Neurosci.*, 3(5):962–976.

[Cova et al., 1979] Cova, S., Longoni, A., and Freitas, I. (1979). Versatile digital lock-in detection technique: application to spectrofluorometry and other fields. *Rev Sci Instrum*, 50:296.

[Crank and Nicolson, 1996] Crank, J. and Nicolson, P. (1996). A practical method for numerical evaluation of solutions of partial differential equations of the heat-conduction type. *Adv. Comput. Math.*, 6(1):207–226.

[Crawford et al., 1991] Crawford, A., Evans, M., and Fettiplace, R. (1991). The actions of calcium on the mechano-electrical transducer current of turtle hair cells. *J. Physiol.*, 434(1):369.

[Crispino et al., 2011] Crispino, G., Di Pasquale, G., Scimemi, P., Rodriguez, L., Galindo Ramirez, F., De Siati, R. D., Santarelli, R. M., Arslan, E., Bortolozzi, M., Chiorini, J. A., and Mammano, F. (2011). BAAV mediated GJB2 gene transfer restores gap junction coupling in cochlear organotypic cultures from deaf Cx26Sox10Cre mice. *PLoS One*, 6:e23279.

[Cui et al., 2007] Cui, G., Meyer, A. C., Calin-Jageman, I., Neef, J., Haeseleer, F., Moser, T., and Lee, A. (2007). Ca2+-binding proteins tune Ca2+-feedback to Cav1.3 channels in mouse auditory hair cells. *J Physiol*, 585:791–803.

[Dallos, 2008] Dallos, P. (2008). Cochlear amplification, outer hair cells and prestin. *Curr Opin Neurobiol*, 18(4):370–376.

[Dallos et al., 1997] Dallos, P., He, D. Z., Lin, X., Sziklai, I., Mehta, S., and Evans, B. N. (1997). Acetylcholine, outer hair cell electromotility, and the cochlear amplifier. *J Neurosci*, 17:2212–2226.

[Davies et al., 2013] Davies, R., Graham, J., and Canepari, M. (2013). Light sources and cameras for standard in vitro membrane potential and high-speed ion imaging. *J Microsc*, 251:5–13.

[De Pittà et al., 2009] De Pittà, M., Goldberg, M., Volman, V., Berry, H., and Ben-Jacob, E. (2009). Glutamate regulation of calcium and IP3 oscillating and pulsating dynamics in astrocytes. *J. Biol. Phys.*, 35(4):383–411.

[De Vuyst et al., 2006] De Vuyst, E., Decrock, E., Cabooter, L., Dubyak, G. R., Naus, C. C., Evans, W. H., and Leybaert, L. (2006). Intracellular calcium changes trigger connexin 32 hemichannel opening. *EMBO J*, 25(1):34–44.

[De Vuyst et al., 2009] De Vuyst, E., Wang, N., Decrock, E., De Bock, M., Vinken, M., Van Moorhem, M., Lai, C., Culot, M., Rogiers, V., Cecchelli, R., Naus, C. C., Evans, W. H., and Leybaert, L. (2009). Ca(2+) regulation of connexin 43 hemichannels in C6 glioma and glial cells. *Cell Calcium*, 46(3):176–87.

[De Young and Keizer, 1992] De Young, G. W. and Keizer, J. (1992). A single-pool inositol 1,4,5-trisphosphate-receptor-based model for agonist-stimulated oscillations in Ca2+ concentration. *Proc. Natl. Acad. Sci. U. S. A.*, 89(20):9895–9899.

[Decrock et al., 2011] Decrock, E., Krysko, D. V., Vinken, M., Kaczmarek, A., Crispino, G., Bol, M., Wang, N., De Bock, M., De Vuyst, E., Naus, C. C., Rogiers, V., Vandenabeele, P., Erneux, C., Mammano, F., Bultynck, G., and Leybaert, L. (2011). Transfer of IP(3) through gap junctions is critical, but not sufficient, for the spread of apoptosis. *Cell Death Differ*, 19(6):947–957.

[Defourny et al., 2011] Defourny, J., Lallemend, F., and Malgrange, B. (2011). Structure and development of cochlear afferent innervation in mammals. *Am J Physiol Cell Physiol*, 301(4):C750–61.

[del Castillo and del Castillo, 2011] del Castillo, F. J. and del Castillo, I. (2011). The DFNB1 subtype of autosomal recessive non-syndromic hearing impairment. *Front Biosci*, 16:3252–3274.

[Di Virgilio, 1989] Di Virgilio, F. S. T. S. S. (1989). Ca2+ with Fura-2. *Methods Cell Biol.*

[Dolmetsch et al., 1997] Dolmetsch, R. E., Lewis, R. S., Goodnow, C. C., and Healy, J. I. (1997). Differential activation of transcription factors induced by Ca2+ response amplitude and duration. *Nature*, 386:855–858.

[Dolmetsch et al., 1998] Dolmetsch, R. E., Xu, K., and Lewis, R. S. (1998). Calcium oscillations increase the efficiency and specificity of gene expression. *Nature*, 392:933–936.

[Drescher et al., 1997] Drescher, M., Khan, K., Beisel, K., Karadaghy, A., Hatfield, J., Kim, S., Drescher, A., Lasak, J., Barretto, R., Shakir, A., and Others (1997). Expression of adenylyl cyclase type I in cochlear inner hair cells. *Mol. brain Res.*, 45(2):325–330.

[Dumont et al., 2001] Dumont, R. A., Lins, U., Filoteo, A. G., Penniston, J. T., Kachar, B., and Gillespie, P. G. (2001). Plasma membrane Ca2+-ATPase isoform 2a is the PMCA of hair bundles. *J Neurosci*, 21:5066–5078.

[Dumont et al., 2002] Dumont, R. A., Zhao, Y. D., Holt, J. R., Bahler, M., and Gillespie, P. G. (2002). Myosin-I isozymes in neonatal rodent auditory and vestibular epithelia. *J Assoc Res Otolaryngol*, 3:375–389.

[Eggston and Wolff, 1947] Eggston, A. A. and Wolff, D. (1947). Embryology of the ear. *Histopathol. ear, nose, throat.*, pages 37–64.

[Ehret, 1977] Ehret, G. (1977). Postnatal development in the acoustic system of the house mouse in the light of developing masked thresholds. *J. Acoust. Soc. Am.*, 62(1):143–148.

[Ek-Vitorin et al., 2006] Ek-Vitorin, J. F., King, T. J., Heyman, N. S., Lampe, P. D., and Burt, J. M. (2006). Selectivity of connexin 43 channels is regulated through protein kinase C-dependent phosphorylation. *Circ Res*, 98:1498–1505.

[Elledge et al., 2010] Elledge, H. M., Kazmierczak, P., Clark, P., Joseph, J. S., Kolatkar, A., Kuhn, P., and Muller, U. (2010). Structure of the N terminus of cadherin 23 reveals a new adhesion mechanism for a subset of cadherin superfamily members. *Proc Natl Acad Sci U S A*, 107:10708–10712.

[Evans et al., 2000] Evans, M. G., Lagostena, L., Darbon, P., and Mammano, F. (2000). Cholinergic control of membrane conductance and intracellular free Ca2+ in outer hair cells of the guinea pig cochlea. *Cell Calcium*, 28:195–203.

[Evans et al., 2006] Evans, W. H., De Vuyst, E., and Leybaert, L. (2006). The gap junction cellular internet: connexin hemichannels enter the signalling limelight. *Biochem J*, 397:1–14.

[Fechner et al., 2001] Fechner, F. P., Nadol, J. J., Burgess, B. J., and Brown, M. C. (2001). Innervation of supporting cells in the apical turns of the guinea pig cochlea is from type II afferent fibers. *J Comp Neurol*, 429(2):289–298.

[Fettiplace and Ricci, 2003] Fettiplace, R. and Ricci, A. J. (2003). Adaptation in auditory hair cells. *Curr. Opin. Neurobiol.*, 13(4):446–451.

[Fettiplace et al., 2006] Fettiplace, R., Ricci, A. J., Fay, R. R., and Popper, A. N. (2006). Mechanoelectrical transduction in auditory hair cells. In Eatock, R. A., Fay, R. R., and Popper, A. N., editors, *Vertebr. Hair Cells*, volume 27, pages 154–203. Springer Science Inc., New York.

[Ficarella et al., 2007] Ficarella, R., Di Leva, F., Bortolozzi, M., Ortolano, S., Donaudy, F., Petrillo, M., Melchionda, S., Lelli, A., Domi, T., and Fedrizzi, L. (2007). A functional study of plasma-membrane calcium-pump isoform 2 mutants causing digenic deafness. *Proc Natl Acad Sci U S A*, 104:1516–1521.

[Forge et al., 2003] Forge, A., Becker, D., Casalotti, S., Edwards, J., Marziano, N., and Nevill, G. (2003). Gap junctions in the inner ear: comparison of distribution patterns in different vertebrates and assessement of connexin composition in mammals. *J Comp Neurol*, 467:207–231.

[Frolenkov, 2006] Frolenkov, G. I. (2006). Regulation of electromotility in the cochlear outer hair cell. *J Physiol*, 576:43–48.

[Frolenkov et al., 2000] Frolenkov, G. I., Mammano, F., Belyantseva, I. A., Coling, D., and Kachar, B. (2000). Two distinct Ca(2+)-dependent signaling pathways regulate the motor output of cochlear outer hair cells. *J Neurosci*, 20:5940–5948.

[Frolenkov et al., 2003] Frolenkov, G. I., Mammano, F., and Kachar, B. (2003). Regulation of outer hair cell cytoskeletal stiffness by intracellular Ca2+: underlying mechanism and implications for cochlear mechanics. *Cell Calcium*, 33:185–195.

[Fuchs, 2005] Fuchs, P. A. (2005). Time and intensity coding at the hair cell's ribbon synapse. *J Physiol*, 566:7–12.

[Fuchs et al., 2003] Fuchs, P. A., Glowatzki, E., and Moser, T. (2003). The afferent synapse of cochlear hair cells. *Curr Opin Neurobiol*, 13:452–458.

[Fukai et al., 2000] Fukai, H., Doi, S., Nomura, T., and Sato, S. (2000). Hopf bifurcations in multiple-parameter space of the Hodgkin-Huxley equations I. Global organization of bistable periodic solutions. *Biol. Cybern.*, 82(3):215–22.

[Fukami, 2002] Fukami, K. (2002). Structure, regulation, and function of phospholipase C isozymes. *J. Biochem.*, 131(3):293–9.

[Furness et al., 2008] Furness, D. N., Katori, Y., Nirmal Kumar, B., and Hackney, C. M. (2008). The dimensions and structural attachments of tip links in mammalian cochlear hair cells and the effects of exposure to different levels of extracellular calcium. *Neuroscience*, 154:10–21.

[Fussmann, 2000] Fussmann, G. F. (2000). Crossing the Hopf Bifurcation in a Live Predator-Prey System. *Science (80-.).*, 290(5495):1358–1360.

[Gale et al., 2004] Gale, J. E., Piazza, V., Ciubotaru, C. D., and Mammano, F. (2004). A mechanism for sensing noise damage in the inner ear. *Curr. Biol.*, 14(6):526–529.

[Gebhart et al., 2010] Gebhart, M., Juhasz-Vedres, G., Zuccotti, A., Brandt, N., Engel, J., Trockenbacher, A., Kaur, G., Obermair, G. J., Knipper, M., Koschak, A., and Striessnig, J. (2010). Modulation of Cav1.3 Ca2+ channel gating by Rab3 interacting molecule. *Mol Cell Neurosci*, 44:246–259.

[Gillespie et al., 2005] Gillespie, P. G., Dumont, R. A., and Kachar, B. (2005). Have we found the tip link, transduction channel, and gating spring of the hair cell? *Curr. Opin. Neurobiol.*, 15(4):389–396.

[Gillespie and Muller, 2009] Gillespie, P. G. and Muller, U. (2009). Mechanotransduction by hair cells: models, molecules, and mechanisms. *Cell*, 139:33–44.

[Glowatzki and Fuchs, 2000] Glowatzki, E. and Fuchs, P. A. (2000). Cholinergic synaptic inhibition of inner hair cells in the neonatal mammalian cochlea. *Science (80-.).*, 288:2366–2368.

[Glowatzki and Fuchs, 2002] Glowatzki, E. and Fuchs, P. A. (2002). Transmitter release at the hair cell ribbon synapse. *Nat Neurosci*, 5:147–154.

[Glowatzki et al., 2008] Glowatzki, E., Grant, L., and Fuchs, P. (2008). Hair cell afferent synapses. *Curr Opin Neurobiol*, 18:389–395.

[Goldberg et al., 1999] Goldberg, G. S., Lampe, P. D., and Nicholson, B. J. (1999). Selective transfer of endogenous metabolites through gap junctions composed of different connexins. *Nat Cell Biol*, 1:457–459.

[Gomez-Hernandez et al., 2003] Gomez-Hernandez, J. M., de Miguel, M., Larrosa, B., Gonzalez, D., and Barrio, L. C. (2003). Molecular basis of calcium regulation in connexin-32 hemichannels. *Proc Natl Acad Sci U S A*, 100:16030–16035.

[Gonzalez et al., 2007] Gonzalez, D., Gomez-Hernandez, J. M., and Barrio, L. C. (2007). Molecular basis of voltage dependence of connexin channels: an integrative appraisal. *Prog Biophys Mol Biol*, 94:66–106.

[Goodenough and Paul, 2003] Goodenough, D. A. and Paul, D. L. (2003). Beyond the gap: functions of unpaired connexon channels. *Nat. Rev. Mol. Cell Biol.*, 4(4):285–295.

[Goodenough and Paul, 2009] Goodenough, D. A. and Paul, D. L. (2009). Gap junctions. *Cold Spring Harb Perspect Biol*, 1(1):a002576.

[Goutman and Glowatzki, 2007] Goutman, J. D. and Glowatzki, E. (2007). Time course and calcium dependence of transmitter release at a single ribbon synapse. *Proc. Natl. Acad. Sci.*, 104(41):16341.

[Grant and Fuchs, 2008] Grant, L. and Fuchs, P. (2008). Calcium- and Calmodulin-Dependent Inactivation of Calcium Channels in Inner Hair Cells of the Rat Cochlea. *J. Neurophysiol.*, 99(5):2183–2193.

[Grati et al., 2006] Grati, M., Aggarwal, N., Strehler, E. E., and Wenthold, R. J. (2006). Molecular determinants for differential membrane trafficking of PMCA1 and PMCA2 in mammalian hair cells. *J Cell Sci*, 119:2995–3007.

[Grati and Kachar, 2011] Grati, M. and Kachar, B. (2011). Myosin VIIa and sans localization at stereocilia upper tip-link density implicates these Usher syndrome proteins in mechanotransduction. *Proc Natl Acad Sci U S A*, 108:11476–11481.

[Graydon et al., 2011] Graydon, C. W., Cho, S., Li, G. L., Kachar, B., and von Gersdorff, H. (2011). Sharp Ca(2)(+) nanodomains beneath the ribbon promote highly synchronous multivesicular release at hair cell synapses. *J Neurosci*, 31:16637–16650.

[Greenwood et al., 2007] Greenwood, D., Jagger, D. J., Huang, L. C., Hoya, N., Thorne, P. R., Wildman, S. S., King, B. F., Pak, K., Ryan, A. F., and Housley, G. D. (2007). P2X receptor signaling inhibits BDNF-mediated spiral ganglion neuron development in the neonatal rat cochlea. *Development*, 134(7):1407–1417.

[Gregory et al., 2011] Gregory, F. D., Bryan, K. E., Pangrsic, T., Calin-Jageman, I. E., Moser, T., and Lee, A. (2011). Harmonin inhibits presynaptic Cav1.3 Ca(2)(+) channels in mouse inner hair cells. *Nat Neurosci*, 14:1109–1111.

[Grifa et al., 1999] Grifa, A., Wagner, C. A., D'Ambrosio, L., Melchionda, S., Bernardi, F., Lopez-Bigas, N., Rabionet, R., Arbones, M., Monica, M. D., and Estivill, X. (1999). Mutations in GJB6 cause nonsyndromic autosomal dominant deafness at DFNA3 locus. *Nat Genet*, 23:16–18.

[Grillet et al., 2009] Grillet, N., Xiong, W., Reynolds, A., Kazmierczak, P., Sato, T., Lillo, C., Dumont, R. A., Hintermann, E., Sczaniecka, A., and Schwander, M. (2009). Harmonin mutations cause mechanotransduction defects in cochlear hair cells. *Neuron*, 62:375–387.

[Grynkiewicz et al., 1985] Grynkiewicz, G., Poenie, M., and Tsien, R. (1985). A new generation of Ca2+ indicators with greatly improved fluorescence properties. *J. Biol. Chem.*, 260(6):3440–3450.

[Guinan Jr., 2006] Guinan Jr., J. J. (2006). Olivocochlear efferents: anatomy, physiology, function, and the measurement of efferent effects in humans. *Ear Hear*, 27(6):589–607.

[Hackney et al., 2003] Hackney, C. M., Mahendrasingam, S., Jones, E. M., and Fettiplace, R. (2003). The distribution of calcium buffering proteins in the turtle cochlea. *J Neurosci*, 23:4577–4589.

[Hackney et al., 2005] Hackney, C. M., Mahendrasingam, S., Penn, A., and Fettiplace, R. (2005). The concentrations of calcium buffering proteins in mammalian cochlear hair cells. *J Neurosci*, 25:7867–7875.

[Harris, 2007] Harris, A. L. (2007). Connexin channel permeability to cytoplasmic molecules. *Prog Biophys Mol Biol*, 94:120–143.

[Hasson et al., 1995] Hasson, T., Heintzelman, M. B., Santos-Sacchi, J., Corey, D. P., and Mooseker, M. S. (1995). Expression in cochlea and retina of myosin VIIa, the gene product defective in Usher syndrome type 1B. *Proc Natl Acad Sci U S A*, 92:9815–9819.

[Hernandez et al., 2007] Hernandez, V. H., Bortolozzi, M., Pertegato, V., Beltramello, M., Giarin, M., Zaccolo, M., Pantano, S., and Mammano, F. (2007). Unitary permeability of gap junction channels to second messengers measured by FRET microscopy. *Nat. Methods*.

[Hibino and Kurachi, 2006] Hibino, H. and Kurachi, Y. (2006). Molecular and physiological bases of the K+circulation in the mammalian inner ear. *Physiol.*, 21:336–345.

[Hilgert et al., 2009] Hilgert, N., Smith, R. J., and Van Camp, G. (2009). Function and expression pattern of nonsyndromic deafness genes. *Curr Mol Med*, 9:546–564.

[Hill et al., 2006] Hill, J. K., Williams, D. E., LeMasurier, M., Dumont, R. A., Strehler, E. E., and Gillespie, P. G. (2006). Splice-site A choice targets plasma-membrane Ca2+-ATPase isoform 2 to hair bundles. *J Neurosci*, 26:6172–6180.

[Hinojosa, 1977] Hinojosa, R. (1977). A note on development of Corti's organ. *Acta Otolaryngol*, 84:238–251.

[Hofer et al., 2001] Hofer, T., Politi, A., and Heinrich, R. (2001). Intercellular Ca2+ wave propagation through gap-junctional Ca2+ diffusion: a theoretical study. *Biophys. J.*, 80(1):75–87.

[Holt et al., 2002] Holt, J. R., Gillespie, S. K., Provance, D. W., Shah, K., Shokat, K. M., Corey, D. P., Mercer, J. A., and Gillespie, P. G. (2002). A chemical-genetic strategy implicates myosin-1c in adaptation by hair cells. *Cell*, 108:371–381.

[Hou et al., 2013] Hou, M., Li, Y., and Paul, D. L. (2013). A novel, highly sensitive method for assessing gap junctional coupling. *J Neurosci Methods*, 220(1):18–23.

[Housley et al., 2009] Housley, G. D., Bringmann, A., and Reichenbach, A. (2009). Purinergic signaling in special senses. *Trends Neurosci*, 32:128–141.

[Howard and Hudspeth, 1987] Howard, J. and Hudspeth, A. (1987). Mechanical relaxation of the hair bundle mediates adaptation in mechanoelectrical transduction by the bullfrog's saccular hair cell. *Proc. Natl. Acad. Sci.*, 84(9):3064.

[Howard and Hudspeth, 1988] Howard, J. and Hudspeth, A. J. (1988). Compliance of the hair bundle associated with gating of mechanoelectrical transduction channels in the bullfrog's saccular hair cell. *Neuron*, 1:189–199.

[Huang et al., 2002] Huang, D., Chen, P., Chen, S., Nagura, M., Lim, D. J., and Lin, X. (2002). Expression patterns of aquaporins in the inner ear: evidence for concerted actions of multiple types of aquaporins to facilitate water transport in the cochlea. *Hear Res*, 165(1-2):85–95.

[Huang et al., 2007] Huang, Y. J., Maruyama, Y., Dvoryanchikov, G., Pereira, E., Chaudhari, N., and Roper, S. D. (2007). The role of pannexin 1 hemichannels in ATP release and cell-cell communication in mouse taste buds. *Proc. Natl. Acad. Sci. U. S. A.*, 104:6436–6441.

[Hubley et al., 1996] Hubley, M. J., Locke, B. R., and Moerland, T. S. (1996). The effects of temperature, pH, and magnesium on the diffusion coefficient of ATP in solutions of physiological ionic strength. *Biochim. Biophys. Acta (BBA)-General Subj.*, 1291(2):115–121.

[Jagger and Forge, 2006] Jagger, D. J. and Forge, A. (2006). Compartmentalized and signal-selective gap junctional coupling in the hearing cochlea. *J Neurosci*, 26(4):1260–1268.

[Jin et al., 2012] Jin, L., Han, Z., Platisa, J., Wooltorton, J. R., Cohen, L. B., and Pieribone, V. A. (2012). Single action potentials and subthreshold electrical events imaged in neurons with a fluorescent protein voltage probe. *Neuron*, 75:779–785.

[Johnson et al., 2007] Johnson, S. L., Adelman, J. P., and Marcotti, W. (2007). Genetic deletion of SK2 channels in mouse inner hair cells prevents the developmental linearization in the Ca2+ dependence of exocytosis. *J Physiol*, 583:631–646.

[Johnson et al., 2011a] Johnson, S. L., Beurg, M., Marcotti, W., and Fettiplace, R. (2011a). Prestin-driven cochlear amplification is not limited by the outer hair cell membrane time constant. *Neuron*, 70:1143–1154.

[Johnson et al., 2011b] Johnson, S. L., Eckrich, T., Kuhn, S., Zampini, V., Franz, C., Ranatunga, K. M., Roberts, T. P., Masetto, S., Knipper, M., Kros, C. J., and Marcotti, W. (2011b). Position-dependent patterning of spontaneous action potentials in immature cochlear inner hair cells. *Nat. Neurosci.*, 14(6):711–717.

[Johnson et al., 2008] Johnson, S. L., Forge, A., Knipper, M., Münkner, S., and Marcotti, W. (2008). Tonotopic variation in the calcium dependence of neurotransmitter release and vesicle pool replenishment at mammalian auditory ribbon synapses. *J. Neurosci.*, 28(30):7670–7678.

[Johnson et al., 2009] Johnson, S. L., Franz, C., Knipper, M., and Marcotti, W. (2009). Functional maturation of the exocytotic machinery at gerbil hair cell ribbon synapses. *J. Physiol.*, 587(8):1715–1726.

[Johnson et al., 2010] Johnson, S. L., Franz, C., Kuhn, S., Furness, D. N., Ruttiger, L., Munkner, S., Rivolta, M. N., Seward, E. P., Herschman, H. R., and Engel, J. (2010). Synaptotagmin IV determines the linear Ca2+ dependence of vesicle fusion at auditory ribbon synapses. *Nat Neurosci*, 13:45–52.

[Johnson et al., 2012] Johnson, S. L., Kennedy, H. J., Holley, M. C., Fettiplace, R., and Marcotti, W. (2012). The resting transducer current drives spontaneous activity in prehearing Mammalian cochlear inner hair cells. *J Neurosci*, 32(31):10479–10483.

[Johnson and Marcotti, 2008] Johnson, S. L. and Marcotti, W. (2008). Biophysical properties of CaV1.3 calcium channels in gerbil inner hair cells. *J Physiol*, 586:1029–1042.

[Johnson et al., 2005] Johnson, S. L., Marcotti, W., and Kros, C. J. (2005). Increase in efficiency and reduction in Ca2+ dependence of exocytosis during development of mouse inner hair cells. *J Physiol*, 563:177–191.

[Kachar et al., 2000] Kachar, B., Parakkal, M., Kurc, M., Zhao, Y., and Gillespie, P. G. (2000). High-resolution structure of hair-cell tip links. *Proc. Natl. Acad. Sci. U. S. A.*, 97(24):13336–13341.

[Kamiya et al., 2001] Kamiya, K., Takahashi, K., Kitamura, K., Momoi, T., and Yoshikawa, Y. (2001). Mitosis and apoptosis in postnatal auditory system of the C3H/He strain. *Brain Res*, 901:296–302.

[Kandler et al., 2009] Kandler, K., Clause, A., and Noh, J. (2009). Tonotopic reorganization of developing auditory brainstem circuits. *Nat. Neurosci.*, 12(6):711–7.

[Kazmierczak et al., 2007] Kazmierczak, P., Sakaguchi, H., Tokita, J., Wilson-Kubalek, E. M., Milligan, R. A., Muller, U., and Kachar, B. (2007). Cadherin 23 and protocadherin 15 interact to form tip-link filaments in sensory hair cells. *Nature*, 449:87–91.

[Keen and Hudspeth, 2006] Keen, E. C. and Hudspeth, A. J. (2006). Transfer characteristics of the hair cell's afferent synapse. *Proc Natl Acad Sci U S A*, 103:5537–5542.

[Kelley et al., 1998] Kelley, P. M., Harris, D. J., Comer, B. C., Askew, J. W., Fowler, T., Smith, S. D., and Kimberling, W. J. (1998). Novel mutations in the connexin 26 gene (GJB2) that cause autosomal recessive (DFNB1) hearing loss. *Am J Hum Genet*, 62:792–799.

[Kelly et al., 2011] Kelly, J. J., Forge, A., and Jagger, D. J. (2011). Development of gap junctional intercellular communication within the lateral wall of the rat cochlea. *Neuroscience*, 180:360–369.

[Kelly and Chen, 2009] Kelly, M. C. and Chen, P. (2009). Development of form and function in the mammalian cochlea. *Curr Opin Neurobiol*, 19:395–401.

[Kennedy and Meech, 2002] Kennedy, H. J. and Meech, R. W. (2002). Fast Ca2+ signals at mouse inner hair cell synapse: a role for Ca2+-induced Ca2+ release. *J Physiol*, 539:15–23.

[Khimich et al., 2005] Khimich, D., Nouvian, R., Pujol, R., Tom Dieck, S., Egner, A., Gundelfinger, E. D., and Moser, T. (2005). Hair cell synaptic ribbons are essential for synchronous auditory signalling. *Nature*, 434:889–894.

[Kikuchi et al., 2000] Kikuchi, T., Adams, J. C., Miyabe, Y., So, E., and Kobayashi, T. (2000). Potassium ion recycling pathway via gap junction systems in the mammalian cochlea and its interruption in hereditary nonsyndromic deafness. *Med Electron Microsc*, 33:51–56.

[Kikuchi et al., 1995] Kikuchi, T., Kimura, R. S., Paul, D. L., and Adams, J. C. (1995). Gap junctions in the rat cochlea: immunohistochemical and ultrastructural analysis. *Anat Embryol*, 191(2):101–118.

[Kofuji and Newman, 2004] Kofuji, P. and Newman, E. A. (2004). Potassium buffering in the central nervous system. *Neuroscience*, 129(4):1045–1056.

[Koschak et al., 2001] Koschak, A., Reimer, D., Huber, I., Grabner, M., Glossmann, H., Engel, J., and Striessnig, J. (2001). alpha 1D (Cav1.3) subunits can form l-type Ca2+ channels activating at negative voltages. *J Biol Chem*, 276:22100–22106.

[Kozel et al., 1998] Kozel, P. J., Friedman, R. A., Erway, L. C., Yamoah, E. N., Liu, L. H., Riddle, T., Duffy, J. J., Doetschman, T., Miller, M. L., Cardell, E. L., and Shull, G. E. (1998). Balance and hearing deficits in mice with a null mutation in the gene encoding plasma membrane Ca2+-ATPase isoform 2. *J Biol Chem*, 273:18693–18696.

[Kros et al., 2002] Kros, C. J., Marcotti, W., van Netten, S. M., Self, T. J., Libby, R. T., Brown, S. D., Richardson, G. P., and Steel, K. P. (2002). Reduced climbing and increased slipping adaptation in cochlear hair cells of mice with Myo7a mutations. *Nat Neurosci*, 5:41–47.

[Kros et al., 1998] Kros, C. J., Ruppersberg, J. P., Rüsch, A., and Rusch, A. (1998). Expression of a potassium current in inner hair cells during development of hearing in mice. *Nature*, 394(6690):281–284.

[Krstic, 1997] Krstic, R. V. (1997). *Human Microscopic Anatomy.* Springer-Verlag, Berlin, corrected edition.

[Kudo, 2003] Kudo, T. (2003). Transgenic expression of a dominant-negative connexin26 causes degeneration of the organ of Corti and non-syndromic deafness. *Hum. Mol. Genet.*, 12(9):995–1004.

[Lagostena et al., 2001] Lagostena, L., Cicuttin, A., Inda, J., Kachar, B., and Mammano, F. (2001). Frequency dependence of electrical coupling in Deiters' cells of the guinea pig cochlea. *Cell Commun Adhes*, 8:393–399.

[Larsson et al., 1999] Larsson, D., Larsson, B., Lundgren, T., and Sundell, K. (1999). The Effect of pH and Temperature on the Dissociation Constant for Fura-2 and Their Effects on [Ca2+]i in Enterocytes from a Poikilothermic Animal, Atlantic Cod (Gadus morhua). *Anal. Biochem.*, 273(1):60–65.

[Lautermann et al., 1999] Lautermann, J., Frank, H. G., Jahnke, K., Traub, O., and Winterhager, E. (1999). Developmental expression patterns of connexin26 and 30 in the rat cochlea. *Dev Genet*, 25:306–311.

[Lautermann et al., 1998] Lautermann, J., ten Cate, W. J., Altenhoff, P., Grummer, R., Traub, O., Frank, H., Jahnke, K., Winterhager, E., and Grümmer, R. (1998). Expression of the gap-junction connexins 26 and 30 in the rat cochlea. *Cell Tissue Res.*, 294(3):415–20.

[Lelli et al., 2009] Lelli, A., Asai, Y., Forge, A., Holt, J. R., and Geleoc, G. S. (2009). Tonotopic gradient in the developmental acquisition of sensory transduction in outer hair cells of the mouse cochlea. *J Neurophysiol*, 101(6):2961–2973.

[Lelli et al., 2003] Lelli, A., Perin, P., Martini, M., Ciubotaru, C. D., Prigioni, I., Valli, P., Rossi, M. L., and Mammano, F. (2003). Presynaptic calcium stores modulate afferent release in vestibular hair cells. *J Neurosci*, 23:6894–6903.

[Lemon et al., 2003] Lemon, G., Gibson, W. G., and Bennett, M. R. (2003). Metabotropic receptor activation, desensitization and sequestration—I: modelling calcium and inositol 1, 4, 5-trisphosphate dynamics following receptor activation. *J. Theor. Biol.*, 223(1):93–111.

[Lenzi et al., 1999] Lenzi, D., Runyeon, J. W., Crum, J., Ellisman, M. H., and Roberts, W. M. (1999). Synaptic vesicle populations in saccular hair cells reconstructed by electron tomography. *J Neurosci*, 19:119–132.

[Lenzi and von Gersdorff, 2001] Lenzi, D. and von Gersdorff, H. (2001). Structure suggests function: the case for synaptic ribbons as exocytotic nanomachines. *Bioessays*, 23:831–840.

[Leybaert et al., 2003] Leybaert, L., Braet, K., Vandamme, W., Cabooter, L., Martin, P. E. M., and Evans, W. H. (2003). Connexin Channels, Connexin Mimetic Peptides and ATP Release. *Cell Commun. Adhes.*, 10(4-6):251–257.

[Li et al., 1998] Li, W., Llopis, J., Whitney, M., Zlokarnik, G., and Tsien, R. Y. (1998). Cell-permeant caged InsP3 ester shows that Ca2+ spike frequency can optimize gene expression. *Nature*, 392:936–941.

[Li and Rinzel, 1994] Li, Y. X. and Rinzel, J. (1994). Equations for InsP3 receptor-mediated [Ca2+] i oscillations derived from a detailed kinetic model: a Hodgkin-Huxley like formalism. *J. Theor. Biol.*, 166(4):461–473.

[Lim and Rueda, 1992] Lim, D. and Rueda, J. (1992). Structural development of the cochlea. *Dev. Audit. Vestib. Syst. - 2*, pages 33–58.

[Lim, 1986] Lim, D. J. (1986). Functional structure of the organ of Corti: a review. *Hear Res*, 22:117–146.

[Lin et al., 2005] Lin, H. W., Schneider, M. E., and Kachar, B. (2005). When size matters: the dynamic regulation of stereocilia lengths. *Curr. Opin. Cell Biol.*, 17(1):55–61.

[Lytton et al., 1992] Lytton, J., Westlin, M., Burk, S., Shull, G., and MacLennan, D. (1992). Functional comparisons between isoforms of the sarcoplasmic or endoplasmic reticulum family of calcium pumps. *J. Biol. Chem.*, 267(20):14483–14489.

[Maeda et al., 2009] Maeda, S., Nakagawa, S., Suga, M., Yamashita, E., Oshima, A., Fujiyoshi, Y., and Tsukihara, T. (2009). Structure of the connexin 26 gap junction channel at 3.5 A resolution. *Nature*, 458:597–602.

[Majumder et al., 2010] Majumder, P., Crispino, G., Rodriguez, L., Ciubotaru, C. D., Anselmi, F., Piazza, V., Bortolozzi, M., and Mammano, F. (2010). ATP-mediated cell-cell signaling in the organ of Corti: the role of connexin channels. *Purinergic Signal*, 6(2):167–187.

[Mammano, 2013] Mammano, F. (2013). ATP-dependent intercellular Ca2+ signaling in the developing cochlea: Facts, fantasies and perspectives. *Semin Cell Dev Biol*, 24:31–39.

[Mammano et al., 2007] Mammano, F., Bortolozzi, M., Ortolano, S., and Anselmi, F. (2007). Ca2+ signaling in the inner ear. *Physiol.*, 22:131–144.

[Mammano et al., 1999a] Mammano, F., Canepari, M., Capello, G., Ijaduola, R. B., Cunei, A., Ying, L., Fratnik, F., and Colavita, A. (1999a). An optical recording system based on a fast CCD sensor for biological imaging. *Cell Calcium*, 25:115–123.

[Mammano et al., 1999b] Mammano, F., Frolenkov, G. I., Lagostena, L., Belyantseva, I. A., Kurc, M., Dodane, V., Colavita, A., and Kachar, B. (1999b). ATP-Induced Ca(2+) release in cochlear outer hair cells: localization of an inositol triphosphate-gated Ca(2+) store to the base of the sensory hair bundle. *J Neurosci*, 19:6918–6929.

[Mann and Whitney, 1947] Mann, H. B. and Whitney, D. R. (1947). On a Test of Whether one of Two Random Variables is Stochastically Larger than the Other. *Ann Math Stat*, 18:50–60.

[Mann et al., 2009] Mann, Z. F., Duchen, M. R., and Gale, J. E. (2009). Mitochondria modulate the spatio-temporal properties of intra- and intercellular Ca2+ signals in cochlear supporting cells. *Cell Calcium*, 46:136–146.

[Marcotti, 2012] Marcotti, W. (2012). Functional assembly of mammalian cochlear hair cells. *Exp Physiol*, 97:438–451.

[Marcotti et al., 2003a] Marcotti, W., Johnson, S. L., Holley, M. C., and Kros, C. J. (2003a). Developmental changes in the expression of potassium currents of embryonic, neonatal and mature mouse inner hair cells. *J. Physiol.*, 548(2):383.

[Marcotti et al., 2004] Marcotti, W., Johnson, S. L., and Kros, C. J. (2004). Effects of intracellular stores and extracellular Ca(2+) on Ca(2+)-activated K(+) currents in mature mouse inner hair cells. *J Physiol*, 557:613–633.

[Marcotti et al., 2003b] Marcotti, W., Johnson, S. L., R\üsch, A., and Kros, C. J. (2003b). Sodium and calcium currents shape action potentials in immature mouse inner hair cells. *J. Physiol.*, 552(3):743.

[Martinez et al., 2009] Martinez, A. D., Acuna, R., Figueroa, V., Maripillan, J., and Nicholson, B. (2009). Gap-junction channels dysfunction in deafness and hearing loss. *Antioxid Redox Signal*, 11:309–322.

[Matthews and Fuchs, 2010] Matthews, G. and Fuchs, P. (2010). The diverse roles of ribbon synapses in sensory neurotransmission. *Nat Rev Neurosci*, 11:812–822.

[McCullough and Tempel, 2004] McCullough, B. J. and Tempel, B. L. (2004). Haploinsufficiency revealed in deafwaddler mice when tested for hearing loss and ataxia. *Hear Res*, 195:90–102.

[Mellstrom et al., 2008] Mellstrom, B., Savignac, M., Gomez-Villafuertes, R., and Naranjo, J. R. (2008). Ca2+-operated transcriptional networks: molecular mechanisms and in vivo models. *Physiol Rev*, 88:421–449.

[Meyer and Moser, 2010] Meyer, A. C. and Moser, T. (2010). Structure and function of cochlear afferent innervation. *Curr Opin Otolaryngol Head Neck Surg*, 18(5):441–446.

[Michna et al., 2003] Michna, M., Knirsch, M., Hoda, J. C., Muenkner, S., Langer, P., Platzer, J., Striessnig, J., and Engel, J. (2003). Cav1.3 (alpha1D) Ca2+ currents in neonatal outer hair cells of mice. *J Physiol*, 553:747–758.

[Mikaelian et al., 1965] Mikaelian, D., Alford, B. R., and Ruben, R. J. (1965). Cochlear Potentials and 8 Nerve Action Potentials in Normal and Genetically Deaf Mice. *Ann Otol Rhinol Laryngol*, 74:146–157.

[Miller et al., 2012] Miller, E. W., Lin, J. Y., Frady, E. P., Steinbach, P. A., Kristan, W. B., and Tsien, R. Y. (2012). Optically monitoring voltage in neurons by photo-induced electron transfer through molecular wires. *Proc. Natl. Acad. Sci. U. S. A.*, 109(6):2114–9.

[Mistrik and Ashmore, 2009] Mistrik, P. and Ashmore, J. (2009). The role of potassium recirculation in cochlear amplification. *Curr Opin Otolaryngol Head Neck Surg*, 17:394–399.

[Moser and Beutner, 2000] Moser, T. and Beutner, D. (2000). Kinetics of exocytosis and endocytosis at the cochlear inner hair cell afferent synapse of the mouse. *Proc. Natl. Acad. Sci.*, 97(2):883.

[Muller et al., 2002] Muller, D. J., Hand, G. M., Engel, A., and Sosinsky, G. E. (2002). Conformational changes in surface structures of isolated connexin 26 gap junctions. *EMBO J*, 21:3598–3607.

[Nayagam et al., 2011] Nayagam, B. A., Muniak, M. A., and Ryugo, D. K. (2011). The spiral ganglion: connecting the peripheral and central auditory systems. *Hear Res*, 278(1-2):2–20.

[Nickel and Forge, 2008] Nickel, R. and Forge, A. (2008). Gap junctions and connexins in the inner ear: their roles in homeostasis and deafness. *Curr Opin Otolaryngol Head Neck Surg*, 16:452–457.

[Noben-Trauth et al., 2003] Noben-Trauth, K., Zheng, Q. Y., and Johnson, K. R. (2003). Association of cadherin 23 with polygenic inheritance and genetic modification of sensorineural hearing loss. *Nat Genet*, 35:21–23.

[Noben-Trauth et al., 1997] Noben-Trauth, K., Zheng, Q. Y., Johnson, K. R., and Nishina, P. M. (1997). mdfw: a deafness susceptibility locus that interacts with deaf waddler (dfw). *Genomics*, 44:266–272.

[Nouvian et al., 2006] Nouvian, R., Beutner, D., Parsons, T., and Moser, T. (2006). Structure and Function of the Hair Cell Ribbon Synapse. *J. Membr. Biol.*, 209(2-3):153–165.

[Nouvian et al., 2011] Nouvian, R., Neef, J., Bulankina, A. V., Reisinger, E., Pangrsic, T., Frank, T., Sikorra, S., Brose, N., Binz, T., and Moser, T. (2011). Exocytosis at the hair cell ribbon synapse apparently operates without neuronal SNARE proteins. *Nat Neurosci*, 14:411–413.

[Okamura et al., 2001] Okamura, H., Spicer, S., and Schulte, B. (2001). Immunohistochemical localization of phospholipase C isozymes in mature and developing gerbil cochlea. *Neuroscience*, 102(2):451–459.

[Oliver et al., 2000] Oliver, D., Klocker, N., Schuck, J., Baukrowitz, T., Ruppersberg, J. P., and Fakler, B. (2000). Gating of Ca2+-activated K+channels controls fast inhibitory synaptic transmission at auditory outer hair cells. *Neuron*, 26:595–601.

[Ortolano and Pasquale, 2008] Ortolano, S. and Pasquale, G. D. (2008). Coordinated control of connexin 26 and connexin 30 at the regulatory and functional level in the inner ear. *Proc. . . .*, 105(48):18776.

[Ozbudak et al., 2004] Ozbudak, E. M., Thattai, M., Lim, H. N., Shraiman, B. I., and Van Oudenaarden, A. (2004). Multistability in the lactose utilization network of Escherichia coli. *Nature*, 427(6976):737–40.

[Palacios-Prado et al., 2010] Palacios-Prado, N., Briggs, S. W., Skeberdis, V. A., Pranevicius, M., Bennett, M. V., and Bukauskas, F. F. (2010). pH-dependent modulation of voltage gating in connexin45 homotypic and connexin45/connexin43 heterotypic gap junctions. *Proc Natl Acad Sci USA*, 107:9897–9902.

[Palacios-Prado et al., 2009] Palacios-Prado, N., Sonntag, S., Skeberdis, V. A., Willecke, K., and Bukauskas, F. F. (2009). Gating, permselectivity and pH-dependent modulation of channels formed by connexin57, a major connexin of horizontal cells in the mouse retina. *J Physiol*, 587:3251–3269.

[Pangrsic et al., 2010] Pangrsic, T., Lasarow, L., Reuter, K., Takago, H., Schwander, M., Riedel, D., Frank, T., Tarantino, L. M., Bailey, J. S., and Strenzke, N. (2010). Hearing requires otoferlin-dependent efficient replenishment of synaptic vesicles in hair cells. *Nat Neurosci*, 13:869–876.

[Patuzzi, 2011a] Patuzzi, R. (2011a). Ion flow in cochlear hair cells and the regulation of hearing sensitivity. *Hear Res*, 280(1):3–20.

[Patuzzi, 2011b] Patuzzi, R. (2011b). Ion flow in stria vascularis and the production and regulation of cochlear endolymph and the endolymphatic potential. *Hear Res*, 280:4–19.

[Pawley, 2006] Pawley, J. (2006). *Handbook of Biological Confocal Microscopy, Volume 236*. Springer.

[Peng et al., 2011] Peng, A. W., Salles, F. T., Pan, B., and Ricci, A. J. (2011). Integrating the biophysical and molecular mechanisms of auditory hair cell mechanotransduction. *Nat Commun*, 2:523.

[Piazza et al., 2007] Piazza, V., Ciubotaru, C. D., Gale, J. E., and Mammano, F. (2007). Purinergic signalling and intercellular Ca2+ wave propagation in the organ of Corti. *Cell Calcium*, 41(1):77–86.

[Platzer et al., 2000] Platzer, J., Engel, J., Schrott-Fischer, A., Stephan, K., Bova, S., Chen, H., Zheng, H., and Striessnig, J. (2000). Congenital deafness and sinoatrial node dysfunction in mice lacking class D L-type Ca2+ channels. *Cell*, 102:89–97.

[Plazas et al., 2005] Plazas, P. V., Katz, E., Gomez-Casati, M. E., Bouzat, C., and Elgoyhen, A. B. (2005). Stoichiometry of the alpha9alpha10 nicotinic cholinergic receptor. *J Neurosci*, 25:10905–10912.

[Prank et al., 2000] Prank, K., Gabbiani, F., and Brabant, G. (2000). Coding efficiency and information rates in transmembrane signaling. *Biosystems*, 55:15–22.

[Purves et al., 2001] Purves, D., Augustine, G. J., Fitzpatrick, D., Katz, L. C., LaMantia, A.-S., McNamara, J. O., and Williams, S. M. (2001). *Neuroscience, 2nd edition*, volume 1. Sinauer Associates;, Sunderland (MA), 2nd edition.

[Raphael and Altschuler, 2003] Raphael, Y. and Altschuler, R. A. (2003). Structure and innervation of the cochlea. *Brain Res Bull*, 60(5-6):397–422.

[Reisinger et al., 2011] Reisinger, E., Bresee, C., Neef, J., Nair, R., Reuter, K., Bulankina, A., Nouvian, R., Koch, M., Buckers, J., and Kastrup, L. (2011). Probing the functional equivalence of otoferlin and synaptotagmin 1 in exocytosis. *J. Neurosci.*, 31:4886–4895.

[Ricci and Fettiplace, 1997] Ricci, A. and Fettiplace, R. (1997). The effects of calcium buffering and cyclic AMP on mechano-electrical transduction in turtle auditory hair cells. *J. Physiol.*, 501(1):111–124.

[Ricci et al., 2005] Ricci, A., Kennedy, H., Crawford, A., and Fettiplace, R. (2005). The transduction channel filter in auditory hair cells. *J. Neurosci.*, 25(34):7831.

[Ricci et al., 1998] Ricci, A., Wu, Y., and Fettiplace, R. (1998). The endogenous calcium buffer and the time course of transducer adaptation in auditory hair cells. *J. Neurosci.*, 18(20):8261.

[Richardson et al., 2011] Richardson, G. P., de Monvel, J. B., and Petit, C. (2011). How the Genetics of Deafness Illuminates Auditory Physiology. *Annu. Rev. Physiol. Vol 73*, pages 311–334.

[Rickheit et al., 2008] Rickheit, G., Maier, H., Strenzke, N., Andreescu, C. E., De Zeeuw, C. I., Muenscher, A., Zdebik, A. A., and Jentsch, T. J. (2008). Endocochlear potential depends on Cl- channels: mechanism underlying deafness in Bartter syndrome IV. *EMBO J*, 27(21):2907–2917.

[Rio et al., 2002] Rio, C., Dikkes, P., Liberman, M. C., and Corfas, G. (2002). Glial fibrillary acidic protein expression and promoter activity in the inner ear of developing and adult mice. *J Comp Neurol*, 442(2):156–162.

[Robertson, 2009] Robertson, D. (2009). Centrifugal control in mammalian hearing. *Clin Exp Pharmacol Physiol*, 36(7):603–611.

[Rodriguez et al., 2012] Rodriguez, L., Simeonato, E., Scimemi, P., Anselmi, F., Cali, B., Crispino, G., Ciubotaru, C. D., Bortolozzi, M., Ramirez, F. G., Majumder, P., Arslan, E., De Camilli, P., Pozzan, T., and Mammano, F. (2012). Reduced phosphatidylinositol 4,5-bisphosphate synthesis impairs inner ear Ca2+ signaling and high-frequency hearing acquisition. *Proc Natl Acad Sci U S A*, 109(35):14013–14018.

[Roux et al., 2006] Roux, I., Safieddine, S., Nouvian, R., Grati, M., Simmler, M. C., Bahloul, A., Perfettini, I., Le Gall, M., Rostaing, P., and Hamard, G. (2006). Otoferlin,

defective in a human deafness form, is essential for exocytosis at the auditory ribbon synapse. *Cell*, 127:277–289.

[Rusznak and Szucs, 2009] Rusznak, Z. and Szucs, G. (2009). Spiral ganglion neurones: an overview of morphology, firing behaviour, ionic channels and function. *Pflugers Arch*, 457(6):1303–1325.

[Rutherford et al., 2012] Rutherford, M. A., Chapochnikov, N. M., and Moser, T. (2012). Spike encoding of neurotransmitter release timing by spiral ganglion neurons of the cochlea. *J Neurosci*, 32(14):4773–4789.

[Rutherford and Roberts, 2006] Rutherford, M. A. and Roberts, W. M. (2006). Frequency selectivity of synaptic exocytosis in frog saccular hair cells. *Proc Natl Acad Sci U S A*, 103:2898–2903.

[Rybak et al., 1992] Rybak, L. P., Whitworth, C., and Scott, V. (1992). Development of endocochlear potential and compound action potential in the rat. *Hear Res*, 59:189–194.

[Rzadzinska et al., 2004] Rzadzinska, A. K., Schneider, M. E., Davies, C., Riordan, G. P., and Kachar, B. (2004). An actin molecular treadmill and myosins maintain stereocilia functional architecture and self-renewal. *J Cell Biol*, 164:887–897.

[Saez et al., 2005] Saez, J. C., Retamal, M. A., Basilio, D., Bukauskas, F. F., and Bennett, M. V. (2005). Connexin-based gap junction hemichannels: gating mechanisms. *Biochim Biophys Acta*, 1711:215–224.

[Safieddine and Wenthold, 1999] Safieddine, S. and Wenthold, R. J. (1999). SNARE complex at the ribbon synapses of cochlear hair cells: analysis of synaptic vesicle- and synaptic membrane-associated proteins. *Eur J Neurosci*, 11:803–812.

[Santos-Sacchi, 1991] Santos-Sacchi, J. (1991). Isolated supporting cells from the organ of Corti: some whole cell electrical characteristics and estimates of gap junctional conductance. *Hear Res*, 52:89–98.

[Schaechinger et al., 2011] Schaechinger, T. J., Gorbunov, D., Halaszovich, C. R., Moser, T., Kugler, S., Fakler, B., and Oliver, D. (2011). A synthetic prestin reveals protein domains and molecular operation of outer hair cell piezoelectricity. *EMBO J*, 30(14):2793–2804.

[Schmidt and Fernandez, 1963] Schmidt, R. S. and Fernandez, C. (1963). Development of Mammalian Endocochlear Potential. *J Exp Zool*, 153:227–235.

[Schnee et al., 2005] Schnee, M. E., Lawton, D. M., Furness, D. N., Benke, T. A., and Ricci, A. J. (2005). Auditory hair cell-afferent fiber synapses are specialized to operate at their best frequencies. *Neuron*, 47:243–254.

[Schnee et al., 2011] Schnee, M. E., Santos-Sacchi, J., Castellano-Munoz, M., Kong, J. H., and Ricci, A. J. (2011). Calcium-dependent synaptic vesicle trafficking underlies indefatigable release at the hair cell afferent fiber synapse. *Neuron*, 70:326–338.

[Schneider et al., 2006] Schneider, M. E., Dose, A. C., Salles, F. T., Chang, W., Erickson, F. L., Burnside, B., and Kachar, B. (2006). A new compartment at stereocilia tips defined by spatial and temporal patterns of myosin IIIa expression. *J Neurosci*, 26:10243–10252.

[Schultz et al., 2005] Schultz, J., Yang, Y., Caride, A., Filoteo, A., Penheiter, A., Lagziel, A., Morell, R., Mohiddin, S., Fananapazir, L., Madeo, A., and Others (2005). Modification of human hearing loss by plasma-membrane calcium pump PMCA2. *N. Engl. J. Med.*, 352(15):1557–1564.

[Schutz et al., 2011] Schutz, M., Auth, T., Gehrt, A., Bosen, F., Korber, I., Strenzke, N., Moser, T., and Willecke, K. (2011). The connexin26 S17F mouse mutant represents a model for the human hereditary keratitis-ichthyosis-deafness syndrome. *Hum Mol Genet*, 20:28–39.

[Schutz et al., 2010] Schutz, M., Scimemi, P., Majumder, P., De Siati, R. D., Crispino, G., Rodriguez, L., Bortolozzi, M., Santarelli, R., Seydel, A., Sonntag, S., Schütz, M., Ingham, N., Steel, K. P., Willecke, K., and Mammano, F. (2010). The human deafness-associated connexin 30 T5M mutation causes mild hearing loss and reduces biochemical coupling among cochlear non-sensory cells in knock-in mice. *Hum. Mol. Genet.*, 19(24):4759–4773.

[Schwander et al., 2010] Schwander, M., Kachar, B., and Muller, U. (2010). Review series: The cell biology of hearing. *J Cell Biol*, 190(1):9–20.

[Sneyd et al., 2006] Sneyd, J., Tsaneva-Atanasova, K., Reznikov, V., Bai, Y., Sanderson, M. J., and Yule, D. I. (2006). A method for determining the dependence of calcium oscillations on inositol trisphosphate oscillations. *Proc. Natl. Acad. Sci. U. S. A.*, 103(6):1675–80.

[Sneyd et al., 1995] Sneyd, J., Wetton, B. T., Charles, A. C., and Sanderson, M. J. (1995). Intercellular calcium waves mediated by diffusion of inositol trisphosphate: a two-dimensional model. *Am. J. Physiol.*, 268(6 Pt 1):C1537–45.

[Sobkowicz et al., 1975] Sobkowicz, H. M., Bereman, B., and Rose, J. E. (1975). Organotypic development of the organ of Corti in culture. *J Neurocytol*, 4(5):543–572.

[Sobkowicz et al., 1993] Sobkowicz, H. M., Loftus, J. M., and Slapnick, S. M. (1993). Tissue culture of the organ of Corti. *Acta Otolaryngol Suppl*, 502:3–36.

[Sotomayor et al., 2010] Sotomayor, M., Weihofen, W. A., Gaudet, R., and Corey, D. P. (2010). Structural determinants of cadherin-23 function in hearing and deafness. *Neuron*, 66:85–100.

[Spassova et al., 2001] Spassova, M., Eisen, M. D., Saunders, J. C., and Parsons, T. D. (2001). Chick cochlear hair cell exocytosis mediated by dihydropyridine-sensitive calcium channels. *J Physiol*, 535:689–696.

[Spassova et al., 2004] Spassova, M. A., Avissar, M., Furman, A. C., Crumling, M. A., Saunders, J. C., and Parsons, T. D. (2004). Evidence that rapid vesicle replenishment of the synaptic ribbon mediates recovery from short-term adaptation at the hair cell afferent synapse. *J Assoc Res Otolaryngol*, 5:376–390.

[Spicer and Schulte, 1998] Spicer, S. S. and Schulte, B. A. (1998). Evidence for a medial K+ recycling pathway from inner hair cells. *Hear Res*, 118(1-2):1–12.

[Spicer et al., 1999] Spicer, S. S., Thomopoulos, G. N., and Schulte, B. A. (1999). Novel membranous structures in apical and basal compartments of inner hair cells. *J Comp Neurol*, 409:424–437.

[Spiden et al., 2008] Spiden, S. L., Bortolozzi, M., Di Leva, F., de Angelis, M. H., Fuchs, H., Lim, D., Ortolano, S., Ingham, N. J., Brini, M., and Carafoli, E. (2008). The novel mouse mutation Oblivion inactivates the PMCA2 pump and causes progressive hearing loss. *PLoS Genet*, 4:e1000238.

[Sridhar et al., 1997] Sridhar, T. S., Brown, M. C., and Sewell, W. F. (1997). Unique postsynaptic signaling at the hair cell efferent synapse permits calcium to evoke changes on two time scales. *J Neurosci*, 17:428–437.

[Stepanyan and Frolenkov, 2009] Stepanyan, R. and Frolenkov, G. I. (2009). Fast adaptation and Ca2+ sensitivity of the mechanotransducer require myosin-XVa in inner but not outer cochlear hair cells. *J Neurosci*, 29:4023–4034.

[Street et al., 1998] Street, V. A., McKee-Johnson, J. W., Fonseca, R. C., Tempel, B. L., and Noben-Trauth, K. (1998). Mutations in a plasma membrane Ca2+-ATPase gene cause deafness in deafwaddler mice. *Nat Genet*, 19:390–394.

[Strenzke et al., 2009] Strenzke, N., Chanda, S., Kopp-Scheinpflug, C., Khimich, D., Reim, K., Bulankina, A. V., Neef, A., Wolf, F., Brose, N., Xu-Friedman, M. A., and Moser, T. (2009). Complexin-I is required for high-fidelity transmission at the endbulb of Held auditory synapse. *J Neurosci*, 29:7991–8004.

[Strogatz, 2000] Strogatz, S. H. (2000). *Nonlinear dynamics and chaos: with applications to physics, biology, chemistry, and engineering*. Westview Press.

[Sudhof, 2004] Sudhof, T. C. (2004). The synaptic vesicle cycle. *Annu Rev Neurosci*, 27:509–547.

[Sun et al., 2009] Sun, Y., Tang, W., Chang, Q., Wang, Y., Kong, W., and Lin, X. (2009). Connexin30 null and conditional connexin26 null mice display distinct pattern and time course of cellular degeneration in the cochlea. *J. Comp. Neurol.*, 516(6).

[Takahashi and Kitamura, 1999] Takahashi, K. and Kitamura, K. (1999). A point mutation in a plasma membrane Ca(2+)-ATPase gene causes deafness in Wriggle Mouse Sagami. *Biochem Biophys Res Commun*, 261:773–778.

[Teubner, 2003] Teubner, B. (2003). Connexin30 (Gjb6)-deficiency causes severe hearing impairment and lack of endocochlear potential. *Hum. Mol. Genet.*, 12(1):13–21.

[Thiers et al., 2008] Thiers, F. A., Nadol Jr., J. B., and Liberman, M. C. (2008). Reciprocal synapses between outer hair cells and their afferent terminals: evidence for a local neural network in the mammalian cochlea. *J Assoc Res Otolaryngol*, 9(4):477–489.

[Tritsch and Bergles, 2010] Tritsch, N. X. and Bergles, D. E. (2010). Developmental regulation of spontaneous activity in the Mammalian cochlea. *J Neurosci*, 30(4):1539–1550.

[Tritsch et al., 2007] Tritsch, N. X., Yi, E., Gale, J. E., Glowatzki, E., and Bergles, D. E. (2007). The origin of spontaneous activity in the developing auditory system. *Nature*, 450(7166):50–55.

[Tsai et al., 2006] Tsai, Y. S., Pendse, A., Moy, S. S., Mohri, I., Perez, A., Crawley, J. N., Suzuki, K., and Maeda, N. (2006). A de novo deafwaddler mutation of Pmca2 arising in ES cells and hitchhiking with a targeted modification of the Pparg gene. *Mamm Genome*, 17:716–722.

[Tsien and Tsien, 1990] Tsien, R. W. and Tsien, R. Y. (1990). Calcium channels, stores, and oscillations. *Annu. Rev. Cell Biol.*, 6:715–60.

[Uthaiah and Hudspeth, 2010] Uthaiah, R. C. and Hudspeth, A. J. (2010). Molecular anatomy of the hair cell's ribbon synapse. *J. Neurosci. Off. J. Soc. Neurosci.*, 30(37):12387–12399.

[Uziel et al., 1981] Uziel, A., Romand, R., and Marot, M. (1981). Development of cochlear potentials in rats. *Audiology*, 20(2):89–100.

[Van de Water and Ruben, 1971] Van de Water, T. R. and Ruben, R. J. (1971). Organ culture of the mammalian inner ear. *Acta Otolaryngol*, 71(4):303–312.

[Verselis and Srinivas, 2013] Verselis, V. K. and Srinivas, M. (2013). Connexin channel modulators and their mechanisms of action. *Neuropharmacology*.

[Vetter et al., 2007] Vetter, D. E., Katz, E., Maison, S. F., Taranda, J., Turcan, S., Ballestero, J., Liberman, M. C., Elgoyhen, A. B., and Boulter, J. (2007). The alpha10 nicotinic acetylcholine receptor subunit is required for normal synaptic function and integrity of the olivocochlear system. *Proc Natl Acad Sci U S A*, 104:20594–20599.

[Vlajkovic et al., 2002] Vlajkovic, S. M., Thorne, P. R., Sevigny, J., Robson, S. C., and Housley, G. D. (2002). Distribution of ectonucleoside triphosphate diphosphohydrolases 1 and 2 in rat cochlea. *Hear Res*, 170:127–138.

[Wade et al., 1986] Wade, M. H., Trosko, J. E., and Schindler, M. (1986). A fluorescence photobleaching assay of gap junction-mediated communication between human cells. *Sci*, 232:525–528.

[Waguespack et al., 2007] Waguespack, J., Salles, F. T., Kachar, B., and Ricci, A. J. (2007). Stepwise morphological and functional maturation of mechanotransduction in rat outer hair cells. *J Neurosci*, 27:13890–13902.

[Wangemann, 2002] Wangemann, P. (2002). K+cycling and the endocochlear potential. *Hear Res*, 165:1–9.

[Wangemann, 2006] Wangemann, P. (2006). Supporting sensory transduction: cochlear fluid homeostasis and the endocochlear potential. *J Physiol*, 576(Pt 1):11–21.

[Warren et al., 2010] Warren, N. J., Tawhai, M. H., and Crampin, E. J. (2010). Mathematical modelling of calcium wave propagation in mammalian airway epithelium: evidence for regenerative ATP release. *Exp. Physiol.*, 95(1):232–49.

[Weisz et al., 2012] Weisz, C. J., Lehar, M., Hiel, H., Glowatzki, E., and Fuchs, P. A. (2012). Synaptic Transfer from Outer Hair Cells to Type II Afferent Fibers in the Rat Cochlea. *J Neurosci*, 32(28):9528–9536.

[Wood et al., 2004] Wood, J., Muchinsky, S., Filoteo, A., Penniston, J., and Tempel, B. (2004). Low Endolymph Calcium Concentrations in deafwaddler2J Mice Suggest that PMCA2 Contributes to Endolymph Calcium Maintenance. *J. Assoc. Res. Otolaryngol.*, 5(2).

[Wu et al., 1999] Wu, Y., Ricci, A., and Fettiplace, R. (1999). Two components of transducer adaptation in auditory hair cells. *J. Neurophysiol.*, 82(5):2171.

[Yamasaki et al., 2000] Yamasaki, M., Komune, S., Shimozono, M., Matsuda, K., and Haruta, A. (2000). Development of monovalent ions in the endolymph in mouse cochlea. *ORL J Otorhinolaryngol Relat Spec*, 62(5):241–246.

[Yamoah et al., 1998] Yamoah, E. N., Lumpkin, E. A., Dumont, R. A., Smith, P. J., Hudspeth, A. J., and Gillespie, P. G. (1998). Plasma membrane Ca2+-ATPase extrudes Ca2+ from hair cell stereocilia. *J Neurosci*, 18:610–624.

[Yang et al., 2006] Yang, P. S., Alseikhan, B. A., Hiel, H., Grant, L., Mori, M. X., Yang, W., Fuchs, P. A., and Yue, D. T. (2006). Switching of Ca2+-dependent inactivation of Ca(v)1.3 channels by calcium binding proteins of auditory hair cells. *J Neurosci*, 26:10677–10689.

[Yasunaga et al., 1999] Yasunaga, S., Grati, M., Cohen-Salmon, M., El-Amraoui, A., Mustapha, M., Salem, N., El-Zir, E., Loiselet, J., and Petit, C. (1999). A mutation in OTOF, encoding otoferlin, a FER-1-like protein, causes DFNB9, a nonsyndromic form of deafness. *Nat Genet*, 21:363–369.

[Yum et al., 2007] Yum, S. W., Zhang, J., Valiunas, V., Kanaporis, G., Brink, P. R., White, T. W., and Scherer, S. S. (2007). Human connexin26 and connexin30 form functional heteromeric and heterotypic channels. *Am J Physiol Cell Physiol*, 293:C1032–1048.

[Zampini et al., 2010] Zampini, V., Johnson, S. L., Franz, C., Lawrence, N. D., Munkner, S., Engel, J., Knipper, M., Magistretti, J., Masetto, S., and Marcotti, W. (2010). Elementary properties of CaV1.3 Ca(2+) channels expressed in mouse cochlear inner hair cells. *J Physiol*, 588:187–199.

[Zdebik et al., 2009] Zdebik, A. A., Wangemann, P., and Jentsch, T. J. (2009). Potassium ion movement in the inner ear: insights from genetic disease and mouse models. *Physiol.*, 24:307–316.

[Zhao et al., 2006] Zhao, H. B., Kikuchi, T., Ngezahayo, A., and White, T. W. (2006). Gap junctions and cochlear homeostasis. *J Membr Biol*, 209:177–186.

[Zhao et al., 2005] Zhao, H. B., Yu, N., and Fleming, C. R. (2005). Gap junctional hemichannel-mediated ATP release and hearing controls in the inner ear. *Proc. Natl. Acad. Sci. U. S. A.*, 102(51):18724.

[Zhao et al., 1996] Zhao, Y., Yamoah, E. N., and Gillespie, P. G. (1996). Regeneration of broken tip links and restoration of mechanical transduction in hair cells. *Proc Natl Acad Sci U S A*, 93:15469–15474.

[Zheng et al., 2000] Zheng, J., Shen, W., He, D. Z., Long, K. B., Madison, L. D., and Dallos, P. (2000). Prestin is the motor protein of cochlear outer hair cells. *Nature*, 405(6783):149–155.

[Zonta et al., 2013] Zonta, F., Polles, G., Sanasi, M. F., Bortolozzi, M., and Mammano, F. (2013). The 3.5 angstrom X-ray structure of the human connexin26 gap junction channel is unlikely that of a fully open channel. *Cell Commun Signal*, 11:15.

[Zonta et al., 2012] Zonta, F., Polles, G., Zanotti, G., and Mammano, F. (2012). Permeation pathway of homomeric connexin 26 and connexin 30 channels investigated by molecular dynamics. *J Biomol Struct Dyn*, 29:985–998.

[Zuo et al., 2008] Zuo, P., Picher, M., Okada, S. F., Lazarowski, E. R., Button, B., Boucher, R. C., and Elston, T. C. (2008). Mathematical model of nucleotide regulation on airway epithelia. Implications for airway homeostasis. *J. Biol. Chem.*, 283(39):26805–19.